APPLIED COMPUTER SCIENCE

Vol. 12, No. 3, 2016

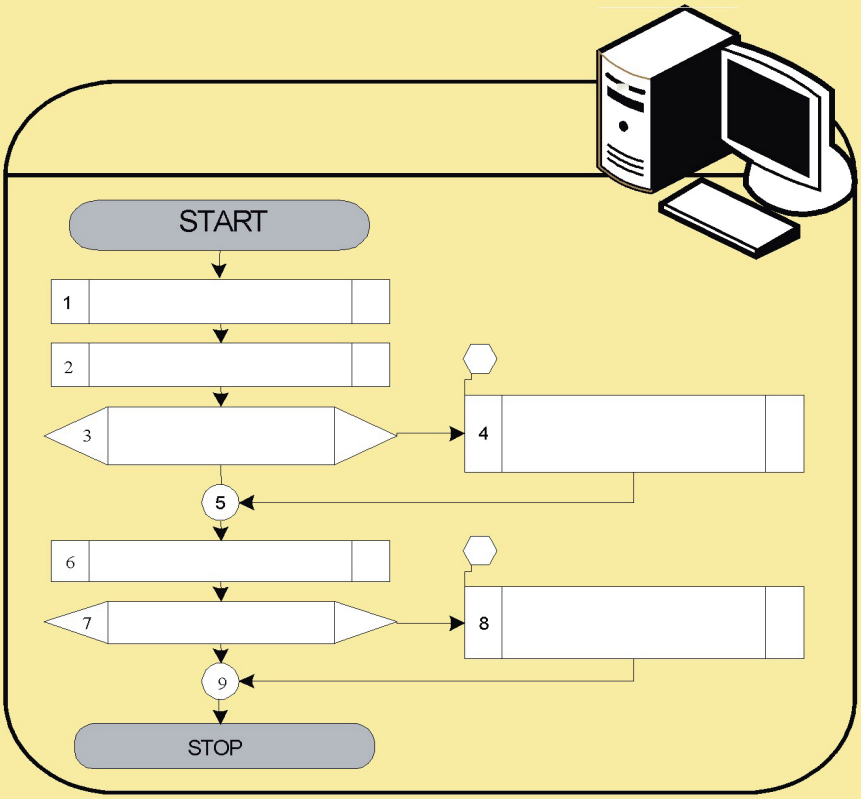

LUBLIN UNIVERSITY OF TECHNOLOGY

INSTITUTE OF TECHNOLOGICAL SYSTEMS OF INFORMATION

www.acs.pollub.pl

ISSN 1895-3735

Editorial Board:	**Arkadiusz Gola** (Editor-in-Chief, Secretary of the Scientific Board) **Jakub Szabelski** (Proof Reading) **Monika Kulisz** (Editorial secretary) **Katarzyna Piotrowska** (Editorial secretary) **Dariusz Wołos** (Editorial secretary) **Lukasz Sobaszek** (DTP specjalist) **Daniel Gąska** (Webmaster)
Redactioral Board:	**Bozena Skołud** - Computer Science in Production Engineering (Subject Redactor) **Zbigniew Pastuszak -** Computer Science in Economy and Management (Subject Redactor) **Marek Janczarek** - Computer Science in Technology (Subject Redactor) **Alex Bodnar** - English Instructor at Kyushu University, Japan (Language Redactor) **Paweł Zaprawa** (Statistical Redactor)
Publisher:	Polish Association for Knowledge Promotion
Editorial Office:	„Applied Computer Science" Editorial Office 20-619 Lublin, ul. Nowomiejska 18/23, Poland Tel.: +48 81 538 45 35, +48 507 387 307 e-mail: acs@pollub.pl www.acs.pollub.pl
Circulation:	100 copies (the digital version is available at the journal's website: **www.acs.pollub.pl** and at Digital Library of Lublin University of Technology: **www.bc.pollub.pl**

APPLIED COMPUTER SCIENCE

The Journal is a peer-reviewed, international, multidisciplinary journal covering a broad spectrum of topics of computer application in production engineering, technology, management and economy.

The main purpose of Applied Computer Science is to publish the results of cutting-edge research advancing the concepts, theories and implementation of novel solutions in computer technology. Papers presenting original research results related to applications of computer technology in production engineering, management, economy and technology are welcomed.

We welcome original papers written in English. The Journal also publishes technical briefs, discussions of previously published papers, book reviews, and editorials. Especially we welcome papers which deals with the problem of computer applications in such areas as:

- manufacturing,
- engineering,
- technology,
- designing,
- organization,
- management,
- economics,
- innovations,
- competitiveness,
- quality and costs.

The Journal is published quarterly and is indexed in: BazTech, Cabell's Directory, CNKI Scholar (China National Knowledge Infrastucture), ERIH PLUS, Index Copernicus, J-Gate, Google Scholar, TEMA Technik und Management.

Letters to the Editor-in-Chief or Editorial Secretary are highly encouraged.

CONTENTS

Applied Computer Science, vol. 12, no. 3, pp. 5–16

Submitted: 2016-06-25
Revised: 2016-08-29
Accepted: 2016-09-12

disk spring, reliability, traction lift, safety progressive gears, lift

Paweł LONKWIC[*], *Patryk RÓŻYŁO*[**], *Ireneusz USYDUS*[*]

NUMERICAL ANALYSIS AND EXPERIMENTAL INVESTIGATION OF DISK SPRING CONFIGURATIONS WITH REGARD TO LOAD CAPACITY OF SAFETY PROGRESSIVE GEARS

Abstract

The paper investigates the effect of various disk spring package configurations on brake load of safety progressive gears. The numerical analysis is performed using the Abaqus/CAE software and the designed 3D models. The numerical results are then verified in experimental tests. The tests also examine the effect of lubrication on brake load of spring packages. In addition, the paper investigates the work conditions of safety progressive gears at emergency braking. The experimental results show agreement with the numerical results.

1. STATE OF THE ART OF THE PROBLEM

The problem of selecting disk springs for technical objects is widely investigated in the field of metal forming. When it comes to the application of safety systems in traction lifts, however, the number of available studies devoted to this issue is very scarce. The authors of the study (Dharan & Bauman, 2007) examine composite disk springs. The results they report demonstrate that composites can satisfactorily replace steel in disk springs with mass savings of almost 80%. These authors also investigate the effects of different spring

[*] The State School of Higher Education, Pocztowa Street 54, 22-100 Chełm, Poland, plonkwic@gmail.com
[**] Lublin University of Technology, Mechanical Engineering Faculty, Department of Machine Design, Nadbystrzycka Street 36, 20-618 Lublin, Poland, p.rozylo@pollub.pl

geometries on load deflection responses. In the studies (Dębski, Kubiak & Teter, 2012; Ozaki, Tsuda & Tominaga 2012), the authors apply the finite element method to predict load deflection curves based on the results of obtained using different friction factors. The authors of (Atxaga, Pelayo & Irisarri, 2006) discuss the effect of temperature and excessive environmental salinity on the life and reliability of stainless steel disk springs. In the study (Kayaoglu, Salman & Candas, 2011), the authors investigate stress and displacement of a lift safety gear brake block using the Abaqus/CAE software. They compare the numerical and experimental results. According to these authors, the numerical results agree with the results of the experimental tests. In the study (Taplak, Erkaya, Yildirim & Uzmay, 2014), the authors deal with the problem of using neural network predictors for the analysis of lift vibrations caused by variable load weight. The neural networks were applied to estimate vibration symptoms and, therefore, to identify failure of either one element of the lift or the entire lifting equipment. The authors of (Onur & Imrak, 2012) discuss the application of the reduction method to estimation of lift dynamics. In their analysis, the lift car model is reduced to a flat system with one vertical degree of freedom. This reduction-based methodology is then applied to describe a specific goods lift using analytical and finite element methods. Moreover, the above authors examine the effect of parameters of lift work on acceleration characteristics of the entire lift system. In the studies (Jong, 2004; Feng, Bao, Zhou & Wang, 2012), the authors discuss the application of the finite element method to estimation of rigidity and strength of a lift car frame in various types of lifts, focusing on the problem of safety gears, too. The FEM was applied to optimize the carrying frame design and thus to reduce both the sections of frame beams and frame weight as well as determine safety factors. Based on the results, they also undertake to determine failure-prone areas of the lift frame system. The problems of lift brake system dynamics, materials and safety gears are also investigated in the studies (Filas & Mudron, 2012; Lonkwic, Różyło & Dębski, 2015; Lonkwic & Różyło, 2016; Lonkwic & Szydło, 2014; Lonkwic & Gardyński, 2014; Lonkwic, Szydło & Molski, 2016). The authors of these publications analyze, among others, the lift brake system and compare the design and operation of safety gears produced by European manufacturers with a new developed solution. In the publication (Zhu & Ren, 2013), the authors raise the problem of the effect of weight of car lifting feeders and hoisting ropes on the operation of so-called tall lifts that are used in building above 40 stories tall. Due to the considerable lifting height, this type of lifts requires the application of an adjusting belt to compensate for the weight of hoisting ropes and feeders, so that other lift components are not excessively loaded. The authors describe the behavior of the adjusting belt and its effect on the linear model of lift operation. They examine the effect of horizontal displacements of the adjusting belt on free vibration frequency of the system. The above-mentioned studies provide information with regard to the methodology of disk spring package

selection and the use of different materials for disk springs. Nonetheless, there is lack of studies reporting numerical results of the application of spring packages in safety gears. Given the above, it seems justified that this problem be investigated by both numerical modeling and experimental tests.

2. RESEARCH METHOD

The objective of the present study is to investigate the effect of different disk spring package configurations and lubrication on the brake load of a safety gear. The investigation of spring disk package deflection was performed following the configurations given in Table 1.

Tab. 1. Characteristics of tested spring packages [source: own study]

Pack	Package	Dry	Lubricated
I	14V_S	X	
II	7X7_S	X	
III	4V5X5_S	X	
IV	14V_Sm		X
V	7X7_Sm		X
VI	4V5X5_Sm		X

The denotation 14V stands for a configuration of 14 disk springs that are arranged in a parallel manner (Fig. 1a). The spring deflection load of this package is 14 times higher than the deflection load of a single spring. The denotation 7X7 (Fig. 1b) means that there are two packages, each containing seven springs, arranged in opposite directions. This configuration has the deflection load that is seven time higher than that of a single spring, while the deflection is two times higher than the deflection of one spring. The denotation 4V5X5 (Fig. 1c) stands for a mixed configuration of springs with the packages arranged in opposite directions, where deflection is three times higher than the deflection of a single spring and the deflection load is the multiplicity of load of one spring in the package. Given the design of the safety gear CHP 2000, the tested disk springs had the following dimensions:

- outside diameter: 31.5 mm,
- inside diameter: 16.3 mm,
- thickness: 2 mm,
- height of unloaded spring: 2.75 mm,
- spring travel: 0.75 mm.

Figures 1a–1c illustrate the package models used in the numerical simulations.

1a)

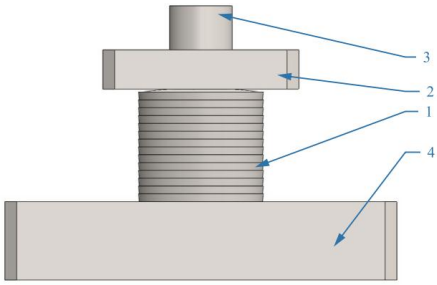

1b)

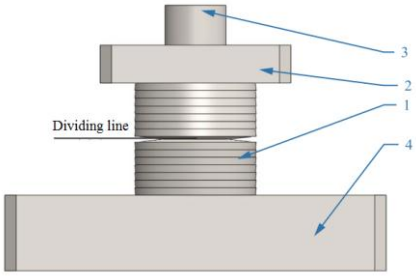

1c)

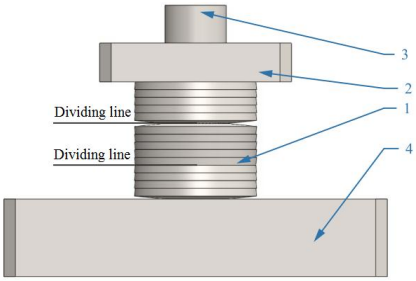

Fig. 1. Models of disk spring packages designed in Solid Works: 1 – disk spring package, 2 – pusher, 3 – guiding bolt, 4 – base, a) configuration 14V, b) configuration 7V7, c) own study

The numerical results were verified in experimental tests conducted using the testing machine HT-2402. The measurement of package deflection and load was done in two ways: with no lubricant applied (dry) and with lubrication to decrease the friction factor between individual springs in the package, following the scheme given in Table 1. The lubricating agent applied in the experiments was Megol SL-68.

The package deflection paths were obtained by averaging the results of 15 consecutive measurements. The measurements were averaged using dependence (1).

$$\bar{z} = \frac{\sum_{i=1}^{i=k} z_i}{k} \tag{1}$$

where: z_i – the path of package deflection in the n-th measurement cycle,
k – the number of measurement cycles,
i – the number of consecutive measurement.

Fig. 2. 4V5X5 disk spring package configuration to be tested using HT-2402 machine (own study)

Fig. 2 shows one example of a disk spring package to be measured using the HT-2402 machine along with all necessary measurement instruments.

3. DISCRETE MODEL

The discrete model of a disk spring package was modeled with Abaqus. The discrete modeling was the fundamental stage of the numerical analysis. The FEM analysis illustrated operation of the lift under load applied to three disk spring packages with different configurations. The contact parameters were based on the interaction between lift components in tangential and normal directions. The load was defined for each spring package configuration separately. All packages were subjected to axial load. The aim of the simulation was to do the following: first, to generate a disk spring deflection package and, then, to determine the maximum axial load applied to the package. The spring package deflection was simulated in the range from 0% to 75% of the unloaded package height, which is the effective operating range of springs.

The material properties of the applied components are compared in Table 2. The objective of the present study is to investigate the effect of different disk.

Tab. 2. Characteristics of tested spring packages (Banaszek, 1996)

	Material	**Young's modulus E [MPa]**	**Poisson's ratio ν**	**Yield strength Re [MPa]**	**Tensile strength Rm [MPa]**
Disk springs	Steel 51CrV4	210000	0.3	1080	1280
Other components	Steel C45	210000	0.3	360	610

The numerical analysis was statics-based, therefore the lift's weight was not taken into account. The configurations contained several contact interactions between components that were active during the simulation. The assigning of boundary conditions to the lift depended on suitable fastening of the system and load determination, as shown in Fig. 3a. The component that produces spring package compression was prevented from displacement in all axes, except for the Y-axis. The bottom plane of the component with the spring package was made totally fixed in compliance with the real fastening. The load was applied as a point-concentrated force. To this end, a reference point was established in the axis of the spring package compressing component. Next, the concentrated force was assigned to the newly established point; the force was assumed to act opposite to the Y-axis (Fig. 3a). The reference point was tied by a coupling in the interaction module with the upper plane of the compression-generating component. The coupling of the point with the surface-acting load enabled us to perform further stages of the numerical analysis. The key stage of the FEM analysis included assigning the mesh to a system and dividing it into finite elements. To obtain the highest quality meshes, the elements were partitioned into smaller parts. In this way, we obtained a linear geometry mesh; the mesh was hexagonal (structured) for the springs, while for the spring fastenings it was arranged hexagonally (sweep) relative to the centre line. The size of mesh elements was set to 2, while the size of spring fastenings was set to 4. The assigned mesh element was C3D8R, i.e. a brick element with three degrees of freedom and eight nodes, with reduced integration. Reduced integration is the technique that can lessen the blockage effect, i.e. the removal of incorrect object shape deformations. As a result, the components of high-order polynomials are eliminated, which improves the numerical analysis (Zienkiewicz & Taylor, 2000). The total number of mesh elements in the entire system, in each analyzed case, is 5862. For detailed information about the mesh see Fig. 3b.

a) **b)**

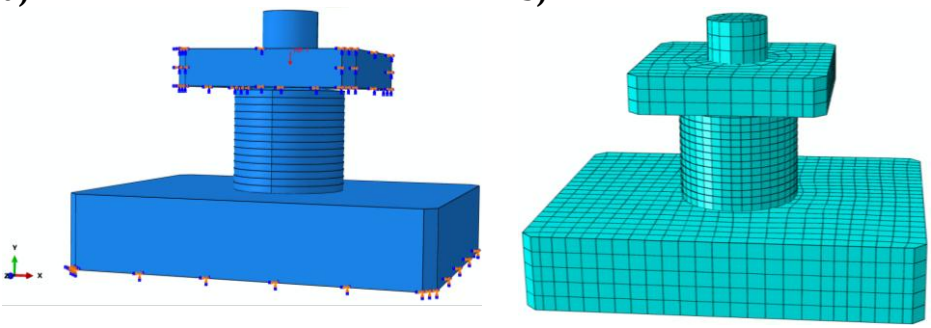

Fig. 3. a) Boundary conditions of the system , b) FEM mesh – total numbers of nodes: 10292; total numbers of elements: 5862, 5862 linear hexahedral elements of type C3D8R (own study)

The FEM analysis shows the results in integration points that were geometrically distant from the node points. The node results are the interpolated values measured in the integration points.

4. NUMERICAL AND EXPERIMENTAL RESULTS

The numerical results are illustrated as distribution patterns of stresses in crucial points. The FEM results are also compared with the experimental results of load-elongation relationships produced for three configurations. The simulation results of stresses are shown in Fig. 4.

5a)

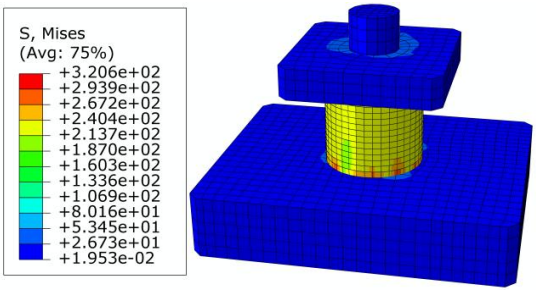

5b)

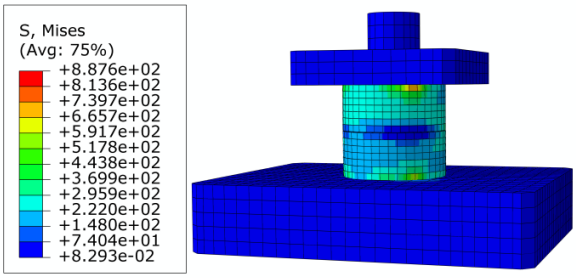

5c)

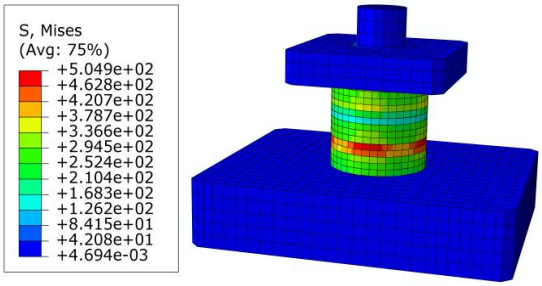

Fig. 4. Numerical results of stresses: a) package 14V under load of 21kN, b) package 7V7 under load of 38kN, c) package 4V5X5 under load of 38kN (own study)

The above results demonstrate that the package 14V exhibits the lowest stresses that are of about 321MPa. The stresses observed for the package 4V5X5 amount to about. 500MPa are considerably lower than is the case with the package 7V7, where the stresses equal 888MPa. The analysis of the three cases does not reveal that the yield strength was exceeded, therefore the system is free from plasticization and plastic strains. The numerical results of displacements are shown as axial sections of spring packages in Fig. 5.

6a)

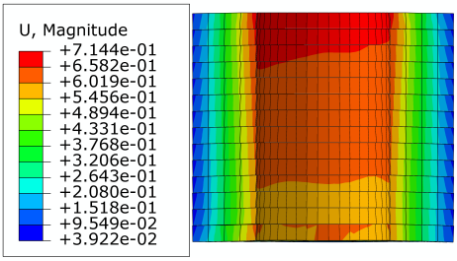

6b)

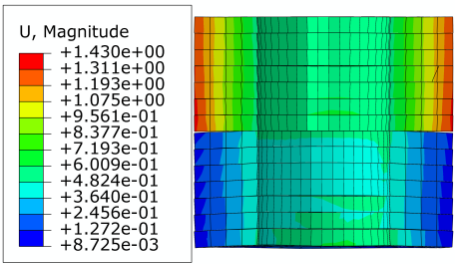

6c)

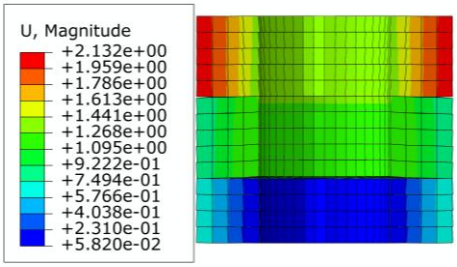

Fig. 5. Numerical results of spring displacement (deflection) [mm]: a) package 14V, b) package 7V7, c) package 4V5X5 (source: own study)

The experimental results are given in Fig. 6. At the beginning of the experiment, each disk spring configuration was pre-loaded in order to remove redundant clearance and determine the 0 measuring point. The dry-loaded packages of springs were degreased with degreasing agents.

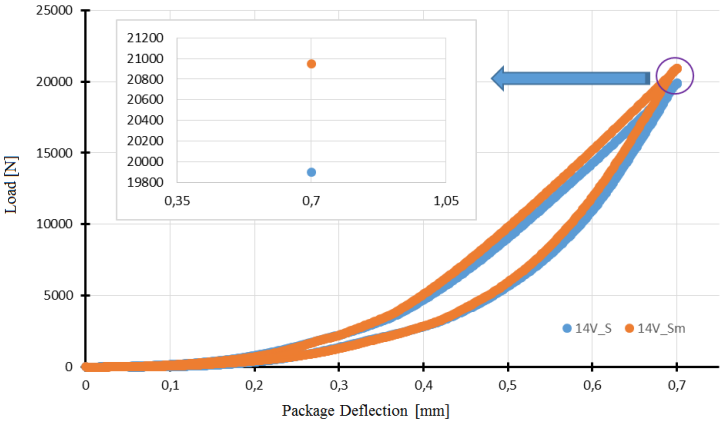

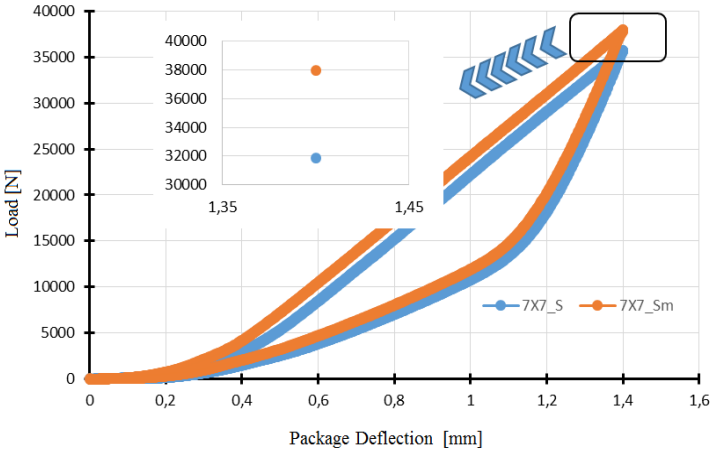

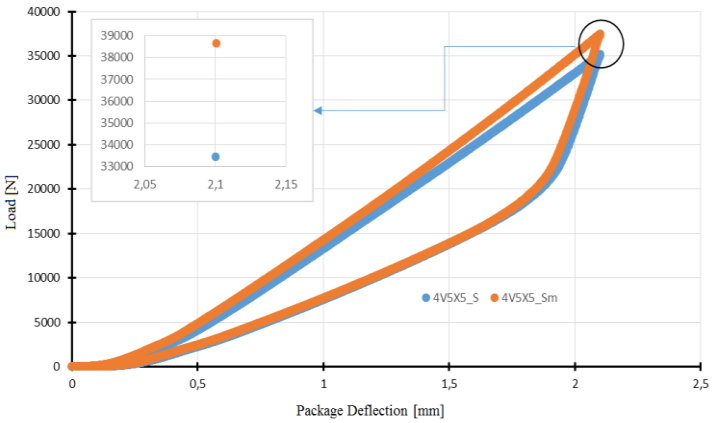

Fig. 6. Experimental results of spring package deflection (own study)

The numerical and experimental results show agreement with regard to displacements. As for the first spring package configuration, the displacement is equal to 0.7 mm, while the results measured for other configurations are a multiple of the displacement recorded for the first case. In effect, the elongation observed for the second case was approximately 1.4 mm, while for the third case it amounted to 2.1 mm. The application of different configurations of disk packages affects both stress and displacement of the system. Fig. 7 gives the comparison between the experimental and numerical results of deflection of disk spring packages.

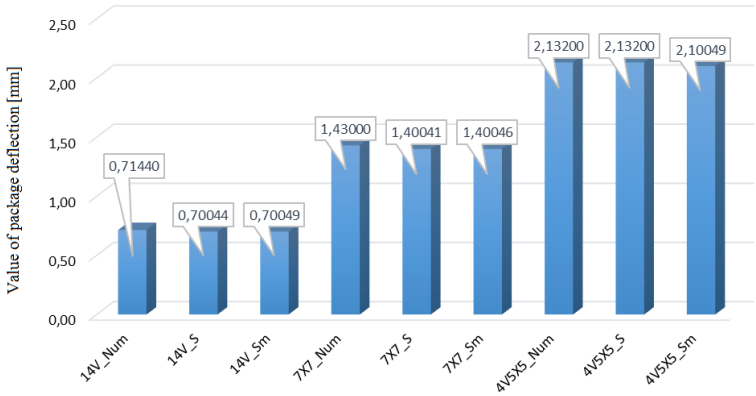

Fig. 7. Comparison of the numerical and experimental results (own study)

Analyzing the data given in Fig. 7, it can be observed that there is no significant difference between the numerical and experimental results. Despite the lack of lubrication, the generated package load is not disturbed in any way. A similar dependence can be observed for the numerical and experimental results of a dry-working (non-lubricated) spring package.

5. CONCLUSIONS

Based on the above results, the following conclusion have been drawn:

- The FEM and experimental results of the effect of load on disk spring package deflection show a good agreement. In addition, the numerical results demonstrate that stresses in crucial points of the three applied spring package configurations do not have negative effect on system operation, which means that the tested spring packages can be used in safety gears.
- The numerical and experimental results of package deflections are almost the same.

- In terms of safety gear operation, the spring package 4V5X5 seems optimum. Although the package configuration is asymmetric, the experimental results reveal that it is characterized by a high package deflection (2.1 mm) and the highest load (almost 40kN). The results demonstrate that the safety gear has the most unified structure in this particular configuration, which means that it can be used at a wide range of load.
- The symmetric package 14V has the most disadvantages out of the tested spring package configurations. Theoretically, this package should exhibit the highest load at the lowest package deflection, yet the experimental results do not confirm this relationship. This can be attributed to a high number of interacting surfaces, which had a significant impact on the experimental results.
- The numerical and experimental results confirm the suitability of using asymmetric spring packages (4V5X5) in safety gears owing to the fact that they exhibit the highest brake load and package deflection. The high package deflection in spring disks means that the energy of the lift car system will be gently reduced until the lift car's stop.
- The lubrication did not have significant effect on the experimental results. Nonetheless, lubricating agents should be applied when safety gears are used in order to prolong service life of spring packages.
- Due to lack of publications on such issues as safety gears and passenger lift brake systems in both national and international journals, it is justified that the research on this problem be continued.

Acknowledgments

We gratefully acknowledge the financial support of NOVA TRADING, Toruń, and Rywal-RCH, Lublin, which made this research possible.

REFERENCES

Atxaga, G., Pelayo, A., & Irisarri, A. M. (2006). Failure analysis of a set of stainless steel disc springs. *Engineering Failure Analysis, 13*(2), 226-234. doi:10.1016/j.engfailanal.2005.01.011

Banaszek, J. (Ed.). (1996). *Przykłady obliczeń z podstaw konstrukcji maszyn cz. II.* Lublin: Wyd. Uczelniane PL.

Dębski, H., Kubiak, T., & Teter, A. (2012). Buckling and postbuckling behavior of thin-walled composite channel section beam. *Composite Structures, 100*, 195-204. doi:10.1016/j.compstruct.2012.12.033

Dharan, C. K. H., & Bauman, J. A. (2007). Composite disc springs. *Composites Part A: Applied Science and Manufacturing, 38*(12), 2511-2516. doi:10.1016/j.compositesa.2007.08.008

Feng, L., Bao, Y., Zhou, X., & Wang, Y. (2012). High Speed Elevator Car Frame's Finite Elements Analysis. *Advanced Materials Research, 510*, 298-303. doi:10.4028/www.scientific.net/AMR.510.298

Filas, J., & Mudron, M. (2012). The dynamic equation of motion of driving mechanism of a freight elevator. *Modelling of Mechanical and Mechatronics Systems, 48*, 149-152. doi:10.1016/j.proeng.2012.09.498

Jong de, J. (2004). Understanding the natural behavior of elevator safety gears and their triggering. *The International Congress on Vertical transportation technologies*, Turkey.

Kayaoglu, E., Salman, O., & Candas, A. (2011). Study on Stress and Deformation of an Elevator Safety Gear Brake Block Using Experimental and FEA Methods. *Advanced Design Technology, 308-310*, 1513-1518. doi:10.4028/www.scientific.net/AMR.308-310.1513

Lonkwic, P., & Gardyński, L. (2014). Testing polymer rollers memory in the context of passenger lift car comfort. *Journal of Vibroegineering, 16*(1), 225-230.

Lonkwic, P., & Szydło, K. (2014). Selected Parameters of the Work of Speed Limiter Line Straining System in a Frictional Lift. *Advances in Science and Technology, 8*(21), 73-77. doi: 10.12913/22998624.1091882

Lonkwic, P., & Różyło, P. (2016). Theoretical and experimental analysis of loading impact from the progressive gears on the lift braking distance with use of the free fall method. *Advances in Science and Technology Research Journal, 10*(30), 103-109. doi:10.12913/22998624/62628

Lonkwic, P., Różyło, P., & Dębski, H. (2015). Numerical and experimental analysis of the progressive gear body with the use of finite-element method. *Eksploatacja I Niezawodność-Maintenance and Reliability, 17*(4), 544-550. doi: 10.17531/ein.2015.4.9

Lonkwic, P., Szydło, K., & Molski, S. (2016). The impact of progressive gear geometry on the braking distance length under changeable operating conditions. *Advances in Science and Technology-Research Journal, 10*(29), 161-167. doi: 10.12913/22998624/61948

Onur, Y. A., & Imrak, C. E. (2012). Reliability analysis of elevator car frame using analytical and finite element methods. *Building Services Engineering Research & Technology, 33*(3), 293-305. doi: 10.1177/0143624411413168

Ozaki, S., Tsuda, K., & Tominaga, J. (2012). Analyses of static and dynamic behavior of coned disk springs: Effects of friction boundaries. *Thin-Walled Structures, 59*, 132-143. doi:10.1016/j.tws.2012.06.001

Taplak, H., Erkaya, S., Yildirim, S., & Uzmay, I. (2014). The Use of Neural Network Predictors for Analyzing the Elevator Vibrations. *Arabian Journal for Science and Engineering, 39*(2), 1157-1170. doi: 10.1007/s13369-013-0632-z

Zhu, W. D., & Ren, H. (2013). A linear model of stationary elevator traveling and compensation cables. *Journal of Sound and Vibration, 332*(12), 3086-3097. doi:10.1016/j.jsv.2013.01.009

Zienkiewicz, O.C., & Taylor, R.L. (2000). *Finite Element Method (5th Edition) Volume 2 – Solid Mechanics*, Elsevier.

Applied Computer Science, vol. 12, no. 3, pp. 17–28

Submitted: 2016-07-27
Revised: 2016-09-05
Accepted: 2016-09-09

Compression detection, Image quality, JPEG

Grzegorz KOZIEL[*]

PRIOR IMAGE JPEG-COMPRESSION DETECTION

Abstract

The paper presents two methods of prior JPEG-compression detection. In the first method the histogram of chrominance is analysed. In JPEG-compressed images the histogram contains significantly more local maxima than in uncompressed files. The second method is based on neighbouring pixel Ø value difference. In JPEG-compressed image the distribution of these values is different than the distribution counted on the edges of compression 8x8 blocks. These differences are summed up to create a classifier that allows to assess if the image was compressed.

1. INTRODUCTION

Steganography is the science of hiding information in another carrier called a container. A carrier can be an image. Further in the article we will focus on images, thus the container will be understood to be an image. In this case the data of the image chosen to hide data inside itself are modified in such a way as to hide a portion of information by including it directly in the image data. During this operation it is important to keep the image quality and not introduce detectable changes.

By detectable changes we understand any visual distortions that can be notified by observer or any statistical interference or characteristic artefacts in the image data. The problem is that in some containers it is much more difficult to meet these conditions. Especially when the image was previously compressed. After compression some characteristic features are introduced into the compressed image. If the steganographic method interferes with these

[*] Lublin University of Technology, Nadbystrzycka 38D, 20-618 Lublin, Poland,
phone: +48 81 538 46 08, e-mail: g.koziel@pollub.pl

features and changes the supposed characteristics of the previously compressed image, the steganalyst who examines the image to check for hidden data will be able to easily detect the presence of hidden information. Also the forgery of the previously compressed file can be detected by image features analysis.

1.1. Problem formulation

Because of problems which may occur while using a compressed image it is worth examining it for former compression. This is important especially when we do not know the file origin. Files downloaded from the Internet are very popular among users but they are often compressed. Even if the file is delivered to user in uncompressed form it could be converted from compressed format. This article discusses the problem of detection of prior JPEG compression. The following thesis was formulated: "It is possible, without a complex analysis, to detect if the analysed image was previously JPEG-compressed."

1.2. Background

The subject of prior image compression is widely discussed in the literature. This is important in steganography (Fridrich, 2005; Kodovsky & Fridrich, 2013; Lukáš & Fridrich, 2003; Pevny & Fridrich, 2008), image processing (Yang, Zhu & Huang, 2015) and forensics (Bianchi, Piva & Perez-Gonzalez, 2013; Fridrich, 2005; Piva, 2013; Popescu & Farid, 2005). In (Triantafyllidis, Tzovaras & Strintzis, 2002) a frequency-domain technique for image blocking artefact detection is proposed. The algorithm detects the image regions which contain visible blocking artefacts. The detection is done in the frequency domain. Blocking artefact inconsistencies are also used in (Ye, Sun & Chang, 2007) to detect digital forgeries of images. Authors of (Lin, Chang & Chen, 2011) propose the use of quantisation table estimation to measure the inconsistency among images to detect forgeries. The authors of (Liu & Bovik, 2002) propose a method of numerical assessment of the degree of artefact blocking in a visual signal. The method works in DCT domain. The steganalytic algorithm based on examining the compatibility of 8x8 pixel blocks with JPEG compression with a given quantisation matrix is presented in (Fridrich, Goljan & Du, 2001). In (Kodovsk`Y & Fridrich, 2013) the authors develop a JPEG-based steganalysis by examining the difference between an image with hidden data and an estimate of the cover image obtained by recompression with a JPEG quantisation table estimated from the stego image.

2. JPEG COMPRESSION

JPEG compression relies on the YCbCr colour model and discrete cosine transform (DCT). It contains the following stages (Przybyłowicz, 2008):

1. transformation to YCbCr colour model and resolution reduction,
2. image decomposition into blocks,
3. discrete cosine transform on each image block,
4. quantisation,
5. DCT matrix zigzag shift and Huffmann coding.

In the first stage RGB image representation is transformed into a YCbCr colour model. This means that each pixel will be described by three components: luminance (Y) and two chrominance components: anti-red (Cr) and anti-blue (Cb). Transformation from RGB model is done for each pixel separately according to Formula 1:

$$\begin{cases} Y = 0.299 * R + 0.587 * G + 0.114 * B \\ Cr = 128 - 0.168736 * R - 0.331264 * G + 0.53 * B \\ Cb = 128 + 0.5 * R - 0.4186688 * G - 0.081312 * B \end{cases} \quad (1)$$

where: R – value of red colour component,
G – value of green colour component,
B – value of blue colour component (Przybyłowicz, 2008).

After the transformation a vertical and horizontal resolution of chrominance components can be reduced because of lower human visual system (HVS) sensitivity to chrominance components than to luminance (Przybyłowicz, 2008).

An image prepared in this way is divided into blocks sized 8x8 pixels. Next, each block is independently processed with DCT and quantised. Quantisation is an operation during which each DCT coefficient is divided by a corresponding value taken from the predefined array Q. Each result is rounded to the closest integer. This operation allows for higher frequencies reduction. The human eye has a low sensitivity on quick luminance changes so higher frequencies can be reduced. At this stage the user can adjust the quality level (QL). The QL ranges from 1 to 100. Value 1 means the highest compression and the lowest quality. Value 100 means the best image quality and lowest compression level.

As a result of the reduction of the level of higher frequencies we obtain an array of coefficients, where some coefficients representing high frequencies are equal to zero. This array is changed into a vector by reading coefficients from the array in such a way as to place the low frequency coefficients at the beginning of the vector and the high frequency ones at the end of it.

Because of this at the end of the vector multiple zeros are placed. These zeros are replaced by the symbol EOB, which means that the rest of the vector is filled with zeros. This allows for image data size reduction. At the end the data are coded with Hufmann coding (Przybyłowicz, 2008). It is worth noticing that in the JPEG2000 compression format the cosine transform was replaced by a wavelet transform. Thanks to this a better compression can be obtained and an image transmitted through the Internet can be presented to the user in lower resolution before the whole image data are transferred. Today most of JPEG images are compressed in JPEG2000 format.

3. JPEG COMPRESSION DETECTION

Some images that can be download from the Internet look as if they are uncompressed. Unfortunately, there is a high chance that they were compressed earlier to store or transmit them effectively. Such images can be uncompressed before putting in the repository available for users. In the case of lossy compression the images keep the compressed format characteristics and some of their features. To prove this statement, a simple experiment was done. A raw picture (taken by Nikon D90, without any processing) was compressed and the differences between corresponding pixels in the original and the compressed file were calculated. In this way it was possible to determine how big the examined pixel's value change was. In this experiment a set of 10 different pictures were examined. Average values were calculated and presented in Figure 1. There we can see the results obtained after compression to JPEG format at various quality levels (25, 50 and 90). In the case of transforming raw image to JPEG a large number of pixels are changed. Only 20%–30% of pixels have the same value. The rest of them changes during compression. In Figure 1 only the value changes up to 22 were presented, but the biggest changes of pixel value are up to 50. Because of a small number of pixels having such a significant value change it was not possible to present them on the chart.

In the next step of the experiment the compressed image was uncompressed and saved in both bmp and png format. In this case the pixel value change was also examined according to the above-presented algorithm. In this experiment we found that all pixels had the same value after image format change. There were no pixels changing value. Changing format from JPEG to uncompressed form does not change pixel value – all the difference between the corresponding pixels is zero. This proves that no changes were introduced into the image during the examined process and all the characteristics and features of the compressed image are kept in its uncompressed form.

Each image has a set of various features that can be examined to check if the image was earlier compressed or not. It is not necessary to analyse all of them, only a selection of parameters, to detect if the image has any features that indicate prior compression. During the work over the problem in question various aspects were analysed, the final selection being:

- luminance and chrominance distribution,
- value differences between neighbouring pixels.

The presented research was prepared with a set of 280 images. Pictures were taken by Nikon D90 and written simultaneously in two formats: raw (NEF) and JPEG. The quality of JPEG files was various. As a result, two sets of images were collected. One set contained compressed files, the other uncompressed ones.

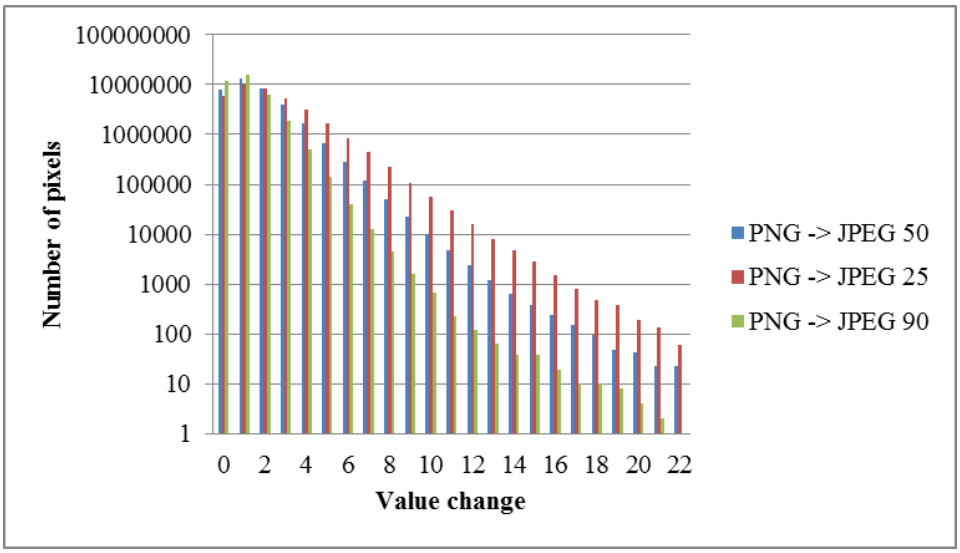

Fig. 1. Pixel value differences after image format change (own study)

3.1. Luminance and chrominance analysis

As mentioned in Section 2, during JPEG compression the colours are transformed to YCbCr model. The compression is done with the use of this colour model (Bianchi et al., 2013). This causes changes in the pixels value. To verify this the common histogram of luminance and chrominance components was prepared. The histogram obtained from the raw file is presented in Figure 2. Figure 3 presents the histogram obtained from the JPEG file.

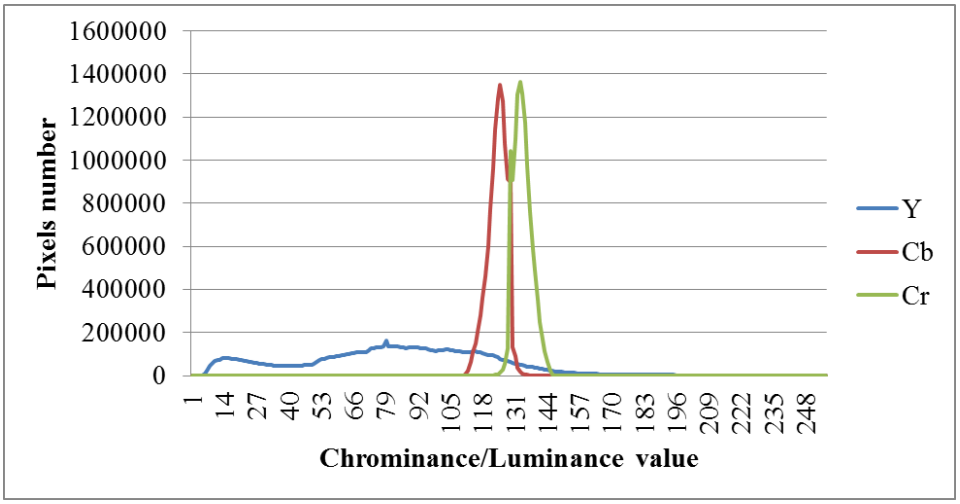

Fig. 2. Luminance and chrominance histogram for a raw image (own study)

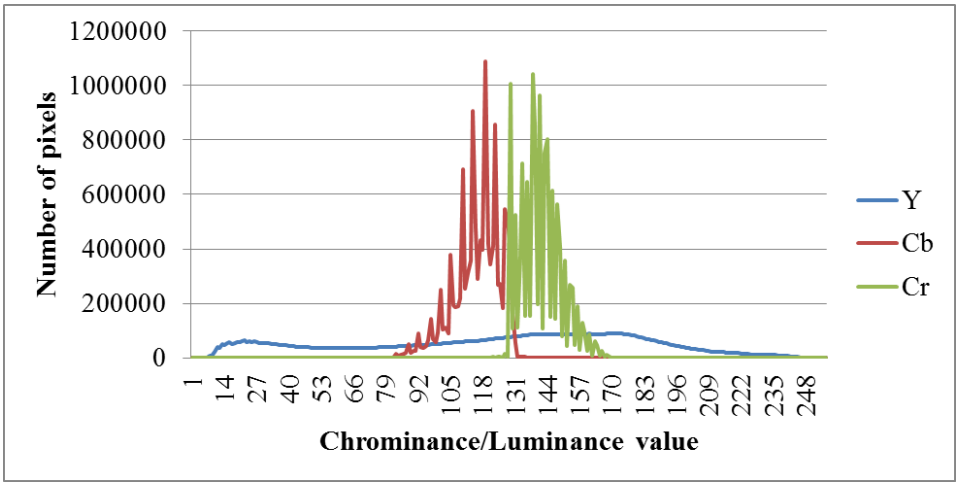

Fig. 3. Luminance and chrominance histogram for a JPEG image (own study)

Analysis of Figures 2 and 3 allows to notice a significant change of the chrominance components histogram. On the base of this change an attempt to create an image classifier was taken. The analysis of local maxima number in the luminance and chrominance components was done. The obtained results are presented in Figure 4.

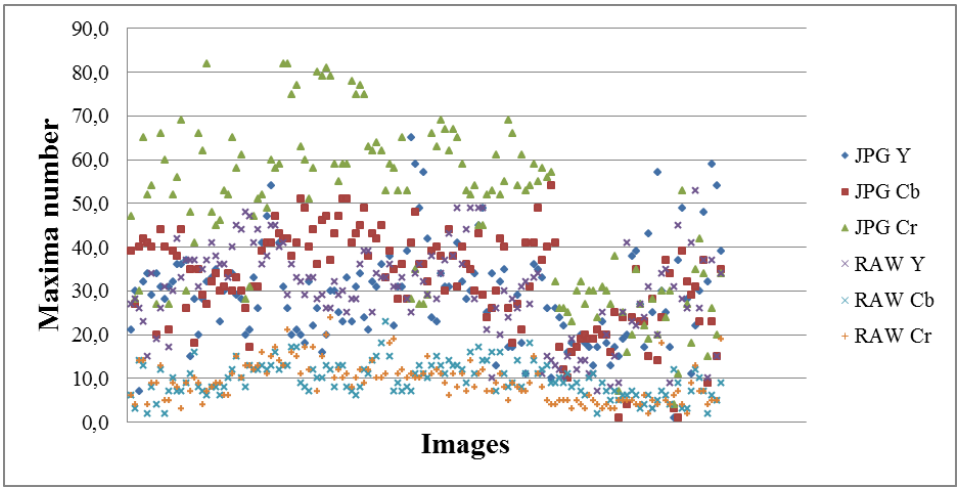

Fig. 4. Number of maxima in the luminance and chrominance histograms for JPEG and raw image (own study)

As we can see in Figure 4, there exists a significant difference between the number of chrominance maxima for JPEG and raw images. The number of maxima for JPEG images is higher. The numerical analysis of the obtained results was done as presented in Table 1.

Tab. 1. Numerical analysis of chrominance and luminance local maxima number (own study)

	JPEG			RAW		
	Y	Cb	Cr	Y	Cb	Cr
Biggest maxima number	65	54	82	53	23	24
Smallest maxima number	1	1	4	3	2	2
Biggest maxima number (VR=10%)	45	45	69	44	15	15
Smallest maxima number (VR=10%)	17	17	24	13	5	4
Biggest maxima number (VR=6%)	49	48	78	45	16	17
Smallest maxima number (VR=6%)	13	14	20	10	3	3

As can be seen, the number of maxima in chrominance histograms (Cb and Cr) should be bigger in the case of JPEG images. The biggest maxima number found in any image is presented in the first line of Table 1. Unfortunately, in some cases JPEG images have a small number of analysed maxima (the smallest numbers of maxima found in a JPEG image are presented in the second line of Table 2). The algorithm of finding a threshold for the Cr histogram is as follows:

1. count local maxima in the Cr histogram for JPEG images and put obtained values into table JPEG_Cr_max; sort the JPEG_Cr_max table in ascending order;
2. count local maxima in the Cr histogram for raw images and put obtained values into table RAW_Cr_max; sort the RAW_Cr_max table in descending order;
3. set the percent of values to remove VR=1%;
4. remove one percent of the first values from both tables;
5. check if the first value form the table RAW_Cr_max is smaller than the first value from the table JPEG_Cr_max; if yes, then return VR and first and last values from both tables; if not, then increase VR=VR+1% and go back to point 4.

According to the same algorithm the Cb histogram maxima were processed independently. The obtained results are presented in the last four rows of Table 1. These results show that for the component Cb the threshold should be set to 16 maxima (compare blue-marked cells). Each image having more maxima will be classified as JPEG-compressed. The accuracy of this classifier, according to the present research, is 90%, because 10% of values are out of the determined set. More precise results can be obtained with Cr component analysis. Cells form Table 1 marked orange show that there is still a big gap between raw and JPEG maxima number. Two last lines in Table 1 show results obtained for the set where only 6% of extreme results were removed. Cells marked green show that the JPEG files from the analysed set have in each case more maxima than the raw files. In this case the Cr component threshold can be set to 18 maxima. Each image having more maxima will be recognised as JPEG. The examined accuracy of this classifier is 94%.

3.2. Neighbouring pixel values difference

JPEG compression processes image data in blocks sized 8x8 pixels. Each block is processed independently. It causes an additional interference on the blocks edges. In the case of strong compression blocks could be visible as small squares having a slightly different colour than the neighbouring blocks. It is caused by a bigger value difference between border pixels coming from different blocks. This difference was examined and compared with the value differences among the pixels coming from the whole picture. The value difference between neighbouring pixels was counted in the RGB colour model according to the following algorithm:

1. create table RES for results having size 3x256; each row will keep results for another colour (R, G and B); initialise table RES with zeros;
2. set the read pixel index (PixIndex) to first pixel;

3. read first pixel from the image (marked ORG) and pixel placed below it (marked NGB);
4. for each colour:
   - read first pixel from the image (marked ORG) and pixel placed below it (marked NGB),
   - count index= |ValORG-ValNGB|,
   - increment RES[colour][index] by one;
5. set the read PixIndex to next pixel;
6. if the PixIndex indicates pixel from the image and not form the last line then go to point 3 of this algorithm;
7. count the pixel number (PixNum) in the image but the last line;
8. divide all values in RES table by PixNum;
9. return to RES table.

For the pixels placed on block edges value differences were counted according to the same algorithm, but ORG pixels were taken from the 8th line and next every eighth line. The RES table contains information about the percent of neighbouring pixels that differ about a defined value, for example the first cell in the first row keeps what percent of neighbouring pixels do not differ, the second cell tells what percent of neighbouring pixels differs about one, and so one.

As can be noticed, the differences between pixels are examined only vertically. It is possible to check them in other directions but it is not necessary because of good results obtained with the present method. Figure 5 presents the results obtained for the raw file, Figure 6 the results obtained for the JPEG. Symbols R, G, B mark differences among neighbouring pixels in the whole image. Symbols R edge, G edge, B edge mark differences among neighbouring pixels placed on the block edges. Series R difference, G difference, B difference are used to show the value differences between values obtained for the whole image and for the edges. These values were counted according to the formula 2:

$$\begin{cases} R_{difference} = R - R_{edge} \\ G_{difference} = G - G_{edge} \\ B_{difference} = B - B_{edge} \end{cases} \tag{2}$$

It can be noticed that the value differences between pixels are similar in the raw file, in contrast to the JPEG file. There, because of compression, differences are noticeable. On the basis of these differences a classifier was defined according to Formula 3:

$$C = \sum_{c=0}^{2} \sum_{i=0}^{N-1} \left| RES[c,i] \right|, N = 0..255 \tag{3}$$

where: c – colour index in the RES table,
N – value difference between pixels.

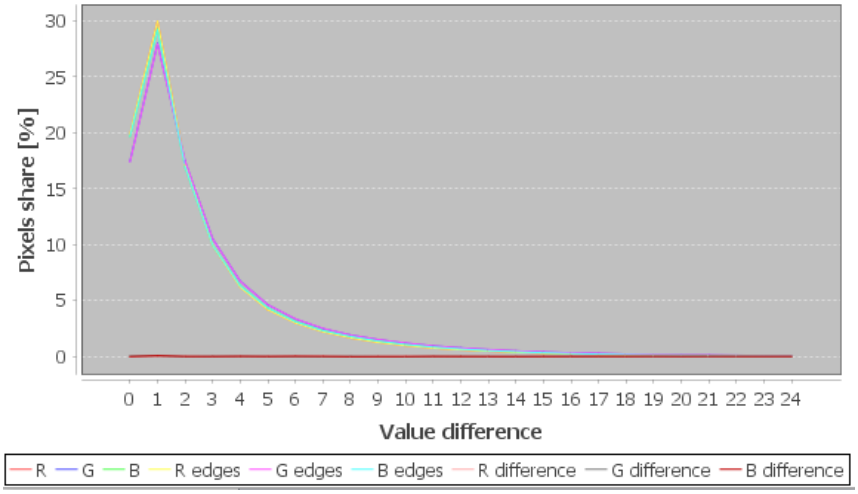

Fig. 5. Value differences between neighbouring pixels in a raw file (own study)

As can be seen in Figure 7, the classifier C has bigger values for JPEG images. The minimal classifier value found for the JPEG image is 5,01 whereas the biggest value found for the raw file is 1,77. The big gap between these results allows to define a treshold at the level of 3,38. Each image having a bigger value of the presented classifier will be recognised as JPEG-compressed. During tests all files were classified correctly by this classifier, so its acuracy is 100%.

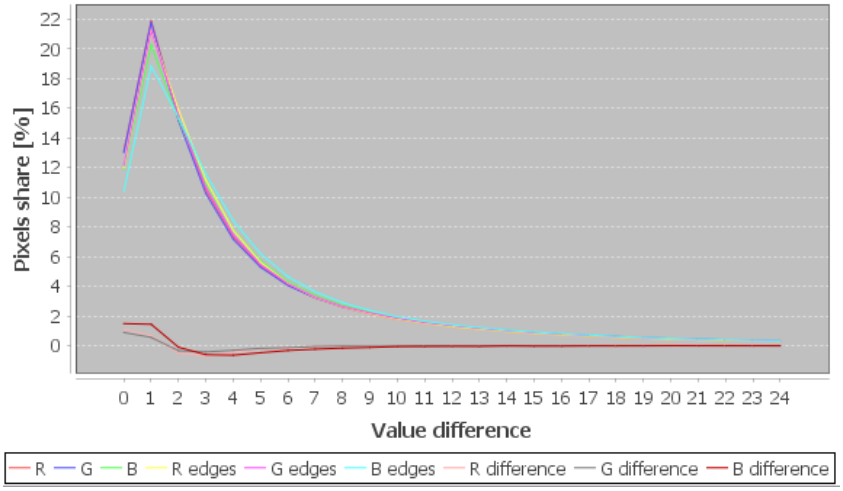

Fig. 6. Value differences between neighbouring pixels in a JPEG file (own study)

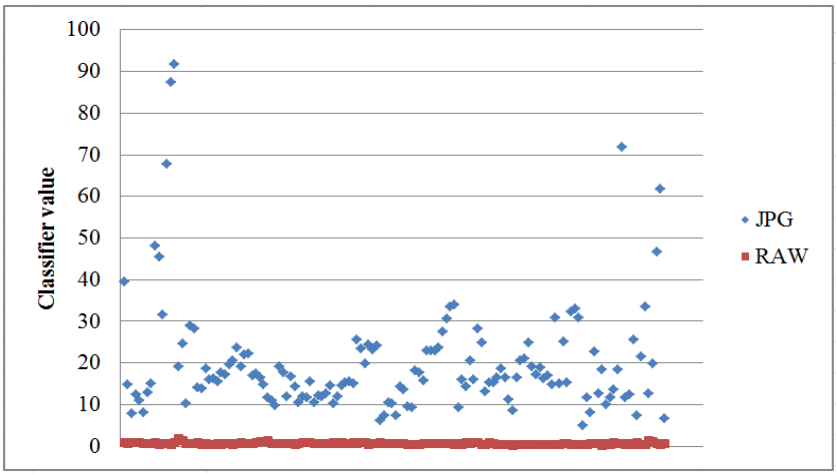

Fig. 7. Classifier values for JPEG and raw files (own study)

5. CONCLUSIONS

It is possible to efficiently detect prior JPEG compression with high accuracy. The methods presented recognise characteristic features introduced to the image during JPEG compression. The present article does not exhaust the topic. Future research will focus on frequency analysis and an attempt to build further classifiers will be made. The topic of prior compression detection is important in steganography, because previously compressed image usage will weaken the security of the applied protection. The prior potential container analysis allows for obtaining better results in steganography and ensures a higher level of hidden information security.

REFERENCES

Bianchi, T., Piva, A., & Perez-Gonzalez, F. (2013). Near optimal detection of quantized signals and application to JPEG forensics. *IEEE International Workshop on Information Forensics and Security (WIFS)*, 168-173. doi: 10.1109/WIFS.2013.6707813

Fridrich, J. (2005). Feature-based steganalysis for JPEG images and its implications for future design of steganographic schemes. *Information Hiding. 6th International Workshop, 3200*, 67-81. doi: 10.1007/978-3-540-30114-1_6

Fridrich, J., Goljan, M., & Du, R. (2001). Steganalysis based on JPEG compatibility. In A. G. Tescher, B. Vasudev, & V. M. Bove (Eds.), *Multimedia Systems and Applications Iv* (vol. 4518, pp. 275-280). doi:10.1117/12.448213

Kodovsky, J., & Fridrich, J. (2013). JPEG-Compatibility Steganalysis Using Block-Histogram of Recompression Artifacts. *Information Hiding. 14th International Conference, 7692*, 78-93. doi: 10.1007/978-3-642-36373-3_6

Lin, G. S., Chang, M. K., & Chen, Y. L. (2011). A Passive-Blind Forgery Detection Scheme Based on Content-Adaptive Quantization Table Estimation. *IEEE Transactions on Circuits and Systems for Video Technology*, *21*(4), 421-434. doi:10.1109/tcsvt.2011.2125370

Liu, S. Z., & Bovik, A. C. (2002). Efficient DCT-Domain blind measurement and reduction of blocking artifacts. *IEEE Transactions on Circuits and Systems for Video Technology*, *12*(12), 1139-1149. doi:10.1109/tcsvt.2002.806819

Lukáš, J., & Fridrich, J. (2003). Estimation of primary quantization matrix in double com-pressed JPEG images. *Proc. Digital Forensic Research Workshop, 2*, 5-8.

Pevny, T., & Fridrich, J. (2008). Detection of double-compression in JPEG images for applications in steganography. *IEEE Transactions on Information Forensics and Security, 3*(2), 247-258.

Piva, A. (2013). An overview on image forensics. *ISRN Signal Process, 2013*, Article ID 496701, 22 pages. doi:10.1155/2013/496701

Popescu, A.C., & Farid, H. (2005). Statistical tools for digital forensics. *Information Hiding. 6th International Workshop, 3200,* 128-147. doi:10.1007/978-3-540-30114-1_10

Przybyłowicz, P. (2008). Matematyczne podstawy kompresji JPEG. *Centrum Modelowania Matematycznego Sigma*

Triantafyllidis, G. A., Tzovaras, D., & Strintzis, M. G. (2002). Blocking artifact detection and reduction in compressed data. *IEEE Transactions on Circuits and Systems for Video Technology, 12*(10), 877-890. doi:10.1109/tcsvt.2002.804880

Yang, J. Q., Zhu, G. P., Huang, J. W., & Zhao, X. (2015). Estimating JPEG compression history of bitmaps based on factor histogram. *Digital Signal Processing, 41,* 90-97. doi:10.1016/j.dsp.2015.03.014

Ye, S., Sun, Q., & Chang, E. C. (2007). Detecting digital image forgeries by measuring inconsistencies of blocking artifact. *IEEE International Conference on Multimedia and Expo*, 12-15. doi: 10.1109/ICME.2007.4284574

Applied Computer Science, vol. 12, no. 3, pp. 29–36

Submitted: 2016-08-24
Revised: 2016-09-16
Accepted: 2016-09-21

direct metal laser sintering, 3Dprinting, 17-4PH stainless steel

Mariusz WALCZAK[*], *Daniel GĄSKA*[**], *Mirosław GUZIK*[***]

CHARACTERISTICS OF PRODUCTS MADE OF 17-4PH STEEL BY MEANS OF 3D PRINTING METHOD

Abstract

The article presents the results of tests of 17-4PH steel fabricated by means of the method consisting in laser additive manufacturing (LAM) – direct metal laser sintering (DMLS). This grade of steel is characterized by excellent stress corrosion resistance in the first place and is applied as construction material in chemical, aircraft, medical or mould making industry. 3D metal printing is a relatively new method enabling significant change of structural properties of these materials at printing parameters predetermined by printers manufacturer for "offline" printing mode. In order to achieve this goal, the authors have carried out the analysis of chemical composition, SEM tests and the tests of products surface roughness. Furthermore the products have been subjected to X-ray analysis by means of computed tomography (X-ray CT). Structural discontinuities have been found in upper layer and inside printouts subjected to tests.

1. INTRODUCTION

Additive manufacturing technologies called RapidPrototyping techniques occurred about 30 years ago. Initially, they were applied in aircraft and automotive industry where there is a need to apply metal elements characterized by complex shapes and high precision of inner structure. Additive manufacturing

[*] Department of Materials Engineering, Faculty of Mechanical Engineering,
Lublin University of Technology, Nadbystrzycka St. 36, 20-618 Lublin, Poland, m.walczak@pollub.pl

[**] Institute of Technological Systems of Information, Faculty of Mechanical Engineering,
Lublin University of Technology, Nadbystrzycka St. 36, 20-618 Lublin, Poland, d.gaska@pollub.pl

[***] Faculty of Transport and Computer Science, University of Economics and Innovation
in Lublin (WSEI), Projektowa 4, 20-209 Lublin, Poland

method of metal products fabrication by means of laser has been invented by Ciraud in the year 1971 (Borsuk-Nastaj & Młynarski, 2012; Mazzoli, Moriconi & Pauri, 2007).

This technology was based on direct fabrication of successive layers of 3D structures previously designed in computer aided design process. These structures can be tested and modified before engineering design works. The assumptions of this technology proposed by Ciraud have been applied till nowadays, and the process has been developed in the form of 3D printing technology thanks to modern CAD design technologies and laser technology.

Additive manufacturing methods are used for sintering of wide spectrum of metallic powders e.g. light alloys, titanium alloys, steel alloys and Co and Cr superalloys as well as polymer materials (e.g. polyamide) or ceramic and composite materials. This technology enables the fabrication of single elements or small series of elements in accordance with individual market demands, ensuring the forming of cavities, undercuts and inner channels which could be difficult or even impossible by means of conventional methods (Atzeni et al., 2016; Dobrzański & Matula, 2012; Pal, Tiyyagura, Drstvenšek & Kumar, 2016).

The latest technology used for making of complex shapes by means of metallic powders selective melting method consists in DLMS process (Direct Metal Laser Sintering). Thanks to DMLS technology, it is possible to obtain repeatable strength parameters of elements being fabricated. The essence of DMLS technology is the making of complex shapes which could be impossible even by means of casting methods and using difficult-to –cut materials.

The functioning principle of DMLS machines (Fig. 1) consists on application of a layer of precisely composed metallic powder by means of a blade on a working platform and then in selective sintering of successive layers of element being fabricated by means of near infrared laser beam (wave length of about 1064nm).

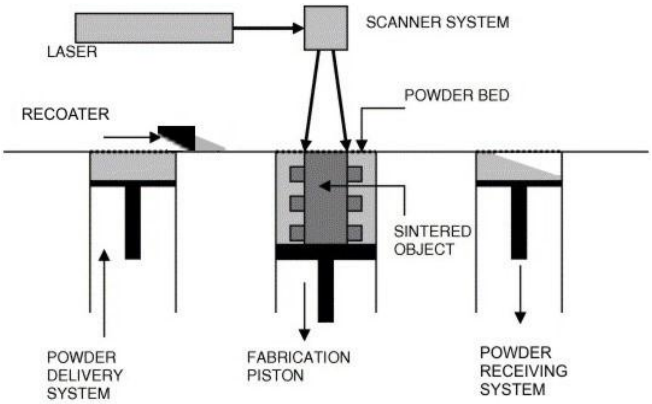

Fig. 1. Direct metal laser sintering apparatus (own study based on (Mazzoli, Moriconi & Pauri, 2007))

The whole process is carried out in protective atmosphere – most frequently in nitrogen or argon presence depending on reactivity of applied alloy. For example, aluminium and titanium alloys are processed in argon atmosphere and tool steels characterized by lower reactivity as well as Co and Cr superalloys are processed in nitrogen atmosphere.

2. RESEARCH METHODOLOGY

EOS StainlessSteel GP1 powder was the subject of tests. Composition of this powder is similar to US classification 17-4 PHand European 1.4542 stainless steel materials. This type of steel is widely applied in engineering applications requiring high strength and good plastic properties as well as wear and corrosion resistance e.g. in chemical, aircraft, medical or mould making industry. Circular specimens 6 mm thick with diameter Ø 30 mm were used for tests. The specimens have been fabricated in laser additive manufacturing (LAM) process by means of 3D printer for metals – EOSINT M280 supplied by EOS. The following parameters have been used in course of printing: laser power of 200W, layerthickness of 0.02 mmand laser spot size of 0.1 mm.

Chemical composition analysis has been carried out by means of Magellan Q8 emission spark spectrometer (Bruker, Germany). The tests were carried out on Fe130 detail testing channel used to complete 5 analyses (sparkings) for each specimen. The purpose of tests was to verify chemical composition with a confrontation with data declared by the manufacturer in technological sheets.

The surface of materials being tested has been subjected to analysis by means of PhenomProX scanning microscope (supplied by Phenom-World B.V.) and by means of Dektak 150 contact profile meter supplied by VeecoInstruments. Measuring needle radius was equal to 2 μm and load to 3 mg.

Additionally, the specimens have been subjected to X-ray analysis by means of computed tomography (X-ray CT) in order to check whether there are any structural discontinuities in the products made in LAM process. Therefore, SkyScan1272 computed tomography equipment (Bruker, Belgium) with XIMEA xiRAY11 camera and software package: Nrecon 1.6.10.1, CTVox 2.1.0 r741 and DataViewer 1.4.2 enabling the analysis of obtained images has been used for tests. The most important parameters which have been used for tests are: camera resolution of 1.6 μm, detector pixel number of 2688x4032, source voltage of 100kV, current of 100 μA, exposure time of 5300ms, rotation angle of 0.15°, average number of photos per rotation is equal to 6; the thickness of applied copper filter is equal to 0.11mm.

3. RESULTS AND DISCUSSION

The results of chemical composition analysis are presented in Tab. 1. The manufacturer – EOS company, does not indicate accurate information on carbon concentration percentage in furnished data except of maximum content. Measured average concentration is included in the scope declared by the manufacturer. In case of nickel, the concentration was slightly exceeded. Remaining elements contained in GP1 steel under analysis meet the requirements for 17-4PH steel. High content of Cu additive additionally increases stress corrosion resistance. In accordance with data (Thijs, Kempen, Kruth & Van Humbeeck, 2013), corrosion resistance of 17-4 PH is similar to this parameter of 18Cr-8Ni steel.

Tab. 1. Chemical composition of the tested GP1 (17-4 PH) stainless steel (masses %) (own study)

	C	Si	Mn	Cr	Mo	Ni	Cu	Nb	Fe
Tested 17-4 PH	0.044	0.717	0.686	15.9	0.118	5.272	4.806	0.274	71.84
SD	0.001	0,008	0.016	0.045	0.002	0.057	0.054	0.001	0.098
Manufac-tures	< 0.07	< 1	< 1	15–17.5	< 0.5	3-5	3-5	0.15–0.45	bal.

Direct metal laser sintering DMLS consists in laser beam scanning on the surface of thin layer of powder deposited on substrate (base plate). The laser beam is directed to the layer of powder distributed on the base plate. Then the laser is used to successively scan the first layer applied by scraper onto previously melted layer which becomes the substrate for the next layer (Yadroitsev, Krakhmalev & Yadroitsava, 2015; Lin et al., 2012). This process takes place in accordance with laser beam scanning direction (Fig. 2). After scanning, substrate is lowered and a new layer is deposited maintaining the powder surface in laser beam focusing plane. The process is repeated until the entire object is fabricated. A laser meltedtrack is created as a result of melted material surface tension. Laser beam penetration into substrate or into previously sintered layer causes an additional stabilizing effect for continuous creation of tracks (Yadroitsev, Gusarov, Yadroitsava & Smurov, 2010) but excessive depth of key hole penetration is not permitted in DMLS mode because such phenomenon can generate pores in the final 3D object as a result of weld pool collapse or gas bubbles in material (*Steelinox BV*,2016). Moreover, greater depth of laser beam penetration (melting depth) i.e. much greater than the thickness of sintered layer is also not useful for energy reasons (Yadroitsev et al., 2015).

SEM analysis of the surface after laser sintering (Fig. 2) indicated defects in the form of structural discontinuities in the area of weld face. Such phenomenon can be undesirable because the structural discontinuities in upper layer can play the role of micro-notches and, as a result of stresses concentration, these areas can jeopardize the reliability of the object being printed.

Surface roughness analysis (Fig. 3) indicates that elements printed at pre-determined parameters are characterized by significant surface area (Sa = 6.05 µm, Sq=7.56 µm, St=55.76 µm).

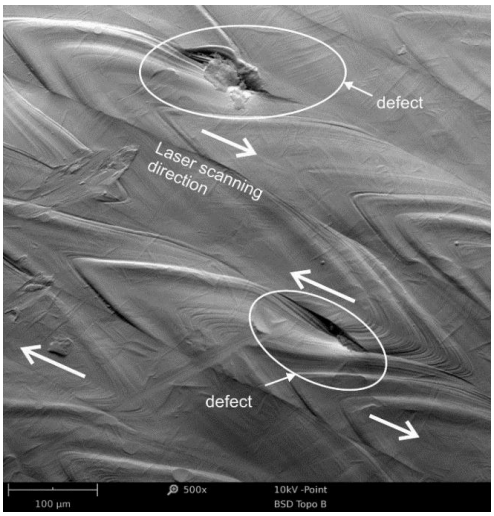

Fig. 2. SEM microphotographs of the tracks surfaces from 17-4 PH powder (own study)

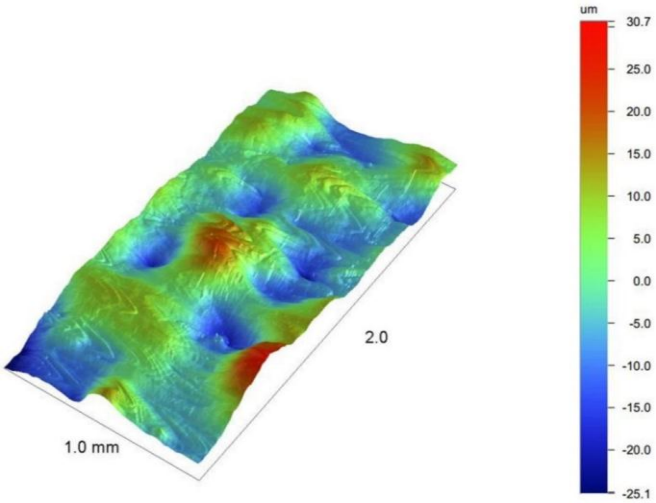

Fig. 3. 3. Dimension of surface roughness in 17-4 PH stainless steel (own study)

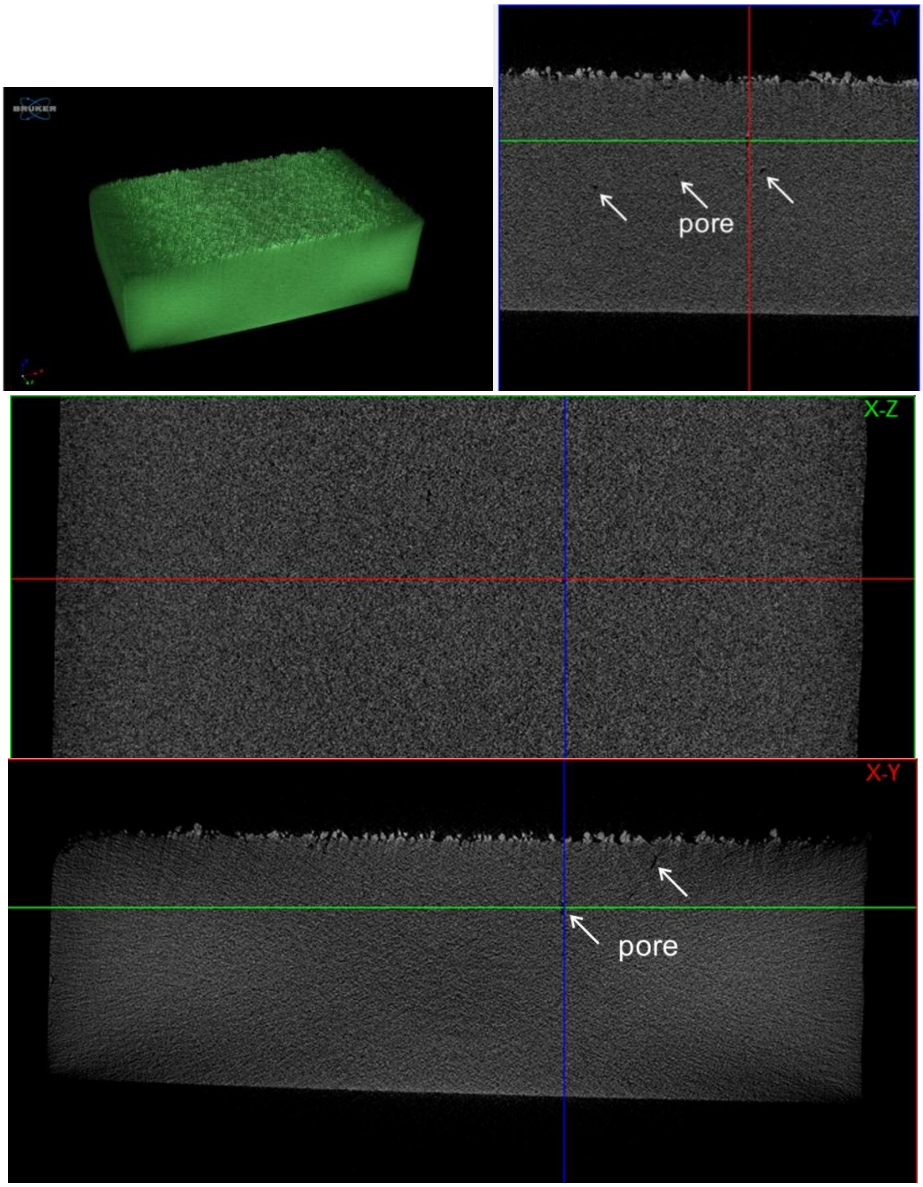

Fig. 4. Visualization of 3D specimen made of 17-4 PH and its cross-section in XYZ planes (camera resolution of 1.6µm) (own study)

Furthermore, the analysis of cross-sections carried out by means of X-ray computed micro-tomography disclosed a discontinuity on XY and ZY planes (Fig.4) in the form of pores exceeding the size of 5 µm. This is a particularly worrying phenomenon in the context of products made of 17-4PH steel applied in aircraft industry.

4. CONCLUSIONS

Thanks to the use of advanced additive techniques, it is possible to fabricate the products which could be difficult to fabricate by means of conventional methods i.e. casting or machining. Furthermore, these techniques make it possible to build complex cooling channels following the contour of an element in injection moulds inserts. Described technique makes it possible to design complex geometries with lattices structures in order to unload the components in aircraft and aerospace industry.

Optimization is required for selection of parameters for elements fabrication by means of direct metal laser sintering DMLS methods. Printouts of elements made of 17-4PH steel using a priori process parameters in "offline" mode in case of highly loaded products can be unsatisfactory because, as confirmed by X-ray analysis, they create the possibility of pores generation in material structure. Furthermore, the surfaces of the products fabricated by means of this method are characterized by significant surface area and accumulation of structural discontinuities is possible in upper layer; their effect can be compared to the effect of micro-notches. Therefore upper layer of such product should be additionally subjected to finishing (grinding or sandblasting). Chemical composition of printed products does not significantly differ from the powder composition declared by the manufacturer.

REFERENCES

Atzeni, E., Barletta, M., Calignano, F., Iuliano, L., Rubino, G., & Tagliaferri, V. (2016). Abrasive Fluidized Bed (AFB) finishing of AlSi10Mg substrates manufactured by Direct Metal Laser Sintering (DMLS). *Additive Manufacturing, 10*, 15-23. doi:http://dx.doi.org/10.1016/j.addma.2016.01.005

Borsuk-Nastaj, B., Młynarski, M. (2012). Selective laser melting (SLM) technique in fixed prosthetic restorations. *Protetyka Stomatologiczna, LXII*(3), 203-210.

Dobrzański, L.A., Matula, G. (2012). *Podstawy metalurgii proszków i materiały spiekane* (vol.8), Gliwice: Open Access Library.

Lin, X., Cao, Y., Wu, X., Yang, H., Chen, J., & Huang, W. (2012). Microstructure and mechanical properties of laser forming repaired 17-4PH stainless steel. *Materials Science and Engineering: A, 553*, 80-88. doi:http://dx.doi.org/10.1016/j.msea.2012.05.095

Mazzoli, A., Moriconi, G., & Pauri, M. G. (2007). Characterization of an aluminum-filled polyamide powder for applications in selective laser sintering. *Materials & Design*, 28(3), 993-1000. doi:http://dx.doi.org/10.1016/j.matdes.2005.11.021

Pal, S., Tiyyagura, H. R., Drstvenšek, I., & Kumar, C. S. (2016). The Effect of Post-processing and Machining Process Parameters on Properties of Stainless Steel PH1 Product Produced by Direct Metal Laser Sintering. *Procedia Engineering, 149*, 359-365. doi:http://dx.doi.org/10.1016/j.proeng.2016.06.679

Steelinox BV. (n.d.). Retrieved March 10, 2016, from Steelinox BV Company website, http://www.steelinox.nl/nl

Thijs, L., Kempen, K., Kruth, J.-P., & Van Humbeeck, J. (2013). Fine-structured aluminium products with controllable texture by selective laser melting of pre-alloyed AlSi10Mg powder. *Acta Materialia, 61*(5), 1809-1819. doi:http://dx.doi.org/10.1016/j.actamat.2012.11.052

Yadroitsev, I., Gusarov, A., Yadroitsava, I., & Smurov, I. (2010). Single track formation in selective laser melting of metal powders. *Journal of Materials Processing Technology, 210*(12), 1624-1631. doi:http://dx.doi.org/10.1016/j.jmatprotec.2010.05.010

Yadroitsev, I., Krakhmalev, P., & Yadroitsava, I. (2015). Hierarchical design principles of selective laser melting for high quality metallic objects. *Additive Manufacturing, 7*, 45-56. doi:http://dx.doi.org/10.1016/j.addma.2014.12.007

Applied Computer Science, vol. 12, no. 3, pp. 37–46

Submitted: 2016-09-12
Revised: 2016-09-20
Accepted: 2016-09-24

fog computing, industry 4.0, cloud computing

Jakub PIZOŃ[*], *Jerzy LIPSKI*[**]

PERSPECTIVES FOR FOG COMPUTING IN MANUFACTURING

Abstract

This article discusses ongoing efforts to enable the fog computing vision in manufacturing. As a new paradigm of computing implementation of fog computing faces many challenges that open perspective of new applications within a field of manufacturing. It is expected that fog computing will be one of factors that will accelerate development of in forth industrial revolution. In this article we discuss the perspectives of manufacturing companies surrounded by new solutions of CPS, CPPS and CM in relation to fog computing.

1. INTRODUCTION

The rapid development of technology, related to the progressive integration of systems and incredible growth of mobile devices number that sends and receives data, further extending quantity of solutions that implements Internet of things (IoT) and cyber-physical systems (CPS) paradigms, increase demand for computation recourses.

Cloud computing (CC) paradigm is in many cases the answer to this extensive need to process and analysis rising data volume. CC mainly provides scalable computation resources to meet customer computing power needs in service model “pay-as-you-go” which means that the fee is charged only for what is used. Computation resources are provided from the level of data centers located globally, depending on capabilities of data centers provider.

[*] Lublin University of Technology, Department of Enterprise Organization, Nadbystrzycka 38, 20-618 Lublin, Poland, +48 81 538 44 80, jakub.pizon@pollub.edu.pl

[**] Lublin University of Technology, Department of Enterprise Organization, Nadbystrzycka 38, 20-618 Lublin, Poland, +48 81 538 44 80, j.lipski@pollub.pl

CC provides a fully functional virtual environment setup that meets performance requirements. Moreover, this setup is available immediately for a price much lower than investment in raw infrastructure that is purchase of new equipment, implementation, configuration and maintenance only to obtain a new computation power.

However, a problem arises when the power of the cloud becomes unavailable or unusable due to the network unavailability, overfull bandwidth transmission or delays associated with data transmission.

These problems may appear due to the fact that a given geographical area is not available to broadband network. Control solution implement in the cloud requires huge data stream from sensors to take action in real case scenario like Smart Connected Vehicle (SCV), autonomous cars, smart cities, industrial automation and Industrial Internet of things (IIoT).

The conclusion that comes from above is that IoT like solutions force us to adopt "system view", rather than an "individual view" of the endpoints (Bonomi, Milito, Natarajan & Zhu, 2014).

There is, for these reasons, a need for looking for some architecture framework that will support future solutions. Attractive option is Fog Computing paradigm which is presented in this article. It is considering the perspectives of implementing a framework inside requirements and characteristics of modern manufacturing.

2. FOG COMPUTING

Fog Computing is a highly virtualized platform that provides compute, storage, and networking services between end devices and traditional Cloud Computing Data Centers, typically, but not exclusively located at the edge of network. Fig.1 presents the idealized information and computing architecture supporting the future IoT applications, and illustrates the role of Fog Computing (Bonomi, Milito, Zhu & Addepalli, 2012).

Gartner Inc. forecasts that 6.4 billion connected things will be in use worldwide in 2016, up 30 percent from 2015, and will reach 20.8 billion by 2020. In 2016, 5.5 million new things will get connected every day (Van der Meulen, 2015).

With regard to this challenging increase in the volume of data generated from millions of new connected devices in terms of smart connected vehicles, autonomous cars, smart cities and industrial Internet of things systems it no longer makes sense to ship all of this data to the Cloud for processing and storage.

In such cases, it begins to be important what is sent and processed in the cloud. Question arises whether the data sent to the cloud is relevant and consistent with the established objectives and the interests of implemented system? What if some part of the data will be processed at the network edge and only critical data will be pushed to cloud? This is where fog computing is proposed.

Keeping the data at the edge of the network, where the connected devices are creating the data offers the possibility to create new and innovative services and process efficiencies not possible with Cloud computing alone.

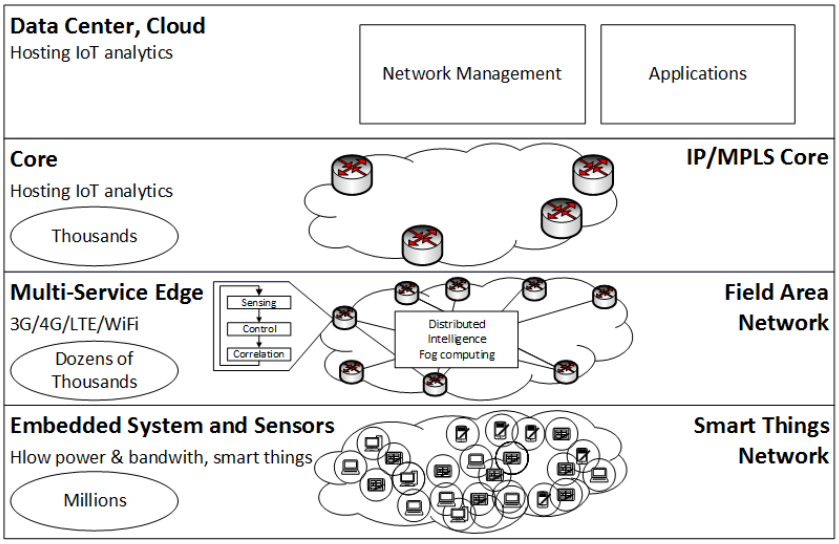

Fig. 1. The Internet of Things architecture and Fog Computing (Van der Meulen, 2015)

Smart solutions will make use of "horizontal" Machine-to-machine (M2M) connectivity in the same way traditional M2M systems typically rely on "vertical" Machine-to-Cloud (M2C) communication only (*Vortex Fog*, 2016). That is presented on Fig. 2.

The idea of implementing fog computing is proposed to deal with problem of data geo-distribution and data flow. Growing volume of raw and processed data cause the need to differentiation among data in the way that accurate data of interest will be directed to right place.

In this situation the fog collectors at the edge ingest the data generated by grid sensors and devices. Some of this data relates to protection and control loops that require real-time processing (from milliseconds to sub seconds).

This first tier of the Fog, designed for machine-to-machine (M2M) interaction, collects, process the data, and issues control commands to the actuators. It also filters the data to be consumed locally, and sends the rest to the higher tiers.

The second and third tier deal with visualization and reporting (human-to-machine [HMI] interactions), as well as with systems and processes (M2M). The time scales of these interactions, all part of the Fog, range from seconds to minutes (real-time analytics), and even days (transactional analytics). As a result of this the Fog must support several types of storage, from ephemeral at the lowest tier to semi-permanent at the highest tier. It also mention that the higher the tier, the wider the geographical coverage, and the longer the time scale.

The ultimate, global coverage is provided by the Cloud, which is used as repository for data that has a permanence of months and years, and which is the bases for business intelligence analytics. This is the typical HMI environment of reports and dashboards presenting key performance indicators (Bonomi et al., 2014).

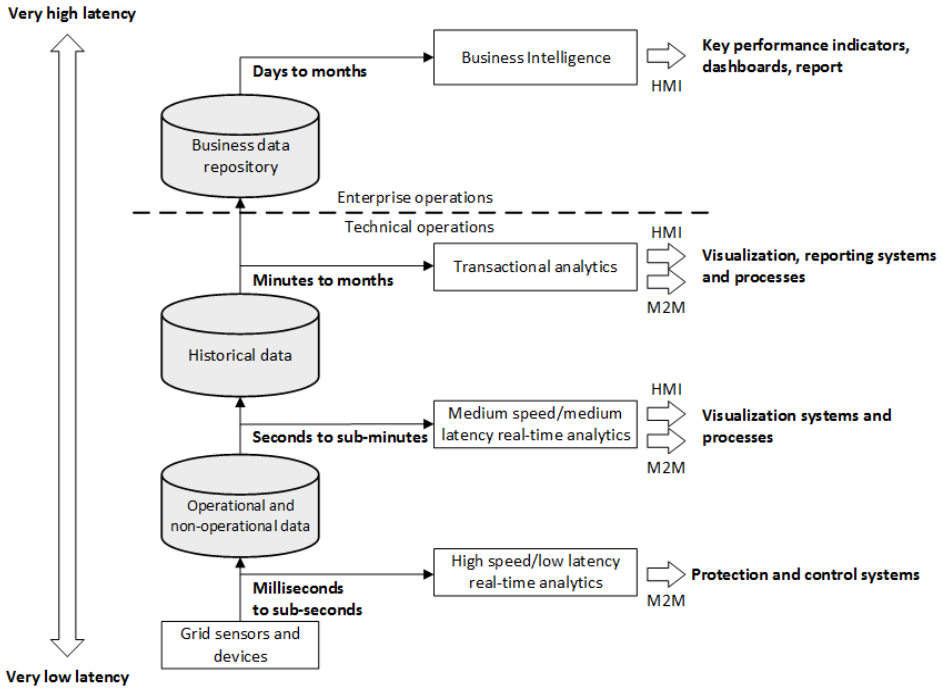

Fig. 2. Data flow in fog computing (Bonomi et al., 2014)

While the fog nodes provide localization, therefore enabling low latency and context awareness, the cloud provides global centralization that opens perspective to new innovative solutions.

The idea is not to replace the existing Cloud architectures but to enhance a system by ensuring that critical data that is available to the places where it can add most value. A Fog computing architecture can help to assure the required determinism and efficiency 'at the edge' by reducing latency and by improving Quality-of-Service (QoS) leading to improved services and a better user experience (*Vortex Fog*, 2016).

In other words, Fog complements of the Cloud, do not substitute it. For the large class of Cloud intended applications the economy of the scale (OPEX, pay as you go model) cannot be beaten. Binding these considerations it is obvious that CC model is critical for new application architectures. On the other hand, fog questions the model's universal application as a platform in relation to emergent IoT applications demand (Bonomi et al., 2014).

3. MODERN MANUFACTURING

Modern shape of manufacturing systems has been formed by successive industrial revolutions (Fig.3). Nowadays manufacturing is affected by many factors related to materials, methods, standards or even political and economic aspects. It is noticeable that growing role of integrated manufacturing information systems support manufacturing processes. Integrated manufacturing systems are organized systems in a way of interrelated production factors supported with the use of integrators (mostly computer systems). The integrators are used for the optimization of production and the products quality, tailored to market requirements and implemented with suitable use of productive resources. The integration made in order to achieve greater added value and to avoid a customer expectation mismatch is determined primarily by complexity of the modern manufacturing processes and products (Szczubełek, 2014).

These days' modern manufacturing support systems development is focused on the implementation of the latest information technology solutions related to leading trends in field of communication, data processing and mobility. These trends are:

- Internet of things – paradigm implying cyber-physical systems development, which are the basis for the development of ideas like Industrie 4.0 (Germany) and Smart Manufacturing (USA)
- Cloud computing paradigm that enables the development of solutions which provide remote access to computing power
- Big Data – methods used to analyze large sets of structured or not structured data.
- Mobility, unmanned and remote operations contribute to the development of automated control. No operators mean lower costs and possibility to fully monitor and interact with the process from anywhere at any time. That gives you the opportunity to control production in the enterprises scale or even globally (Harjunkoski, 2015).

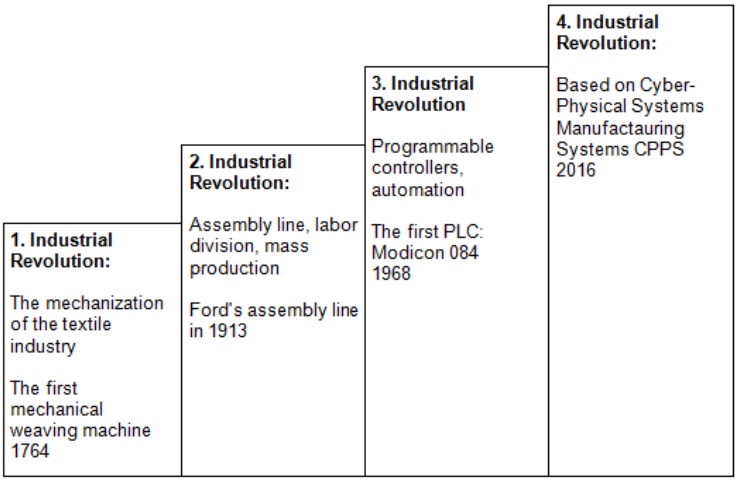

Fig. 3. Industry revolutions (Monostori, 2014)

3.1. Industry 4.0

Industry 4.0 is a strategic initiative of the German government that was adopted as part of the "High-Tech Strategy 2020 Action Plan" in 2011 (Kagermann, Wahlster & Helbig, 2013). In Germany, a major debate on Industry 4.0 has started, which in the meantime has also spread to other countries, like the US or Korea. The idea behind this term is that, the first three industrial revolutions came about as a result of mechanization, electricity and IT. Now, the introduction of the IoT and CPS into the manufacturing environment is ushering in a 4th Industrial Revolution.

In Industry 4.0, field devices, machines, production modules and products are comprised as CPS that are autonomously exchange information, trigger actions and control each other independently. Factories are developing into intelligent environments in which the difference between the real and the digital world is becoming smaller. The strong bias of the electro-technical and hierarchical world of factory automation will transit to smart factory networks, that enable dynamic re-engineering processes and deliver the ability to respond flexibly to disruptions and failures (Weyer, Schmitt, Ohmer & Gorecky, 2015).

3.2. Cyber-physical production systems

Cyber-physical systems are commonly used in aerospace industry, defense industry, power industry, transportation industry (e.g. Intelligent vehicles), medical industry (e.g. Medical devices and systems) and housing (e.g. Intelligent houses).

In a traditional manufacturing environment, where robotic systems, process control and industrial automation are universal, CPS can support both vertical and horizontal integration of IT systems, which integrate entire supply chain, or even all branches of the industry.

This ability gives a broad perspective of solutions for production systems – two-dimensional integration, both vertical and horizontal. That is a key aspect and it gives a rise to a new paradigm of cyber-physical production systems (CPPS) (Yu, Xu & Lu, 2015).

CPPS are composed of autonomous components and subsystems which cooperate in a manner dependent on the situation in all stages of production. Starts from processes that are carried out by means of production devices and logistics network. CPPS systems open prospect for building applications in different areas. The implementation of CPPS systems is identified with manifestation of fourth industrial revolution.

4. PERSPECTIVES

Modern manufacturing environment is characterized by condensation of various devices. Using more advanced and integrated machinery means greater amount of the produced data. Moreover, with the IoT sensor model implemented, the IoT amount of data increases significantly up to terabytes a day. At this point, the control and the processing of the production data gains in importance. Especially where the decision has to be fast – almost instantaneous. Therefore control decisions should be taken as close to the process being monitored, the machines or the things. The decision record should be kept inside of the company network to minimize delay associated with data transfer and storage.

Many current studies address solution to this issue to manufacturing cloud paradigm corresponding with so-called DAMA concept that is design-anywhere and manufacture-anywhere. The implementation of this concept requires the ability to easily exchange data between design and manufacturing of multiple objects remote. DAMA assumptions help to create efficient connections between systems of production planning, resource management systems and customer relationship management. Therefore, the adaptation of this concept can be implemented through types of production based on technology of cloud computing or the cloud predefined production (Cieplak & Malec, 2012).

However, manufacturing cloud is cloud computing based solution so it inherits same limitations. That creates new perspective for application systems that implement fog computing. Nevertheless the perspective of fog computing in manufacturing depends on the answer to the question whether the application of fog computing meets requirements and needs of modern enterprises. The answer to this question will be made on the basis of the analysis of fog computing key possibilities in relation to identified needs of modern manufacturing enterprises.

Modern manufacturing information system that requires computation power can be characterized with a 5C functions, which consist of Connection (sensor and networks), Cloud (data on demand), Content (correlation and meaning), Community (sharing and social), and Customization (personalization and value).

With the advent of smart sensors such as RFID technologies, collecting data for the system has become a simple exercise, but the question remains whether these devices or data provide the right information for the right purpose at the right time. The data is not useful unless it is processed in a way that provides context and meaning that can be understood by the right personnel. Just connecting sensors to a machine or connecting a machine to another machine will not give users the insights needed to make better decisions. Therefore current manufacturing systems require deeper analysis of various data from the machines and the processes (Lee, Lapira, Bagheri & Kao, 2013). Continuous analyze should be implemented to identify many invisible issues and uncertainties in manufacturing that can exist both internal and external to the factory.

Examples of internal issues include degradation of the machine and the manufacturing processes and the occurrence of failure events without any recognizable symptoms (component level). Variation of cycle time due to the inconsistent operation, unplanned systems breakdown and the presence of scraps and rework disrupt normal production planning and scheduling (system or production process level).

Meanwhile, external uncertainties, typically stemming from product development all the way through the supply chain, can manifest as: (1) unreliable downstream capacity, (2) unpredictable variation of raw materials or parts in terms of delivery, quantity and quality, (3) market and customer demand fluctuation, and (4) incomplete product design due to the lack of accurate estimation of product state during production and usage, among others.

These invisible worries and uncertainties have adverse effects in manufacturing if there are no predictive analytics and control strategies implemented. New, smarter technologies are needed for uncertainty reduction to make manufacturing more transparent (Cieplak & Malec, 2012).

The basis for solution of these problems could be the implementation of the manufacturing information system that has algorithms to support fog data processing. In this way, it opens a lot of different perspectives.

One of the key perspectives that fog computing offers is implementation of solutions that require very low and predictable latency. Cloud technology frees users from many implementation details, including the precise knowledge of where the computation or storage takes place.

This opens door for implementation of CAx (computer aided systems) engineering software in „as a service” model. CAx is a group software that support engineers with tools that simplifies and enhances their work. CAx are mostly used to develop and evaluate models of objects, products. From the technical point of view CAx requires a lot computation power to be able to be build and operate on models.

When using the Fog computing, it should be possible to share the entire package of engineering software on „as a service” model within one license model. Such possibility will facilitate deployment of working environment, provision of common repository, data versioning, empower data exchange and security.

Another perspective that fog computing opens is the possibility to implement geo-distributed applications. Fog computing infrastructure allows access to the cloud and its computing everywhere and at the edge of the network. This makes a great perspective for solutions related to technical infrastructure monitoring which is associated with the data acquisition from groups of sensors deployed on major areas. This can be particularly helpful in mining industry, petro-chemical industry (pipeline), metallurgy industry and wherever manufacture technical infrastructure is dispersed within a given geographical area.

Next perspective s are fast mobile applications like smart connected vehicle or connected rail. The proximity of the close fog computing layer opens with prospect of cyber-physical systems implementation. In this case, the virtualization is all about reproduction of equipment and machinery control parameters in virtual reality. In this way it is possible to centrally manage distributed architecture and implementation of algorithms allowing for diagnosis, monitoring, prediction of usage parts and safety in case of hacker and terrorists attacks.

5. CONCLUSION

Fog computing is emerges as an attractive solution to the problem of data processing in the Internet of Things. It relies on devices on the edge of the network that have more processing power than the end devices and are nearer to these devices than the more powerful cloud resources, thus it is reducing latency for applications (Dastjerdi, Gupta, Calheiros, Ghosh & Buyya, 2016).

That is important because of a rich interplay between the edge and the core of the network point of view, because the data generated has different requirements and uses at different time scales (Bonomi et al., 2014).

From the manufacturing perspective fog computing, due to the wide range of applications, has a high prospect of development in the field of production support systems.

Nevertheless the use of this technology to solve issues connected with production tasks execution requires the implementation of special IT ecosystem to build dynamic systems of the production data transfer.

Fog computing opens possibility to implement dynamic monitoring, control and even enable prediction manufacturing.

It should be noted that in the case of the use of fog computing paradigm in the production field it might bring effects represented as selected inventory savings, shortening the manufacturing process, better utilization of machine time and decrease in the value of work in progress.

Discussed ongoing efforts in the academia and industry in pages of this article to enable the fog computing vision still face many challenges with issues ranging from security to resource and energy usage minimization. Protocols and open architectures are also other topics for future research that will make fog computing more attractive for end users.

REFERENCES

Bonomi, F., Milito, R., Natarajan, P., & Zhu, J. (2014). Fog Computing: A Platform for Internet of Things and Analytics. In N. Besis & C. Dobre (Eds.), *Big Data and Internet of Things: A Roadmap for Smart Environments* (pp. 169-186). Cham: Springer International Publishing.

Bonomi, F., Milito, R., Zhu, J., & Addepalli S. (2012). Fog computing and its role in the internet of things. In M. Gerla & D. Huang (Eds.), *Proceedings of the first edition of the MCC workshop on Mobile cloud computing* (pp. 13-16). New York: ACM.

Cieplak. T., & Malec, M. (2012). Practical usage of cloud computing in computer integrated manufacturing. In J. Lipski, A. Świć & A. Bojanowska (Eds.), *New methods in intustrial engineering and production management* (pp. 7-18). Lublin: Politechnika Lubelska.

Dastjerdi, A. V., Gupta, H., Calheiros, R. N., Ghosh, S. K., & Buyya, R. (2016). Chapter 4 - Fog Computing: principles, architectures, and applications. In R. Buyya & A. V. Dastjerdi (Eds.), *Internet of Things. Principles and Paradigms* (pp. 61-75). Morgan Kaufmann.

Harjunkoski, I. (2015). Industrial perspectives on the deployment of scheduling solutions. *Computer Aided Chemical Engineering, 37*, 63-70.

Lee, J., Lapira, E., Bagheri, B., & Kao, H. (2013). Recent advances and trends in predictive manufacturing systems in big data environment. *Manufacturing Letters, 1*(1), 38-41. doi:http://dx.doi.org/10.1016/j.mfglet.2013.09.005

Monostori, L. (2014). Cyber-physical Production Systems: Roots, Expectations and R&D Challenges. *Procedia CIRP, 17*, 9-13. doi:http://dx.doi.org/10.1016/j.procir.2014.03.115

Szczubełek, G. (2014). *Zintegrowane systemy wytwarzania*. Olsztyn: Uniwersytet Warmińsko-Mazurski w Olsztynie.

Van der Meulen, R. (2015, November 10). Gartner Says 6.4 Billion Connected "Things" Will Be in Use in 2016, Up 30 Percent From 2015. *Gartner*. Retrieved from http://www.gartner.com/newsroom/id/3165317

Vortex Fog. (n.d.). from PrismTech's website, http://www.prismtech.com/vortex/vortex-fog

Weyer, S., Schmitt, M., Ohmer, M., & Gorecky, D. (2015). Towards Industry 4.0 - Standardization as the crucial challenge for highly modular, multi-vendor production systems. *IFAC-PapersOnLine, 48*(3), 579-584. doi:http://dx.doi.org/10.1016/j.ifacol.2015.06.143

Yu, C., Xu, X., & Lu, Y. (2015). Computer-Integrated Manufacturing, Cyber-Physical Systems and Cloud Manufacturing – Concepts and relationships. *Manufacturing Letters, 6*, 5-9. doi:http://dx.doi.org/10.1016/j.mfglet.2015.11.005

Applied Computer Science, vol. 12, no. 3, pp. 47–60

Submitted: 2016-08-24
Revised: 2016-09-12
Accepted: 2016-09-21

heat transfer through the walls, the thermal technical chambers, energy saving, temperature sinusoidal signals

Marian JANCZAREK[*], *Oleksij BULYANDRA*[**]

COMPUTER MODELLING OF ENERGY SAVING EFFECTS

Abstract

The paper presents the analysis of the dynamics of the heat transfer through the outer wall of the thermal technical spaces, taking into account the impact of the sinusoidal nature of the changes in atmospheric temperature. These temporal variations of the input on the outer surface of the chamber divider result at the output of the sinusoidal change on the inner wall of the room, but suitably suppressed and shifted in phase. Properly selected phase shift is clearly important for saving energy used for the operation associated with the maintenance of a specific regime of heat inside the thermal technical chamber support. Laboratory tests of the model and the actual object allowed for optimal design of the chamber due to the structure of the partition as well as due to the orientation of the geographical location of the chamber.

1. INTRODUCTION

Designing technical heat chamber, home or any building structure due to their thermal protection, it requires knowledge of the principles and processes described by physics building (Janczarek, 2007; Recknagel & Sprenger1976). Buildings in particular chamber should meet the technical requirements for saving energy required for their operation, while maintaining thermal comfort indoors (Janczarek, Bulyandra, Szapowalenko & Winogradov-Saltykov, 2007). Ignorance of thermal processes occurring in buildings and in particular, keeping the level of the coefficients of thermal conductivity through the wall, may lead to a waste of continuously soaring energy and thus to excessive air pollution.

[*] Institute of Technological Systems of Information, Faculty of Mechanical Engineering, Lublin University of Technology, Nadbystrzycka St. 36, 20-618 Lublin, Poland, m.janczarek@pollub.pl
[**] National University of Food Technologies, Volodymyrska St, 68, Kiev, Ukraina, 01033, phone: 00380442879453, info@nuft.edu.ua

The problem of saving energy in the twenty-first century becomes more important than in the seventies of the last century, when it first appeared the energy crisis associated with the armed conflict in the Middle East. This conflict continues until today varying degrees swollen and also relates to the control of any energy sources (Winogradov-Saltykov, Janczarek, Fiedorow & Kiepko, 2009).

2. DYNAMICS OF ATMOSPHERIC AIR TEMPERATURE AND ITS EFFECT ON THE ENERGY EFFICIENCY OF TECHNICAL CHAMBERS

In the analysis of mathematical-physical technical chambers were not taken into account the heat capacity external partition the design and construction thermal space building, but managed only strength of construction and in the case of wall insulation these outsider partitions (Janczarek & Świć, 2012). Skills of calculating the amount of exchanged heat and maintain the temperature of the medium is the paramount importance for the design and maintenance of proper use in the power of heat, refrigeration, food industry and in construction (Janczarek & Bulyandra, 2007; Janczarek, 2009a, 2009b).

The previously used method for designing the exterior shell of buildings shall take into account of the climatic conditions, unfortunately, only in a static way – the average air temperature in the region. However, as is common knowledge, atmospheric air temperature changes are inherently dynamics occurs in one component of the variable daily, decade, monthly or even yearly. The figures below are presented selected waveforms atmospheric temperature recorded in different seasons in the vicinity of Lublin and also in choosing towns in the world. In order to demonstrate the oscillating behavior in the form of sinusoidal variations measured and also the temperature profile at various time periods.

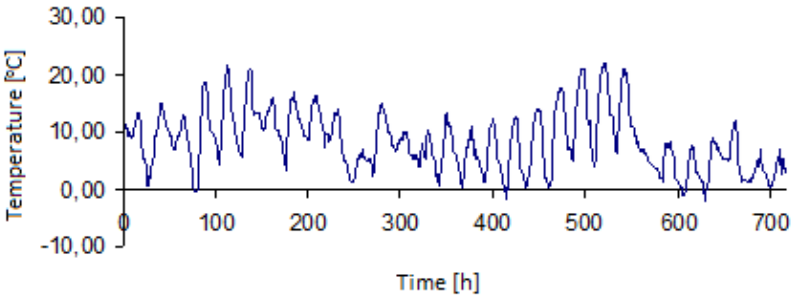

Fig. 1. Air temperature in Lublin, Poland area in the period of one month in the spring – autumn time (own study)

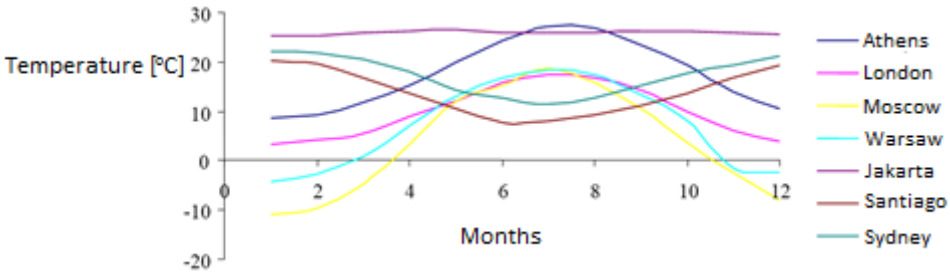

Fig. 2. Average air temperature for selected cities in the 12-month cycle (Recknagel & Sprenger, 1976)

3. MEASUREMENT POSITION FOR THE RESEARCHING COEFFICIENT OF HEAT TRANSFER IN MATERIALS DEPENDENCE OF THE COEFFICIENT OF HEAT TRANSFER

Parameter determining the thermal conductivity, thermal conductivity is λ [Wm^{-1} K^{-1}], which depends inter alia on bulk density and structure of the barrier material, the humidity and temperature (Janczarek, 2006). The heat conduction coefficient is information about a stream of energy that flows through the unit area of the material layer having a thickness of 1 m, the temperature difference on both sides of the layer equal to 1 K (1° C) (Carlslaw & Jaeger, 1959).

The higher the bulk density, the greater the ratio, and thus the material is inferior insulation. In addition, materials of the same chemical substances but different densities are different coefficients of thermal conductivity (Janczarek, 2013). The increase in temperature increases the thermal conductivity of materials. This is because it takes to increase the thermal conductivity of the solid and the air contained in the pores (Janczarek, Skalski & Suchorab, 2007). At the same time the pores of the heat transfer occurs by radiation. The practical application of this phenomenon is relevant only when the materials are used at high or low temperatures, e.g. hot tank insulation. The building envelope variations in temperature are relatively low, allowing you to skip the change in thermal conductivity. However, the value of λ should always be given the temperature at which it has been marked.

The phenomenon of thermal conduction through exterior walls of the rooms makes the largest part of the heat exchange chambers (Janczarek, Skalski, Bulyandra, & Sobczuk, 2006). It dominates in the total heat balance of buildings designed for either permanent residence in them and people as well as facilities where workers are being short-lived. Envelope of chamber fulfill the protective function not only in relation to the heat loss but also it can regulate the conditions of moisture and air in the rooms. External walls should allow a certain degree of penetration of air and water vapor while absorbing moisture.

As is well known, the physical construction materials are unfavorable for the user to change under the influence of moisture wall. Moisture adversely affects the quality of the insulation partition as well and its stability. The objective of effective protection of the building against moisture is to avoid the negative influence of her presence and the resulting defects or damages. The condition of living in the rooms of the building are comfortable microclimate dry bulkhead surrounding the room. Moist partitions much impossible to maintain comfort conditions, it is impossible, even with very intense heating. The protection against moisture is very significant as the flow of steam. Diffusion of water vapor through the building envelope is the process of aligning the partial pressure of water vapor between the two environments, which are separated by the partition. The flow of water vapor takes place from the environment of higher vapor concentration to an environment with a lower concentration, so that steam will always be diffused in this direction, where the air is dry. Material properties related to the diffusion of water vapor through the building materials characterized by the coefficient of steam-permeability δ [mg/mhPa]. It corresponds to the amount of water vapor in milligrams, which diffuses through 1 m^2 of the material layer having a thickness of 1 m for one hour and a differential pressure on both sides of the layer equal to 1 Pa. Similarly, as for the heat transfer through the outer shell of the building, the concept of diffusion resistance of any material layers: $d = Z/\delta$, here: d - thickness [m].Water trapped in the pores has a coefficient λ approx. 0.56 [$Wm^{-1} K^{-1}$] or about 20 times greater than the rate λ of air trapped in pores with a diameter of about 0.05 mm building material. The additional impact on thermal conductivity is the diffusion of water vapor which is connected to increased heat transfer and capillary movement of moisture. With an increase in the humidity of materials is an increase of thermal conductivity. And lowering the value of insulation by humidity due to the fact that in place of the air contained in the pores falls just water.

In aim of determined of coefficient of heat transfer of bricks in dependences upon of degree her moistures one chose method experimental. Research one passed on laboratory – position in Technical University of Lublin (Fig. 3 and 4) and referred of measurement of temperatures, thickness of streams warm and moistures relative bricks. As material to driven researches used brick full red both wet and then this oneself brick dried in stove. In time of a few days' measurements driven former at a help of computer registration of temperatures in four points on external surfaces examined bricks as also in two central points ininterior. Simultaneously driven former computer registration of moisture at help of two searchers of type WHT installed in center of brick. Values of thickness led of warm density became measured at help of electronic sensors of type PTP, which connected former to universal measure APPA.

Position laboratory – to qualifications of coefficient of heat flow in aspect different moistures of equipped brick was in two chambers. Different conditions thermal in chambers held former at help of aggregates cooling and of controlled warmers. Among chambers one installed investigative sample in typical form full red bricks placed tight to capacity in plate of polystyrene about thickness 20 cm. Polystyrene. Plate used former in aim of isolating of surface external bricks from influence undesirable temperatures. Surfaces external bricks surrendered became {remained} to activity from one side of chamber to temperature + 25° C and from second side of chamber to temperature + 1,5°C. Values these of temperatures registered former independently for every from six sensors, and then recorded on disc of computer at measuring – step carrying out 15 of minutes. Simultaneously with measurement of temperature registered former at help of programmed computer values of moisture of brick on two separate files. Obtained from measurements of value of temperatures, of streams and moistures became placed in computer programmer. At the help of suitable mathematical transformations coded values of temperatures and moistures exchanged on suitable individuals on degrees °C and on per cent definite values of relative moisture.

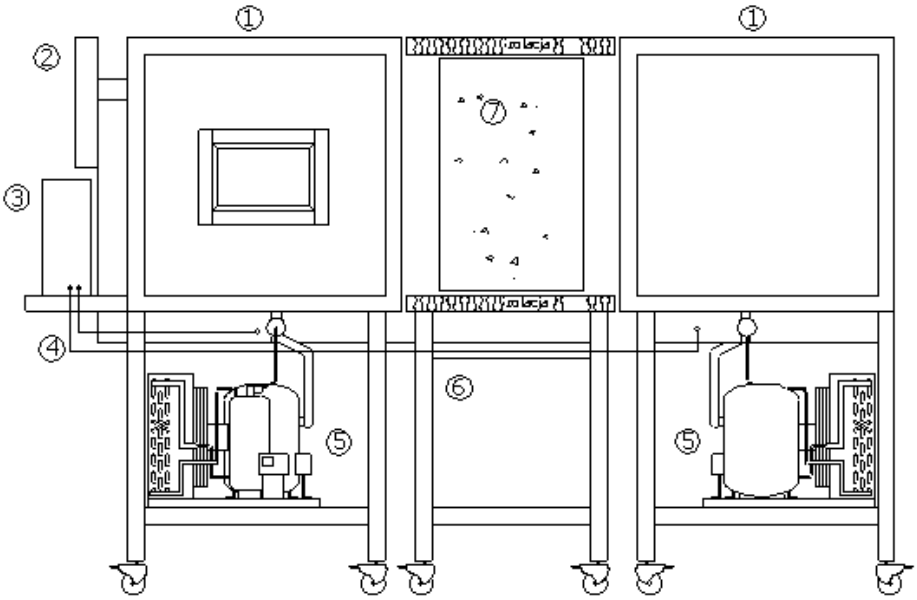

Fig. 3. Schema ideological positions laboratory – to measurement of coefficient of heat transfer (own study)

1. Chamber measuring – executed from aluminum profiles. Thickness of side 10 cm, with full mineral.
2. Display – LCD Samsung SyncMaster about diagonal 15".
3. Driver – computer PC class with operating – system UNIX.
4. Wires driver steering of generative of microclimate in chambers.
5. Laboratory set of Danfoss firm to generating conditions thermal prevalent inside of chambers. Range of temperatures from –40°C to +50°C.
6. Table made from aluminum – profiles with variable construction making possible securing and arrangement of prepared samples to investigations.
7. Primary standard sample of builder's material – full red bricks – placed in polystyrene plate.

Fig. 4. View general positions laboratory – measuring – chambers (own study)

Correlations among obtained values of coefficient of heat conduction permit on determination of characterizations of graphic coefficient for chance dry and wet bricks.

Obtained results of measurements permitted on qualification of dependence of coefficient of heat transfer from internal temperatures in full red brick wet and dry. Example- course of changes of value of coefficient of heat transfer. Simultaneously obtained results of value of coefficient of heat transfer permitted on determination of coefficient lambda. From represented below graphs results difference among courses for wet and dry bricks.

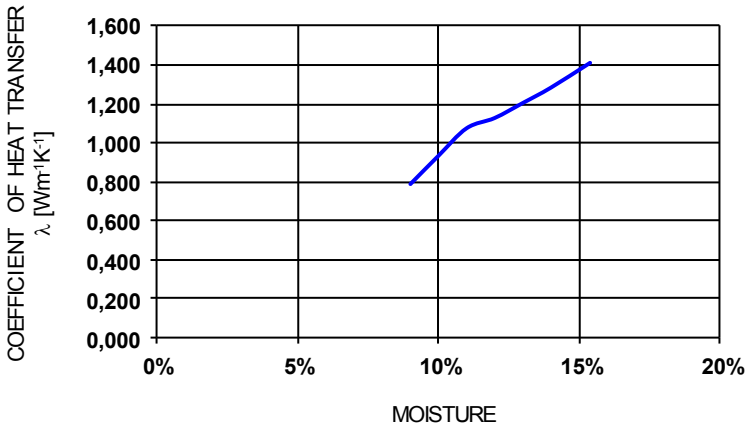

Fig. 5. Characterizations of changes of coefficient of heat transfer in wet full brick (own study)

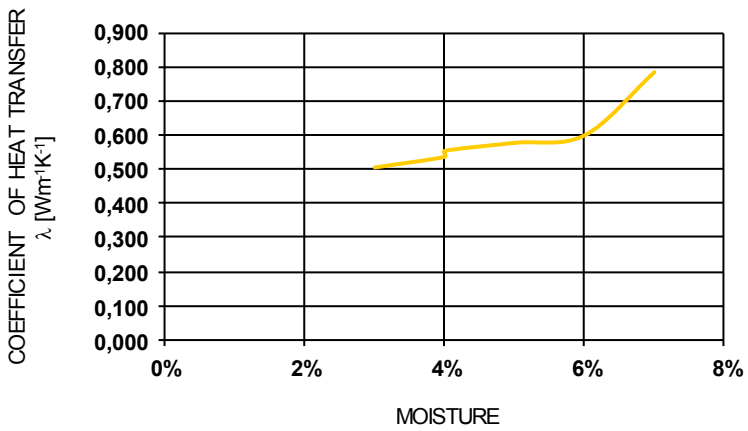

Fig. 6. Characterizations of changes of coefficient of heat transfer in dry full brick (own study)

In order to verify this phenomenon experiment was performed on a laboratory first for the wet material and then a similar experiment was repeated for the material directly taken out of the oven – drying, i.e. The brick dry (Fig. 6). External conditions of the experiment in both cases were the same. The temperature in the hot chamber was programmed at 25°C and the temperature in the cold compartment to the value +1.5°C. Measured temperatures on both surfaces

of brick, and inside it were recorded independently for each of the installed sensors, and then stored on your computer using a measuring step of 15 minutes. In parallel with the measurement temperature was also recorded by a computer program humidity bricks. Obtained from measurements of temperature, heat flux density and moisture content were used for calculations of energy in the heat balance for a variety of technical chambers.

4. MATHEMATICAL ANALYSIS OF THE IMPACT OF A SINUSOIDAL TEMPERATURE CHANGE

With the help of the mathematical-physical analysis as well as with the support of Modelica programmer, shows a simulation of actual conditions of the cooling chamber for example with below temperature regime.

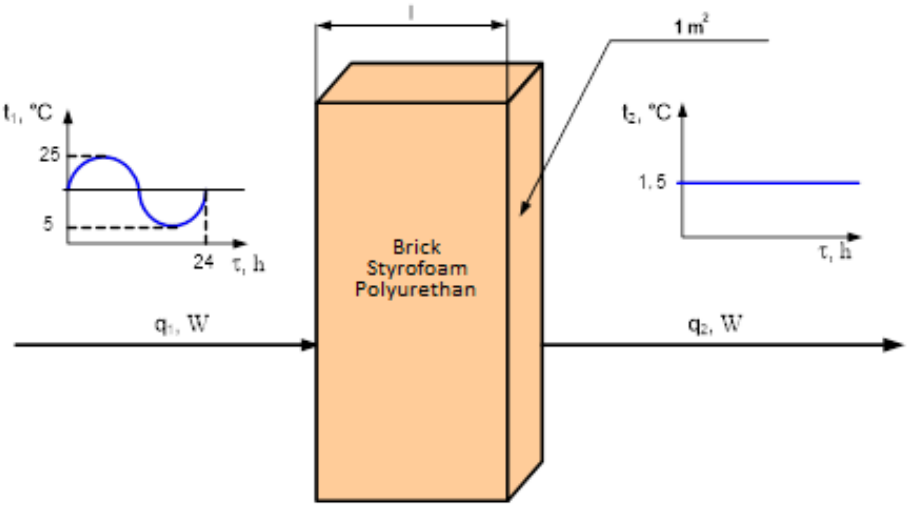

Fig. 7. Effect of the sinusoidal temperature change in order to achieve suppression of the indoor temperature (own study)

The analysis has been performed on the basis of original numerical algorithms. They take into consideration hourly changes of ambient temperature in the central – eastern region of Poland. The accepted methodology of performance takes advantage of temperature dynamics which is necessary to solve physical and mathematical problems related to heat transfer processes occurring in chambers.

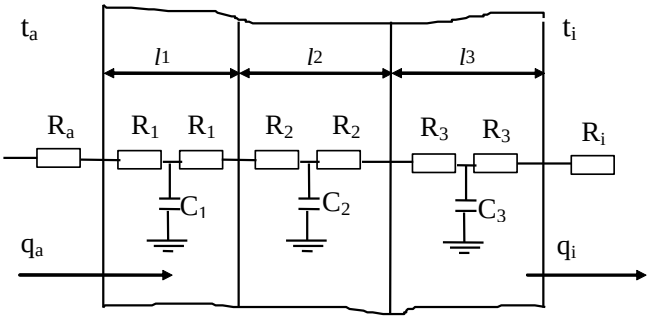

Fig. 8. Model of wall composed of three layers in electrical analogy (own study)

From it we can get matrix notation (eventually for n-layers of wall) and the final result of this calculation is a pair of linear relations between the temperature and fluxes at the two surfaces of the composite slabs (1).

$$[\Delta t_i(p), \Delta q_i(p)] = [\Delta t_a(p); \Delta q_a(p)] \begin{bmatrix} 1 & 0 \\ -R_1 & 1 \end{bmatrix} \begin{bmatrix} 1 & -pC_1 \\ 0 & 1 \end{bmatrix} \cdots \begin{bmatrix} 1 & -pC_n \\ 0 & 1 \end{bmatrix} \cdot \begin{bmatrix} 1 & 0 \\ -R_{n+1} & 1 \end{bmatrix} \quad (1)$$

The relation is precisely analogous to Ohm's law for the steady flow of electric current: the flux corresponds to the electric current and the drop of temperature to the drop of potential. Thus R may be called the thermal resistance of the slab (Fig. 8). Next suppose we have a composite wall composed of n slabs of different thickness and conductivities. If the slabs are in perfect thermal contact mat their surfaces of separation, the fall of temperature over the whole wall will be the sum of the falls over the component slabs and since the flux is the same at every point, this sum is evidently.

This is equivalent to the statement that the thermal resistance of a composite wall is the sum of the thermal resistance's of the separate layers, assuming perfect thermal contact between them. Finally, consider a composite wall as before, but with contact resistances between the layers such that the flux of heat between the surfaces of consecutive layers is H times the temperature difference between these surfaces. The differential equation to be solved is Fourier's equation. These models we can confront with computer program Modelica, which allow to construct the walls of technical chambers (Fig. 9). The diagram of the process of heat transfer through the wall under the program Modelica is shown below. By this modeling, we can simulate any temperature regime and heat flow both inside and outside of the chamber periodically temperature signal on the outside surface of the wall. In Fig.10 and 11 we can obtain suppressed the course of the internal temperature.

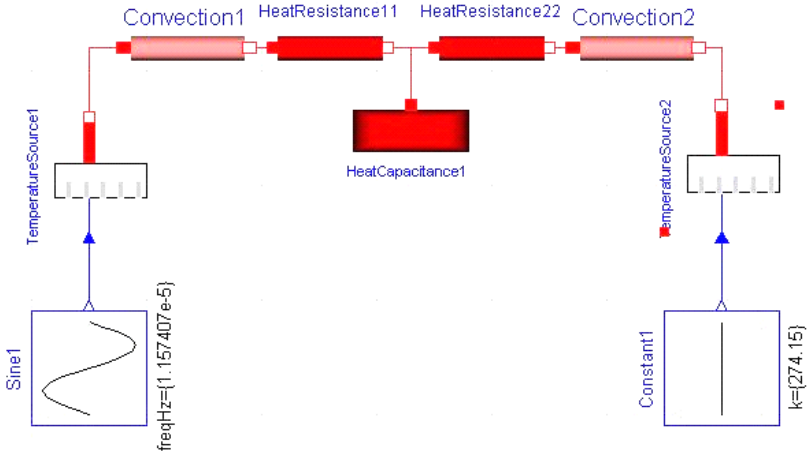

Fig. 9. Ideal model passage of heat through the baffle using an analogy to Ohm's law (own study)

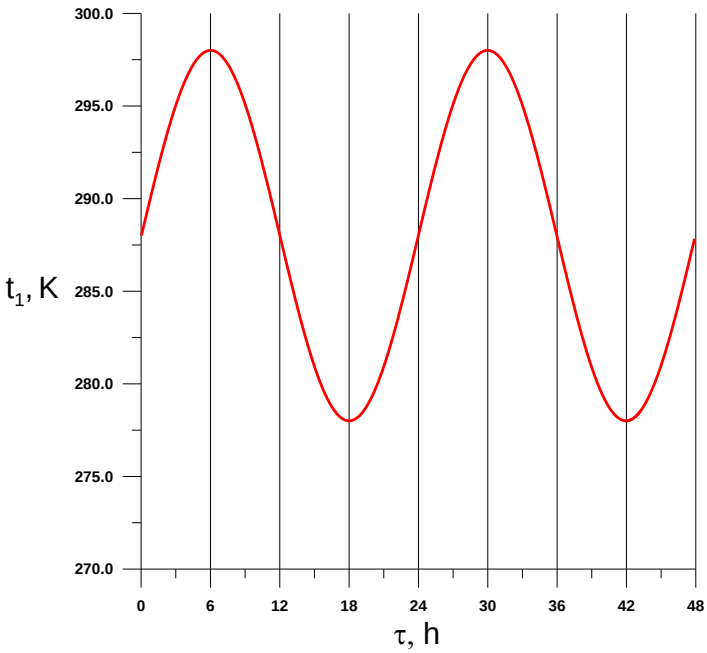

Fig. 10. Temperature t_1 plots obtained from simulations in the Modelica (own study)

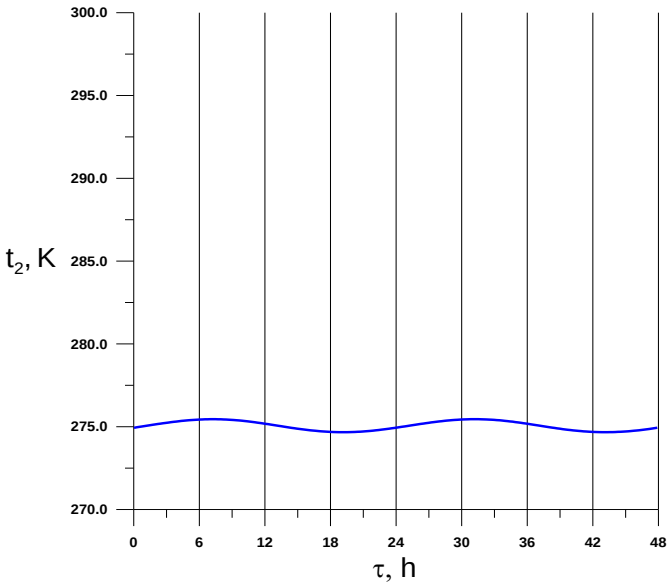

Fig. 11. Temperature t_2 plots obtained from simulations in the Modelica (own study)

Functions of the transition – the transfer – obtained on the basis of these relationships and describing the relationship between the output quantities and input will be helpful also in the design of the construction of exterior walls store-rooms. For the designer and constructor of thermal chambers technical model uses the analogy of electricity to thermal processes is the closest to real physical conditions among all ways of describing and calculating the flow of heat through the outer baffle buildings.

In practice, we can get confirmation of the considerations relating to the stability of heat buildings for example, existing to this day medieval buildings, eg. Churches, libraries and palaces in which there is no need to use air conditioners during the hot days of summer and winter respectively, high-power heating devices. Thus, today we can suitably so designed and constructed partition, which ensures the thermal inertia of the chamber, which would result in significant savings in the energy required to maintain a certain temperature inside a building structure. For example, the daily changes in atmospheric air temperature detrimental to the indoor climate is the effect of heat flow from the interior of space occurring after the 24-hour phase shift. In contrast, most preferred is a case in which the housing is owning outer baffle capable of producing 12-hour phase shift vector heat flux and result in suppression of the temperature change in the building. So in order to achieve measurable economic effects in the process of maintaining the desired temperature in the facility must be in the design of the exterior wall into account not only thermal resistance but also heat capacity of the partition. The product of the thermal resistance – as a function

of the thickness and thermal conductivity of the wall and the heat capacity of the barrier – as a function of the density and specific heat of the construction material which has a dimension of a unit of time is the time constant characterizing the object taken into consideration by inertia applied control and regulation systems.

The higher the bulk density, the greater the ratio, and thus the material is inferior insulation. In addition, materials of the same chemical substances but different densities are different coefficients of thermal conductivity. The increase in temperature increases the thermal conductivity of materials. This is because it takes to increase the thermal conductivity of the solid and the air contained in the pores. At the same time the pores of the heat transfer occurs by radiation. The practical application of this phenomenon is relevant only when the materials are used at high or low temperatures, it means for example hot tank insulation. The building envelope variations in temperature are relatively low, allowing you to skip the change in thermal conductivity. However, the value of λ should always be given the temperature at which it has been marked.

The phenomenon of thermal conduction through exterior walls of the rooms of the largest part of the heat exchange chambers. It dominates in the total heat balance of buildings designed for either permanent residence in them and people as well as facilities where workers are being short-lived. Envelope fulfill the protective function not only in relation to the heat loss but also regulate the conditions of moisture and air in the rooms. External walls should allow a certain degree of penetration of air and water vapor while absorbing moisture.

As is well known, the physical construction materials are unfavorable for the user to change under the influence of moisture wall. Moisture adversely affects the quality of the insulation partition as well and its stability. The objective of effective protection of the building against moisture to avoid the negative influence of her presence and the resulting defects or damages. The condition of living in the rooms of the building are comfortable microclimate dry bulkhead surrounding the room. Moist partitions much impossible to maintain comfort conditions, it is impossible, even with very intense heating. The protection against moisture is very significant as the flow of steam. Diffusion of water vapor through the building envelope is the process of aligning the partial pressure of water vapor between the two environments, which are separated by the partition. The flow of water vapor takes place from the environment of higher vapor concentration to an environment with a lower concentration, so that steam will always be diffused in this direction, where the air is dry. Material properties related to the diffusion of water vapor through the building materials characterized by the coefficient of steam-permeability [mg/(mhPa)]. It corresponds to the amount of water vapor in milligrams, which diffuses through 1 m^2 of the material layer having a thickness of 1 m for one hour and a differential pressure on both sides of the layer equal to 1 Pa. Similarly, as for the heat transfer through the outer shell of the building, the concept of diffusion resistance Z of any material layers.

Water trapped in the pores has a coefficientλ approx. 0.56 [Wm^{-1} K^{-1}] or about 20 times greater than the rate λ of air trapped in pores with a diameter of about 0.05 mm building material. The additional impact on thermal conductivity is the diffusion of water vapor which is connected to increased heat transfer and capillary movement of moisture. With an increase in the humidity of materials is an increase of thermal conductivity. And lowering the value of insulation by humidity due to the fact that in place of the air contained in the pores falls just water.This process does not proceed uniformly in a variety of materials depends on the structure and origin of the material, eg. In the concrete cell is assumed that the gain coefficient λ approx. 4.5% to 1% gain moisture.

5. CONCLUSIONS

The measurement results in the publication are test piece related to the heat flow through the baffle chamber and technical be made in various embodiments of both temperature and time as well as on the actual and model objects. With a variety of probes can be read temperatures and heat fluxes at various locations on the test material. On a laboratory can be simulated on both sides of the baffle different conditions of the course of the atmospheric temperature and the desired regime of heat inside the chamber. The results obtained for optimizing the design of baffles to give the storage chamber, therefore, notable economic impact.

REFERENCES

Carlslaw, H., & Jaeger, J. (1959). *Conduction of heat in solids*. Great Britain: Oxford University.

Janczarek, M., Skalski, P., & Suchorab, Z. (2007). Przewodzenie ciepła przez przegrodę w stanach ustalonych i nieustalonych. *Postępy Nauki i Techniki, 1*, 13-16.

Janczarek, M. (2006). Wyznaczanie bilansu cieplnego komór chłodniczych. In *XII Konferencja Naukowo-Techniczna Rynek Ciepła 2006 - Materiały i Studia*. Lublin: Kaprint.

Janczarek, M. M. (2007). Determining of coefficient of heat transfer in bricks depended from degree of their moisture. *CEEPUS WEB Summer School 2007 "Informatics Systems in Automation"*. Slovenia, Maribor: University of Maribor.

Janczarek, M. M. (2009a). Technological describtion of heat and mass transfer processes in thermal treatment of fruit storage chambers. *Engineering Mechanics 2009*. Czech Republic, Svratka.

Janczarek, M. M. (2009b). The analysis of wall temperatures in a fruit storage in the aspect of transient heat flow. *Engineering Mechanics 2009*. Czech Republic, Svratka.

Janczarek, M. M. (2013). Analiza matematyczno-fizyczna cieplnych komór technicznych. In M. Janczarek & J. Lipski (Eds.), *Technologie informacyjne w technice i kształceniu* (pp. 128-137). Lublin: Politechnika Lubelska.

Janczarek, M. M., & Świć, A. (2012). Scientific and technological description of heat and mass transfer processes in chambers. *Acta technical convinieties – Bulletin of Engineering, 10*, 55-60.

Janczarek, M. M., Bulyandra, O. F., Szapowalenko, O. I., & Winogradov-Saltykov, W. A. (2007). Osobiennosti rasczieta tiepłowowo balansa tiepłowych kamer chranienia fruktow. *Naukowi Praci, 31*(2). Ukraine, Odessa: Odesska nacionalna akademia charczowych technologii.

Janczarek, M., & Bulyandra, O. F. (2007). Zbierigannia fruktiw u gazowich serediwiszczach. *Harchowa Promislowist* (nr 5). Kyiv, Ukraine.

Janczarek, M., Skalski, P., Bulyandra, A., & Sobczuk, H. (2006). Przewodność cieplna zewnętrznych ścian budynków w aspekcie wilgotności i oszczędności energii. *Rynek Energii, 65*(4), 32-35.

Recknagel & Sprenger. (1976). *Ogrzewanie i klimatyzacja – poradnik.* Warszawa: Arkady.

Winogradov-Saltykov, W. A., Janczarek, M. M., Fiedorow, W. G., & Kiepko, O. I. (2009). Tiepłometriczeskije issliedowanie tiepłozaszczitnych swoistw ograżdienij. *Industrial Heat Engineering – International Scientific and Applied Journal, 31*(4), 116-123.

Applied Computer Science, vol. 12, no. 3, pp. 61–73

Submitted: 2016-06-25
Revised: 2016-08-29
Accepted: 2016-09-12

turning, shaft with low rigidity, modelling

Antoni ŚWIĆ[*], *Arkadiusz GOLA*[**], *Mikuláš HAJDUK*[***]

MODELLING OF CHARACTERISTICS OF TURNING OF SHAFTS WITH LOW RIGIDITY

Abstract

Numerical studies were conducted with the use of a computer program permitting the determination of the basic dynamic characteristics of the process of machining and the presentation of graphic characteristics of the numerical simulations performed. Analysis was performed of the relation of the output parameters of the dynamic system to the input parameters, relative stiffness coefficient B to feed rate and depth of machining, change of retardation and time constants to rotary speed and depth of machining, and of the frequency and time characteristics of models of the dynamic system of machining of shafts with low rigidity.

1. INTRODUCTION

The numerical studies of the machining process were performed in the program MATMOD. The program allows the determination of the basic dynamic characteristics of the machining process, numerical simulation of the dynamic system of the machining process, and graphic presentation of the characteristics of the numerical simulations performed (Abakumov, Taranenko & Zubrzycki, 2006).

[*] Institute of Technological Systems of Information, Lublin University of Technology, Nadbystrzycka Street 36, 20-618 Lublin, Poland, e-mail: a.swic@pollub.pl
[**] Department of Enterprise Organization, Lublin University of Technology, Nadbystrzycka Street 38, 20-618 Lublin, Poland, e-mail: a.gola@pollub.pl
[***] Technical University of Košice, Department of Production Systems and Robotics, Slovakia, e-mail: mikulas.hajduk@tuke.sk

Simulations were performed for shafts of steel C45, with dimensions of L_1=500 mm, d_1=20 mm and L_2=300 mm, d_2=10 mm. The variable input parameters were the rotation speed, feed, depth of machining, and the tool cutting edge angle. The machined part was fixed in a chuck and supported by the tailstock centre.

The following relations were analysed: of the output parameters of the dynamic system to the input parameters, of the relative stiffness coefficient *B* to feed rate and machining depth, of change of retardation and time constants to rotary speed and machining depth, as well as the frequency characteristics and the time characteristics of the dynamic system of machining of shafts with low rigidity.

The possibility was found of the approximation of the frequency and time characteristics within the range of actual frequencies of the dynamic system, and of the control system of the operator transmittances of typical dynamic elements: integrating element and aperiodic element of the second or first order. The gain factor and the time constants of the approximated models are subject to change, primarily with a change in the rotary speed of the machined part and in the relative dynamic stiffness coefficient *B*, characterising the ratio of stiffness of the elastic system of the machine tool and the gain factors of the machining process (Świć, 2009; Świć, Gola & Wołos, 2014). In the case of use of universal lathes for the machining of the shafts under analysis, with changing conditions and parameters of machining the model parameters can vary within a broad range (Gola, 2014; Świc & Mazurek, 2011).

Comparative analysis of the relative error in the determination of the time constants of the models indicates that the developed mathematic models of turning of shafts are adequate to the actual process.

2. NUMERICAL ANALYIS OF PARAMETERS OF MACHINED SHAFT WITH LOW RIDIGITY AND OF PARAMETERS OF ITS MACHINING

The simulations were performed for shafts of steel C45, with dimensions of L_1=500 mm, d_1=20 mm and L_2=300 mm, d_2=10 mm. The variable input parameters were the rotary speed n_p=100–2000 rev/min, feed f=0.1–0.8 mm/rev, machining depth a_p=0.5–3 mm, Δa_p=0.5 mm, and the tool cutting edge angle κ_r =45°, 90°. The machined part was fixed in a chuck and supported with the tailstock centre. The results of the simulations for the shafts under analysis and the effect of the input parameters of the dynamic system on the change in the values of the output parameters are presented in Tab. 1.

Tab. 1. Changes of output parameters of dynamic system with change of input parameters (own study)

	Cutting forces [N]	Amplifier gain f [N/mm]	Amplifier gain a_p [N/mm]	Coefficient B	Delay τ [s]	Response to unity pitch f [s]	The amplitude [dB]	The phase [rad/s]
Angle κ_r [°]	only to f_f	only m_x	only n_x	yes	no	slight	slight	slight
a_p [mm]	yes	yes	no	yes	no	yes	yes	yes
f [rpm]	yes	no	yes	yes	no	yes	slight	slight
n_p [rpm]	no	no	no	no	yes	yes	yes	yes

Changes of machining force components in the case of shaft with L=500 mm, d=20 mm, a_p=0.4 mm and a_p=2.5 mm are presented in Fig. 1 a) and 1 b).

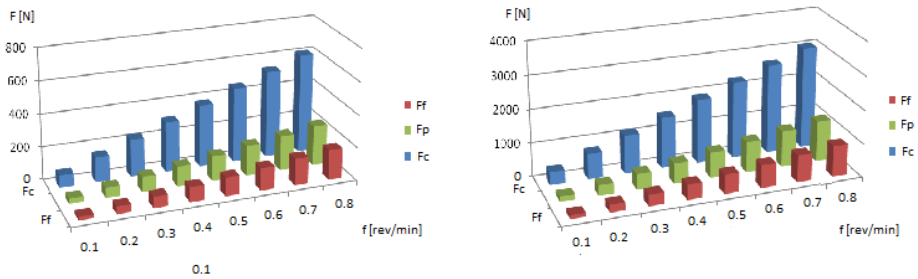

a) b)

Fig. 1. Changes of machining force components in the function of longitudinal feed rate at L=500 [mm], d = 20 [mm], tool cutting edge angle 45°, depth of machining 0.5 [mm] – a) and 2.5 [mm] – b), n_p=1000 [rev/min] (own study)

Analysing Fig. 1 one can conclude that with a change of machining parameters the machining force components change in a linear manner. Irrespective of the depth of machining and of the feed rate, component F_c assumes higher values, while components F_p and F_f – at tool cutting edge angle of 90° – are equal to each other.

We calculated the relative dynamic stiffness coefficient B. The results of the calculations at $\kappa_r = 45^\circ$ and $\kappa_r = 90^\circ$ are presented in Tab. 2 and 3.

Tab. 2. Change of relative stiffness coefficient *B* under the effect of feed rate and machining depth at *L* = 500 [mm], *d* = 20 [mm], rotary speed of machined part n_p=1000 [rev/min], tool cutting edge angle κ_r= 45° (own study)

		Relative stiffness coefficient B							
Depth of cut a_p [mm]	**0.1**	0.020	0.020	0.019	0.019	0.019	0.019	0.019	0.019
	0.2	0.039	0.039	0.039	0.039	0.038	0.038	0.038	0.038
	0.3	0.059	0.059	0.058	0.058	0.058	0.057	0.057	0.057
	0.4	**0.079**	**0.078**	**0.078**	**0.077**	**0.077**	**0.077**	**0.076**	**0.076**
	0.5	0.099	0.098	0.097	0.097	0.096	0.096	0.095	0.095
	0.6	0.118	0.118	0.117	0.116	0.115	0.115	0.114	0.113
	0.7	0.138	0.137	0.136	0.135	0.135	0.134	0.133	0.132
	0.8	0.158	0.157	0.156	0.155	0.154	0.153	0.152	0.151
	0.9	0.177	0.176	0.175	0.174	0.173	0.172	0.171	0.170
	1.0	0.197	0.196	0.195	0.194	0.192	0.191	0.190	0.189
	1.5	0.296	0.294	0.292	0.290	0.289	0.287	0.285	0.284
	2.0	0.394	0.392	0.389	0.387	0.385	0.383	0.380	0.378
	2.5	0.493	0.490	0.487	0.484	0.481	0.478	0.475	0.473
	3.0	0.591	0.588	0.584	0.581	0.577	0.574	0.570	0.567
		0.1	**0.2**	**0.3**	**0.4**	**0.5**	**0.6**	**0.7**	**0.8**

Tab. 3. Change of relative stiffness coefficient *B* under the effect of feed rate and machining depth at *L* = 500 [mm], *d* = 20 [mm], rotary speed of machined part n_p=1000 [rev/min], tool cutting edge angle κ_r= 90° (own study)

		Relative stiffness coefficient B							
Depth of cut a_p [mm]	**0.1**	0.018	0.018	0.018	0.018	0.018	0.018	0.018	0.017
	0.2	0.036	0.036	0.036	0.036	0.036	0.035	0.035	0.035
	0.3	0.055	0.054	0.054	0.054	0.053	0.053	0.053	0.052
	0.4	**0.073**	**0.072**	**0.072**	**0.071**	**0.071**	**0.071**	**0.070**	**0.070**
	0.5	0.091	0.090	0.090	0.089	0.089	0.088	0.088	0.087
	0.6	0.109	0.108	0.108	0.107	0.107	0.106	0.105	0.105
	0.7	0.127	0.127	0.126	0.125	0.124	0.124	0.123	0.122
	0.8	0.146	0.145	0.144	0.143	0.142	0.141	0.140	0.140
	0.9	0.164	0.163	0.162	0.161	0.160	0.159	0.158	0.157
	1.0	0.182	0.181	0.180	0.179	0.178	0.177	0.175	0.174
	1.5	0.273	0.271	0.270	0.268	0.266	0.265	0.263	0.262
	2.0	0.364	0.362	0.359	0.357	0.355	0.353	0.351	0.349
	2.5	0.455	0.452	0.449	0.447	0.444	0.441	0.439	0.436
	3.0	0.546	0.542	0.539	0.536	0.533	0.530	0.527	0.523
		0.1	**0.2**	**0.3**	**0.4**	**0.5**	**0.6**	**0.7**	**0.8**

Analysis of the results shows that the value of the relative stiffness coefficient *B* decreases slightly with increase of the tool cutting edge angle. The change in the value of coefficient *B* under the effect of change in the feed and the machining depth a_p (from 0.5 to 3 mm), and κ_r = 45° and 90° are presented in Fig. 2 and Fig. 3.

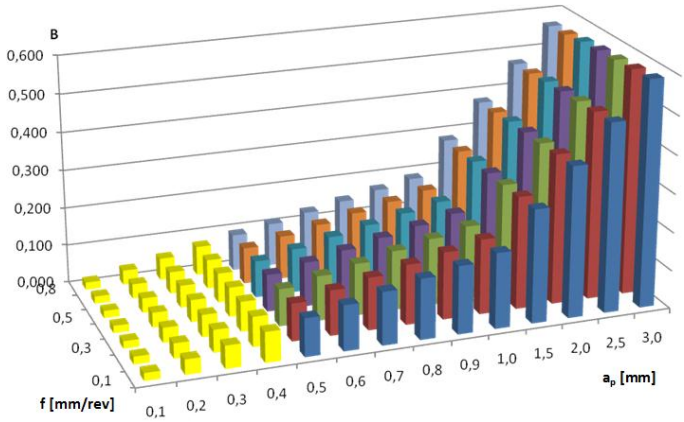

Fig. 2. Change of relative stiffness coefficient *B* under the effect of feed rate and machining depth at *L* = 500 [mm], *d* = 20 [mm], rotary speed of machined part n_p=1000 [rev/min], tool cutting edge angle κ_r= 45° (own study)

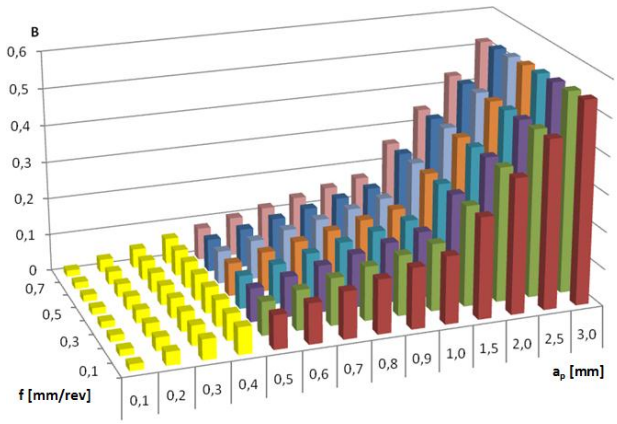

Fig. 3. Change of relative stiffness coefficient *B* under the effect of feed rate and machining depth at *L* = 500 [mm], *d* = 20 [mm], rotary speed of machined part n_p=1000 [rev/min], tool cutting edge angle κ_r= 90° (own study)

Based on the results of modelling (Fig. 2 and 3) we can conclude that the value of coefficient *B* increases in the function of change of machining depth and decreases slightly with increase of feed rate. With the change of tool cutting edge angle from κ_r=90° to κ_r=45° one can observe a slight increase in the value of coefficient *B* (for feed of 0.8 mm/rev and depth of 0.5 mm the difference is 0.008).

Therefore, we need to determine the operator transmittance in control, corresponding to these conditions, as well as the gain factors of the object and the retardation τ. Next, we determine the operator transmittance relative to the interference factor that assumes the form:

$$G_{v_f gi}(s) = \frac{\Delta F_i(s)}{\Delta v_f} = \frac{m_x h_{xx} G_\tau(s)}{s[(T_c s + 1)(T_{us}^2 s^2 + 2\xi T_{us} s + 1) + B_1 G_\tau(s) + n_y h_{yy}]} \quad (1)$$

and the accurate value of coefficient B:

$$B = \frac{m_x h_{xx} + K_{\kappa_r} m_y h_{yy}}{1 + n_y h_{yy}} \quad (2)$$

After calculating the gain factors of the machining process, m_x, m_y and m_z, with the change of feed f and machining depth a_p (these values can be treated as interference), we determine the relative dynamic stiffness coefficient B.

We determine the coefficients of object strengthening K_{ox}, K_{oy}, K_{oz}, retardation τ and coefficients K_{bx}, K_{by}, K_{bz}. The relation to the approximated operator transmittance of the object in control assumes the form (3) (Cardi, Firpi, Bement & Liang, 2008; Świc & Taranenko, 2012; Wu & Liu, 1985):

$$G_o(s) = \frac{\Delta Y_o(s)}{\Delta v_f(s)} = \frac{K_o}{(T_1 s + 1)\,(T_2 s + 1)} \quad (3)$$

After the determination of the operator transmittance we determine coefficients K_{a0x}, K_{a0y}, K_{a0z} and time constants T_1 and T_2.

Analysis of the simulation results presented in Tab. 2, Tab. 3 and in Fig. 2 and Fig. 3 indicates that in those cases the operator transmittances of the approximated object of control have different forms. In the case of coefficient $B \geq 0.077$ (the limit value of B, at which the form of the operator transmittance changes), with changes of feed f and of machining depth a_p (from 0.4 to 3 mm) the operator transmittance has a form conforming to relation (3). At $B < 0.077$ and changes of machining depth a_p (from 0.1 to 0,4 mm) and feed rate, the operator transmittance of the approximated object has the following form (Świć, Wołos, Zubrzycki, Opielak, Gola & Taranenko, 2014; Ratchev, Liu, Huang, & Becker, 2004)

$$G_o(s) = \frac{\Delta Y_o(s)}{\Delta v_f(s)} = \frac{K_o}{(T_1 s + 1)}. \quad (4)$$

The results of calculations of retardation and time constants in relation to changes in rotary speed and machining depth, on the basis of which Fig. 4 was elaborated, are presented in Tab. 4.

Tab. 4. Change of retardation and time constants in relation to rotary speed and machining depth at length L = 500 [mm], diameter d = 20 [mm], tool cutting edge angle κ_r= 90° (own study)

a_p [mm]	0.4				0.6			
n [rpm]	500	1000	1500	2000	500	1000	1500	2000
Delay τ [s]	0.12	0.06	0.04	0.03	0.12	0.06	0.04	0.03
T_1 [s]	0.12	0.06	0.04	0.03	0.048	0.025	0.016	0.012
T_1 [s]	-	-	-	-	0.025	0.012	0.008	0.006
a_p [mm]	1.0				1.5			
n [rpm]	500	1000	1500	2000	500	1000	1500	2000
Delay τ [s]	0.12	0.06	0.04	0.03	0.12	0.06	0.04	0.03
T_1 [s]	0.062	0.031	0.021	0.016	0.076	0.038	0.025	0.019
T_1 [s]	0.019	0.01	0.006	0.005	0.016	0.008	0.005	0.004

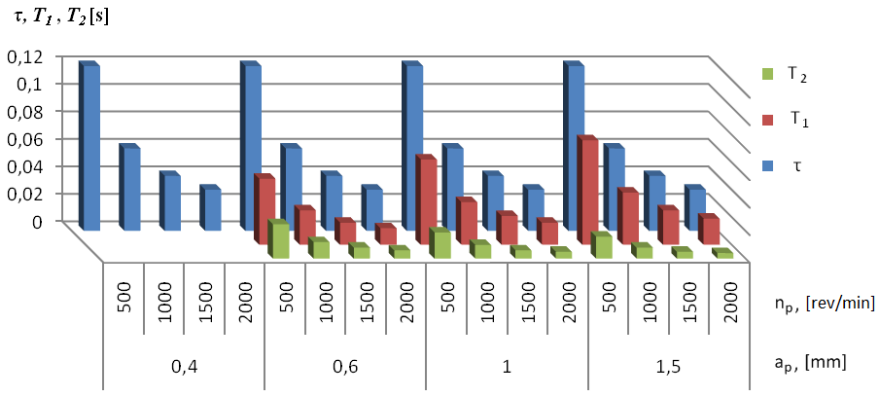

Fig. 4. Change of retardation and time constants in relation to rotary speed and machining depth at length L = 500 [mm], diameter d = 20 [mm] (own study)

Analysis of the data given in Tab. 4 and in Fig. 4 shows that the operator transmittance at $a_p \leq 0{,}4$ mm has a form conforming to relation (4).

3. ANALYSIS OF FREQUENCY AND TIME CHARACTERISTICS OF MODELS OF DYNAMIC SYSTEM OF MACHINING OF SHAFTS WITH LOW RIGIDITY

Transition processes in the dynamic system, at step-wise changes in feed rate and various depths of machining, are illustrated in Fig. 5 a. At machining depth of a_p=0.5 [mm] the approximated characteristic conforms to the operator transmittance (4), while at higher values of a_p it assumes the form of (3). This is due to the change of the operator transmittance at the value of coefficient $B \geq 0.077$, dependent on machining depth. The change of the operator transmittance affects both the approximated and the output characteristics. At higher depths of machining the time of response to unit step of feed increases.

This is due to the inclusion of the change of time constants T_1 and T_2. In Figs. 5–9 solid line represents the characteristics of the accurate model (output), and the broken line the characteristics of the approximated model.

The amplitude characteristics at various depths of machining are presented in Fig. 5 b. Irrespective of the depth of machining, at frequency 0 [rad/s] the curves assume the value of 10 dB. At the depth of a_p=0.5 [mm] the approximated characteristic assumes values higher than those of the initial characteristic, and in the case of greater depths of machining the approximated characteristic assumes lower values. The change of the operator transmittance affects only the approximated characteristic.

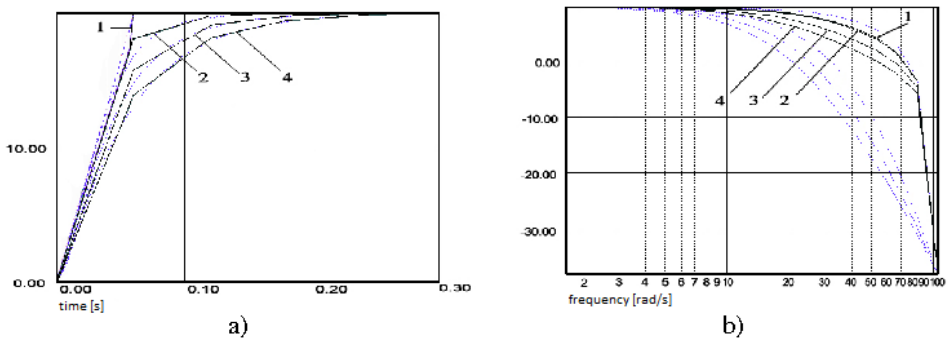

Fig. 5. Responses to unit step of feed rate – a); amplitude characteristic at depth of machining - b); where: 1 – 0.5 [mm], 2 – 0.6 [mm], 3 – 1.5 [mm], 4 – 2.5 [mm], feed 0.4 [mm/rev], speed 1000 [rev/min], angle κ_r= 90° and L = 500 [mm], diameter d = 20 [mm], tool cutting edge angle κ_r= 90° (own study)

The phase-frequency characteristics at various depths of machining are presented in Fig. 6. Irrespective of machining depth the output characteristic attains the value of –180°, at frequency of 100 [rad/s]. The approximated characteristic, in the range from 0° to –90°, assumes higher values at lower depths of machining. At machining depth of 0.6 and higher, after exceeding the value of –45°, the curve of the approximated characteristic diverges increasingly from the curve of the output characteristic.

Within the range from 0^0 to –90°, the approximated characteristic assumes somewhat higher values than the output characteristic in the case of machining depths smaller than 0.5 [mm]. At the angle of –90° the curves cross each other, and therefore the output characteristic assumes higher values with increase of the depth of machining.

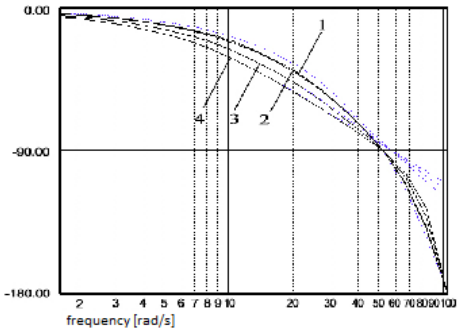

Fig. 6. Phase-frequency characteristics at various values of machining depth, where: 1 – 0.5 [mm], 2 – 0.6 [mm], 3 – 1.5 [mm], 4 – 2.5 [mm], feed 0.4 [mm/rev], speed 1000 [rev/min], angle κ_r = 90° (own study)

The responses to init step of feed are presented in Fig. 6. Irrespective of the feed change, the output characteristic attains the value of –180° at frequency of 100 [rad/s]. Within the range from 0° to –90° the approximated characteristic assumes higher values at smaller machining depths. Feed rate change has no pronounced effect on either the amplitude or the phase characteristics. The feed rate has a slight effect on the relative stiffness coefficient *B*, therefore the change in the shape of the curves of the initial and the approximated characteristics is barely observable. At machining depth of 0.6 mm and higher, and at angles greater than –45°, the curve of the phase approximating characteristic becomes increasingly divergent from the initial characteristic.

In the case of machining depths smaller than 0.5 mm, in the range from 0° to –90° the approximating phase characteristic assumes values higher than those of the initial phase characteristic. At –90° the curves intersect, and thus the initial characteristic assumes higher values with increasing depth of machining.

Feed rate change has only a slight effect on both the amplitude and the phase-frequency characteristics of the dynamic system of machining of parts with low rigidity.

Feed rate change does not have any significant effect on the relative dynamic stiffness coefficient *B*, and therefore the transition, initial and approximated characteristics of the dynamic system remain practically unchanged.

Analysis of the transition characteristics of the system of machining of shafts with low rigidity at step-wise change of unit feeds and at various speeds of shaft rotation indicates that with increase of the rotation speed of the machined part the duration of the transition process is shortened: at 500 rev/min it equals 0.12 s, at 1000 rev/min – 0.06 s, and at 2000 rev/min – 0.03 s. At the same time, there is a reduction in the difference between the values of the characteristics.

The amplitude-frequency characteristics are presented in Fig. 7. The horizontal axis shows various values of part rotation speed: 500, 1000, 2000 rev/min. Analysis of the curves shows that at various speeds of the component

the amplitude=frequency characteristics do not undergo any change in the case of the initial and the approximated models. In the case of the speed of 555 rev/min the curves assume the value of –33 dB, at the speed of 50 rad/s and analogously at 1000 rev/min – 100 rad/s; 2000 obr/min – 200 rad/s.

Irrespective of the change in the speed of rotation, the responses to unit change in feed remain unchanged, whereas there is a change in the response time. With increase of the speed of rotation there is an observable shortening of the response time that at 500 [rev/min] amounts to 0.12 [s], at 1000 [rev/min] – 0.06 [s], at 2000 [rev/min] – 0.03 [s], as well as a decrease of the difference between the values of the characteristics.

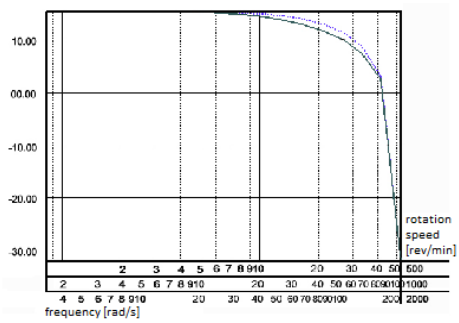

Fig. 7. Amplitude-frequency characteristics, where: a_p = 0.4 [mm], f=0.4 [mm/rev], speed: n=500, 1000, 2000 [rev/min], angle κ_r= 90° (own study)

The axis of abscissae represents three scales referenced to various speeds of rotation: 500, 1000 and 2000 [rev/min]. Analysis of the graph shows that the shape of the curve, both in the case of the approximated and the output characteristics is the same at each of the speeds of rotation. At the speed of 500 [rev/min] the curves attain the value of –33dB at frequency of 50 [rad/s], and analogously, in the remaining cases: 1000 [rev/min] – 100 [rad/s], 2000 [rev/min] – 200 [rad/s]. Also visible is a small difference in values between the curves of the approximated and the initial characteristics. In the case of the phase-frequency characteristic the speed of rotation has an effect only on the frequency [rad/s], and does not affect the shape of the curve.

The responses to unit step of feed are presented in Fig. 8. At machining depth of 0.6 [mm], the approximated characteristics assume the form of ma curve conforming to the operator transmittance (3). Irrespective of feed change, the time of response remains unchanged. With an increase of longitudinal feed rate one can observe an increasing divergence between the approximated characteristic and the initial characteristic. The initial value increases, e.g. at feed rate of 0.1 [mm/rev] it equals 5 [N], at feed rate of 0.4 [mm/rev] – 20 [N], and at feed of 0.8 [mm/rev] – 40 [N]. After 0.15 [s] the initial characteristic coincides with the approximated characteristic.

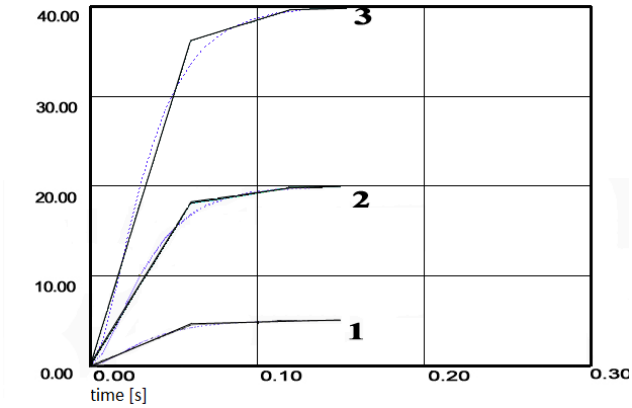

Fig. 8. Response to unit step of feed at machining depth of a_p=0.6 [mm] and feed rate [mm/rev.]: 1 – 0.1; 2 – 0.4; 3 – 0.8; speed 1000 [rev/min], angle κ_r =90° (own study)

The amplitude-frequency characteristic, at machining depth of 0.6 [mm], speed of 1000 [rev/min] and various feed rates, is presented in Fig. 9 a. Based on the Figure it can be concluded that feed change does not affect the shapes of the curves of both the initial and the approximated characteristics. However, there is a visible difference in values between the curves of the initial and the approximated characteristics. Feed rate change has only a slight effect on the relative stiffness coefficient *B*, therefore the change in the shape of the curves is practically non-observable and has no effect on the amplitude characteristic.

The phase-frequency characteristic, at machining depth of 0.6 [mm], speed of rotation of 500 [rev/min] and feed rates of 0.1, 0.4, 0.8 [mm/rev], is presented in Fig. 9 b. The phase-frequency characteristic of the initial model attains the value of –180° at frequency of 100 [rad/s]. After exceeding the value of –45° the curve of the approximated characteristic begins to diverge more and more from the curve of the initial characteristic. Feed rate change has only a slight effect on the relative stiffness coefficient *B*, therefore the change in the shape of the curves is practically non-observable and has no effect on the phase-frequency characteristic.

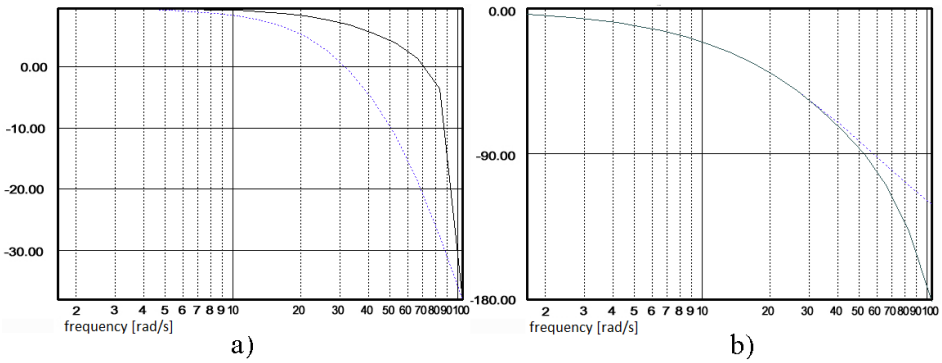

Fig. 9. Amplitude-frequency characteristic at machining depth of 0.6 [mm], feed [mm/rev]: 1 – 0.1; 2 – 0.4; 3 – 0.8; speed 1000 [rev/min] – a); phase characteristic at machining depth of 0.6 [mm], feed [mm/rev]: 1 – 0.1; 2 – 0.4; 3 – 0.8; speed 1000 [rev/min], angle κ_r =90° – b) (own study)

In the determination of the time constants of the models, comparative analysis of the relative error δ (%), that does not exceed 15% (Świć, 2009), indicates that the developed mathematical models of turning of shafts with low rigidity are adequate to the actual process.

4. CONCLUSION

As a result of analysis of the frequency and time models of the dynamic system of machining of shafts with low rigidity, the possibility was found of their approximation within the range of actual frequencies of the dynamic system and of the control system of the operator transmittances of typical dynamic elements: integrating element and aperiodic element of the second or first order. It was determined that the gain factors and the time constants of the approximated models are subject to change, primarily with a change in the speed of rotation of the machined part and in the relative dynamic stiffness coefficient *B*, characterising the ratio of stiffness of the elastic system of the machine tool and the gain factors of the machining process. In the case of use of universal lathes, with relation to the changing conditions and parameters of machining the model parameters can vary within a broad range.

REFERENCES

Abakumov, A., Taranenko, V., & Zubrzycki, J. (2006). Modeling of characteristics of dynamic system of turning process for axial-symmetric shafts. *V-th International Congress "Mechanical Engineering Technologies' 06" (MT''06)* (pp.76-78). Varna, Bulgaria.

Cardi, A. A., Firpi, H. A., Bement, M. T., & Liang, S. Y. (2008). Workpiece dynamic analysis and prediction during chatter of turning process. *Mechanical Systems and Signal Processing*, *22*(6), 1481-1494. doi:10.1016/j.ymssp.2007.11.026

Gola, A. (2014). Economic Aspects of Manufacturing Systems Design. *Actual Problems of Economics*, *156*(6), 205-212.

Ratchev, S., Liu, S., Huang, W., & Becker, A. A. (2004). Milling error prediction and compensation in machining of low-rigidity parts. *International Journal of Machine Tools & Manufacture*, *44*(15), 1629-1641. doi:10.1016/j.ijmachtools.2004.06.001

Świc, A., & Mazurek, L. (2011). Modeling the reliability and efficiency of flexible synchronous production line. *Eksploatacja I Niezawodnosc-Maintenance and Reliability*, *4*, 41-48.

Świc, A., & Taranenko, W. (2012). Adaptive control of machining accuracy of axial-symmetrical low-rigidity parts in elastic-deformable state. *Eksploatacja I Niezawodnosc-Maintenance and Reliability*, *14*(3), 215-221.

Świć, A. (2009). *Technologia obróbki wałów o małej sztywności.* Lublin: Wydawnictwo Politechniki Lubelskiej.

Świć, A., Gola, A., & Wołos, D. (2014). A Method for Increasing the Economic Effectiveness of the Low Rigidity Shafts. *Actual Problems of Economics*, *161*(11), 469-477.

Świć, A., Wołos, D., Zubrzycki, J., Opielak, M., Gola, A., & Taranenko, V. (2014). Accuracy Control in the Machining of Low Rigidity Shafts. *Applied Mechanics and Materials*, *613*, 357-367.

Wu, D. W., & Liu, C. R. (1985). An analytical model of Cutting dynamics. Part 2. Verification. *Journal of Engineering for Industry*, *107*(2), 112. doi:10.1115/1.3185973

Applied Computer Science, vol. 12, no. 3, pp. 74–84

Submitted: 2016-07-20
Revised: 2016-09-05
Accepted: 2016-09-19

involute conical gear, tooth correction,
contact and tribocontact pressures, tooth wear, gear durability

Myron CHERNETS[*], *Yuriy CHERNETS*[**]

CALCULATION METOD FOR THE EVALUATION OF INFLUENCE OF TOOTH ENGAGAMENT PARITY IN CONICAL SPUR GEAR ON CONTACT PRESSURES, WEAR AND DURABILITY

Abstract

The paper presents the results of research undertaken to determine maximum contact pressures, wear and life of conical gears, taking account gear technological correction, tooth engagement and wear-generated changes in curvature of their involute profile. The calculations were made for a reduced cylindrical gear using a method developed by authors. The effect of applied conditions of tooth engagement in the frontal and internal sections of cylindrical gear ring is shown graphically. The initial maximum contact pressures will be higher in the internal section and the highest at the entry of single tooth engagement; the increasing of correcting coefficients will cause the fall of contact and tribocontact pressures; the optimum values of correction coefficients, at which the durability of the gear will be the highest were obtained.

1. INTRODUCTION

The conic gears that allow to transmit torsion moment with the angle $90° \leq 2\delta < 90°$ between axis are widely used. In teeth interaction their two-one-two pair engagement is realized. But the methods allowing to take into account this important circumstance of corrected and uncorrected gears work, including bevel gears, are absent. For a gear with no tooth profile correction, the maximum

[*] Lublin University of Technology, Poland, phone: +48-81-538-12-76, m.czerniec@pollub.pl
[**] Drohobych Ivan Franko State Pedagogical University, Drohobych, Ukraine, jurij_c@yahoo.pl

contact pressures generated during tooth engagement are determined in compliance with a relative ISO standard. However, no such methods have been developed for conical gears with corrected tooth profiles. Also, the methods for assessing wear and life gears reported in the literature (Drozdov, 1975; Grib, 1982; Brauer & Andersson, 2003; Flodin & Andersson, 1997; Flodin & Andersson, 1999; Kahraman, Bajpai & Anderson, 2005; Pasta & Mariotti, 2007) can only be applied to gears with uncorrected profiles. The preliminary results of investigations conducted using methods which take into account gear tooth correction, changes in tooth profile curvature due to wear and the number of engaged tooth pairs are reported in the works (Chernets, 2013; Chernets & Chernets, 2014; Chernets & Chernets, 2015; Chernets, Yarema & Chernets, 2012; Chernets, Kelbinski & Yarema, 2011). The study below was undertaken with respect to the effect of the above factors and tooth interaction conditions on variations in the maximum contact pressures and tribotechnical parameters. The calculationfor a conical gear were made in the same way as for a reduced cylindrical gear with frontal and internal modules of conical engagement made variable over a tooth length $m_{\max} \le m \le m_{\min}$ (Chernets, 2013). To solve the problem, we applied methods for assessing contact strength, wear and life of spur gears.

2. METHOD FOR ESTIMATING GEAR DURABILITY

Tooth wear causes an increase in curvature radii of tooth profiles, which leads to a decrease in initial maximum contact pressures $p_{j\max}$ and contact area width $2b_j$ at every j-th point of contact. The values of $p_{jh\max}$ and $2b_{jh}$ are calculated in accordance with the modified Hertz equations:

$$p_{jh\max} = 0.564\sqrt{N'\theta/\rho_{jh}}\,,\ 2b_{jh} = 2.256\sqrt{\theta N'\rho_{jh}}\,, \qquad (1)$$

where j = 0, 1, 2, 3,… are the contact points of the teeth profiles; $N' = N/w$; $N = 9550P/r_1n_1\cos\alpha$ is the engagement force; P is the power on the drive shaft (pinion); w is the number of engaged tooth pairs; $\theta = (1 - \nu_1^2)/E_1 + (1 - \nu_2^2)/E_2$; E, ν are the Young modulus and Poisson's ratios of toothed gear materials, respectively; r_1 – is the rolling radius of the pinion; r_2 is the number of revolutions of the drive shaft; $\alpha = 20°$ is the pressure angle of engaged teeth; $\rho_{jh} = \dfrac{\rho_{1jh}\rho_{2jh}}{\rho_{1jh} + \rho_{2jh}}$ is the reduced radius of curvature of the gear profile subjected to changes due to wear in a normal section; ρ_{1jh}, ρ_{jh} are the changeable radii of curvature of the pinion and gear teeth profiles, respectively.

In operation, due to the gear's wear, the initial curvature radii ρ_{1j}, ρ_{2j} (Chernets, Yarema & Chernets, 2012) of the gear profiles and the reduced curvature radius ρ_j increase.

The work (Chernets, Yarema & Chernets, 2012) presents a method which takes account of wear-generated changes in the initial radii of gear curvature in every revolution of the gear. Accordingly

$$\rho_{kjh} = \rho_{kj} + D_{jk} \sum^{n} K_{kjn}^{-1}, \; k = 1; 2, \tag{2}$$

where $n = n_k = 1, 2, 3,...$ is the number of revolution of the gear; k is the numeration of gears (1 – pinion, 2 – gear); $D_{jk} = K^2_{kj}$ are the nondimensional constants at every j-th contact point depending on wear.

The wear-generated changes in gear profiles during every tooth interaction is

$$K_{kj} = 8h'_{kj} / l_{kj}^2, \tag{3}$$

where h'_{kj} in the linear wear of gear teeth at any j-th point of the profile; l_{kj} is the length of a gear chord which substitutes the involute between points $j - 1$, $j + 1$;

$$l_{kj} = 2\rho_{kjh} \sin \varepsilon_{kjh} = \text{const}, \tag{4}$$

where $\varepsilon_{kjh} = S_{kj} / \rho_{kjh}$ is the angle between the points j and j +1; $S_{kj} = \left| \frac{mz_k}{4} \left(\frac{1}{\cos^2 \alpha_{kj}} - \frac{1}{\cos^2 \alpha_{k,j+1}} \right) \cos \alpha \right|$ is the length of the involute between the points j, $j + 1$; α_j, α_{j+1} are the angles of tooth engage of selected involute points j, $j + 1$ (Chernets, Yarema & Chernets, 2012); m is the module of engagement; z_1, z_2 is the number of gear teeth.

To make the computation time shorter, we developed a block-based method for solving this problem. With this method, changes in profile curvature radii, reduced curvature radii and maximum contact pressures are determined following a selected number of revolutions (blocks of interactions), and not per every gear revolution (tooth engagement) as was done previously. In a block, computations are made under constant conditions of tooth engagement based on linear cumulative changes in given parameters. In a successive block of computations, the cumulative changes are taken into account after (5), (6) and then the computations are continued using new data. The changeable curvature radii ρ_{kjh} are determined as

$$\rho_{kjh} = \rho_{kj} + E_k \sum_{B_1}^{B_{\max}} D_{kjB} K_{kjB}^{-1}, \tag{5}$$

where B denotes the number of gear revolutions (i.e. the size of a block describing tooth interactions) with the conditions of contact maintained constant; a the size of a block can be selected as: B = 1 revolution (accurate solution), $B = n_1$ (rev/min), $B = n_1$ revolutions per one hour, $B = n_1$ revolutions per 10 hours, and so on; B_1 and $B_{\max}$ are the first and last computational block, respectively; E_k is a nondimensional constant dependent on the maximum acceptable tooth wear h_{k*}; $D_{kjB} = K^2_{kjB}$ is a constant which remains unchanged in one block but changes in every other block.

The wear-induced change in the curvature of a gear tooth profile for every single block of interaction is:

$$K_{kjB} = 8\sum^{B} h'_{kjn} / l^2_{kj}. \tag{6}$$

The unit linear tooth wear h'_{kjn} at any j-th point of gear profiles is calculated for every successive revolution of the block for the time $t'_{jh} = 2b_{kj} / \nu_0$, and it is not subject to accumulation. The width of contact area $2b_{jh}$ is determined at the revolution $n_k - 1$ or at block $B - 1$ in accordance with (1). A value of h'_{kjn} is calculated using the equation (Chernets, Yarema & Chernets, 2012):

$$h'_{kjn} = \frac{v_j t'_{jh} \left(f p_{jh\max} \right)^{m_k}}{C_k \left(0.35 R_m \right)^{m_k}}, \tag{7}$$

where t'_{jh} is the time of tooth wear at displacement along the profile of a j-th contact point over the contact area width $2b_{jh}$; $\nu_0 = \omega_1 r_1 \sin\alpha$ is the velocity of contact point travel along the tooth profile; ω_1 is the angular velocity of the pinion; ν_j is the sliding velocity at a j-th point of the gear profile; f is the sliding friction factor; $p_{jh\max}$ is the maximum tribocontact pressure (at tooth wear) at a j-th contact point; C_k, m_k are the indicators of resistance to wear of tribological pair materials; R_m the immediate tensile strength of material.

The sliding velocity of engaged teeth is calculated as:

$$v_j = \omega_1 r_{b1} \left(\tan\alpha_{1j} - \tan\alpha_{2j} \right), \tag{8}$$

where $r_{b1} = r_1 \cos\alpha$, α_{1j}, α_{2j} in compliance with (Chernets, Kelbinski & Yarema, 2011). Hence, following every interaction or a block of interaction, the parameters h_{1j}, h_{2j},, ρ_{1jh}, ρ_{2jh}, ρ_{jh}, $p_{jh\max}$, $2b_{jh}$, t'_{jh} will change.

For the applied number of pinion revolutions n_{1s} and gear revolutions n_{1s}, and the corresponding number of interaction blocks, the total tooth wear h_{1jn} and h_{2jn} at the j-th points of contact are calculated as:

$$h_{1jn} = \sum_{1}^{n_{1s}} h_{1jB}\,, \qquad h_{2jn} = \sum_{1}^{n_{2s}} h_{2jB}\,, \tag{9}$$

where $n_{2s} = n_{1s} / u$; $h_{kjB} = \sum h'_{kj}$ is the tooth wear in every block of interaction; u is the gear ratio.

The service life $t_{B\min}$ of gear operation for the number of gear revolutions n_{1s} or n_{2s} is determined by:

$$t_{B\min} = n_{1s} / 60 n_1 = n_{2s} / 60 n_2\,. \tag{10}$$

The angles of transition from a double tooth engagement ($\Delta\varphi_{1F_2}$) to a single tooth engagement and, again, to a double tooth engagement ($\Delta\varphi_{1F_1}$) in a cylindrical gear with profile correction are determined in the following way:

$$\Delta\varphi_{1F_2} = \varphi_{10} - \varphi_{1F_2}\,,\ \Delta\varphi_{1F_1} = \varphi_{10} + \varphi_{1F_1}\,; \tag{11}$$

where $\varphi_{1F_2} = \tan\alpha_{F_2} - \tan\alpha$, $\varphi_{1F_1} = \tan\alpha_{F_1} - \tan\alpha$, $\varphi_{10} = \tan\alpha_{10} - \tan\alpha$,

$\tan\alpha_{F_2} = \dfrac{r_1 \sin\alpha - (p_b - e_1)}{r_1 \cos\alpha}$, $\tan\alpha_{F_1} = \dfrac{r_1 \sin\alpha - (p_b - e_2)}{r_1 \cos\alpha}$.

The angle $\Delta\varphi_{1E}$ describing the moment of teeth exit of engagement is:

$$\Delta\varphi_{1E} = \varphi_{10} + \varphi_{1E}\,, \tag{12}$$

where $\varphi_{1E} = \tan\alpha_E - \tan\alpha_t$, $\alpha_E = \arccos(r_{b1} / r_{1s})$, $r_1 = m z_1 / 2$, $p_b = \pi m \cos\alpha$, $\tan\alpha_{10} = (1+u)\tan\alpha - \dfrac{u}{\cos\alpha}\sqrt{(r_{20}/r_2)^2 - \cos^2\alpha}$, $e_1 = \sqrt{r_{1s}^2 - r_{b1}^2} - r_1 \sin\alpha$, $e_2 = \sqrt{r_{20}^2 - r_{b2}^2} - r_2 \sin\alpha$, $r_{20} = r_{a2} - r$, $r_2 = m z_2 / 2$, $r_{a2} = r_2 + m$, $r_{1s} = r_{a1} - r$, $r_{b1} = r_1 \cos\alpha$, $r_{b2} = r_2 \cos\alpha$, $r = 0{,}2m$; r_2 – is the radius of a pitch circle of the gear; p_b is the pitch of teeth; $u = u_K^2$ is the gear ratio of a reduced cylindrical gear; $z_1 = z_{1K} / \cos\delta_1$, $z_2 = z_{2K} / \cos\delta_2$ are the numbers of teeth in reduced cylindrical gears.

3. NUMERICAL SOLUTION

Numerical solution of the problem is made for the data: z_{1K} = 20; u_K = 3; n_1 = 750 rpm; P = 20 kW; b = 50 mm – ring width; $m_{\max}$ = 5 mm – a normal module of tooth engagement in the frontal section; $m_{\min}$ – 3.391 mm – a normal module of tooth engagement in the internal section; $\Delta\varphi$ = 4° – the increment in the pinion's angle of rotation; h_{k*} = 0,5 mm – maximum acceptable wear of gear teeth; B = 900000 revolutions. We applied boundary lubrication with a sliding friction factor set to f = 0.05. The applied technological correction coefficients were: $x_1 = -x_2$ = 0; 0,1; 0,2; 0,3; 0,4. It appears by a double-single-double tooth engagement.

The gears were ascribed the following material properties: the pinion was made of 38HMJA steel after nitriding at a depth ranging from 0.4 mm to 0.5 mm described by 58 HRC, R_m= 1040 MPa, $C_1 = 3{,}5\cdot10^6$, m = 2; the gear was made of bulk hardened 40H steel with 53 HRC, R_m = 981 MPa, $C_2 = 0.17\cdot10^6$, m_2 = 2.5; $E = 2.1\cdot10^5$ MPa, μ = 0.3.

The results are illustrated in the figures below. Fig. 1a shows the diagram that presents changes of initial contact pressures $\boldsymbol{p_{j\max}}$ in the frontal section (external), and Fig. 1b presents their transformations $\boldsymbol{p_{j\max}}$ as a result of tooth wear up to maximum values. Respectively Fig. 2 shows contact and tribocontact pressures in the internal section.

The left- and right-hand sides of the figures show double tooth engagement, while single tooth engagement can be observed in the centre of the figures. An increase in the displacement coefficients leads to decreasing $p_{j\max}$, this decrease is particularly significant on the left. The decrease in the tribocontact pressures $p_{jh\max}$ This value is remarkably high in the entire left-hand zone of double tooth engagement and quite visible at the beginning of the double tooth engagement zone.

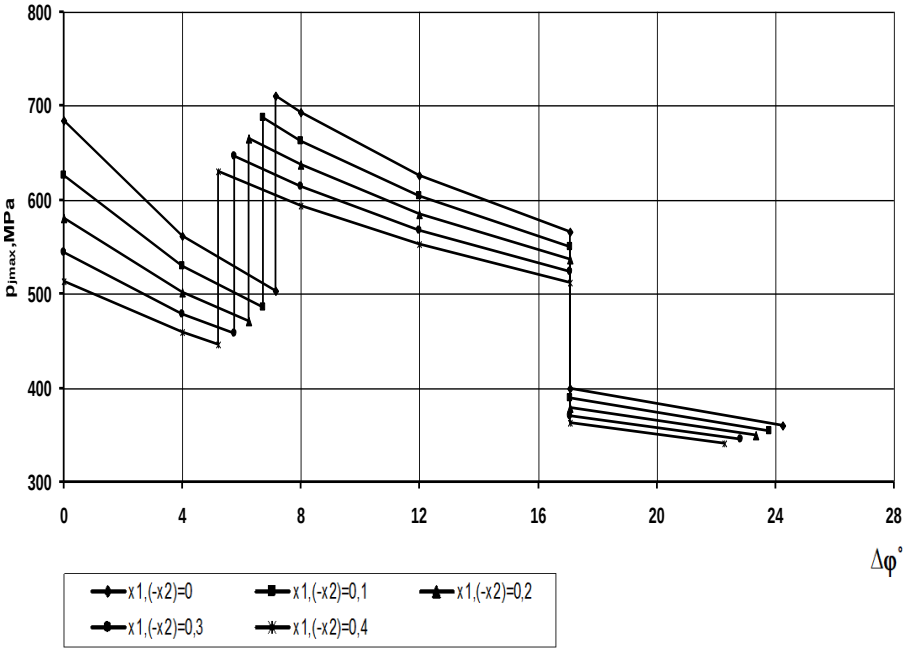

a)

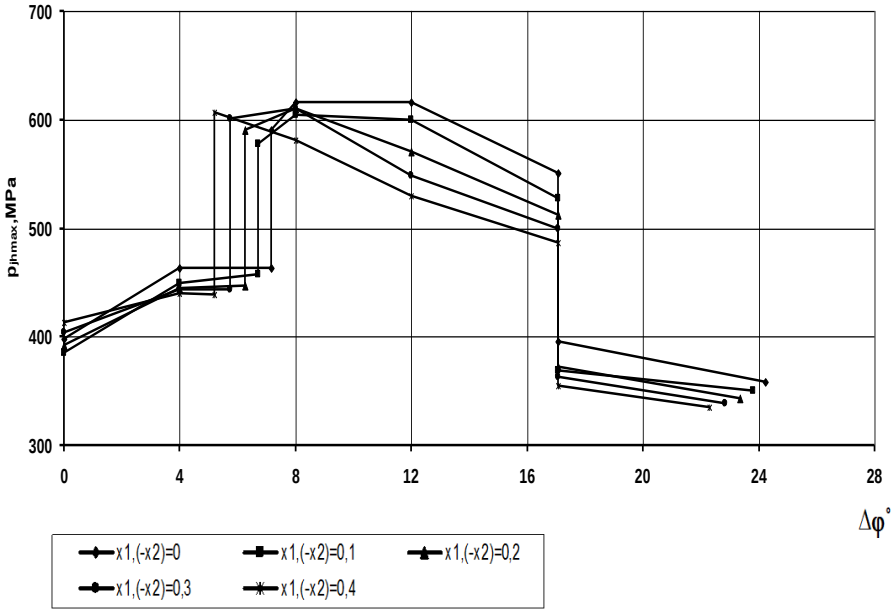

b)

Fig. 1. Contact and tribocontact pressures in the frontal section (own study)

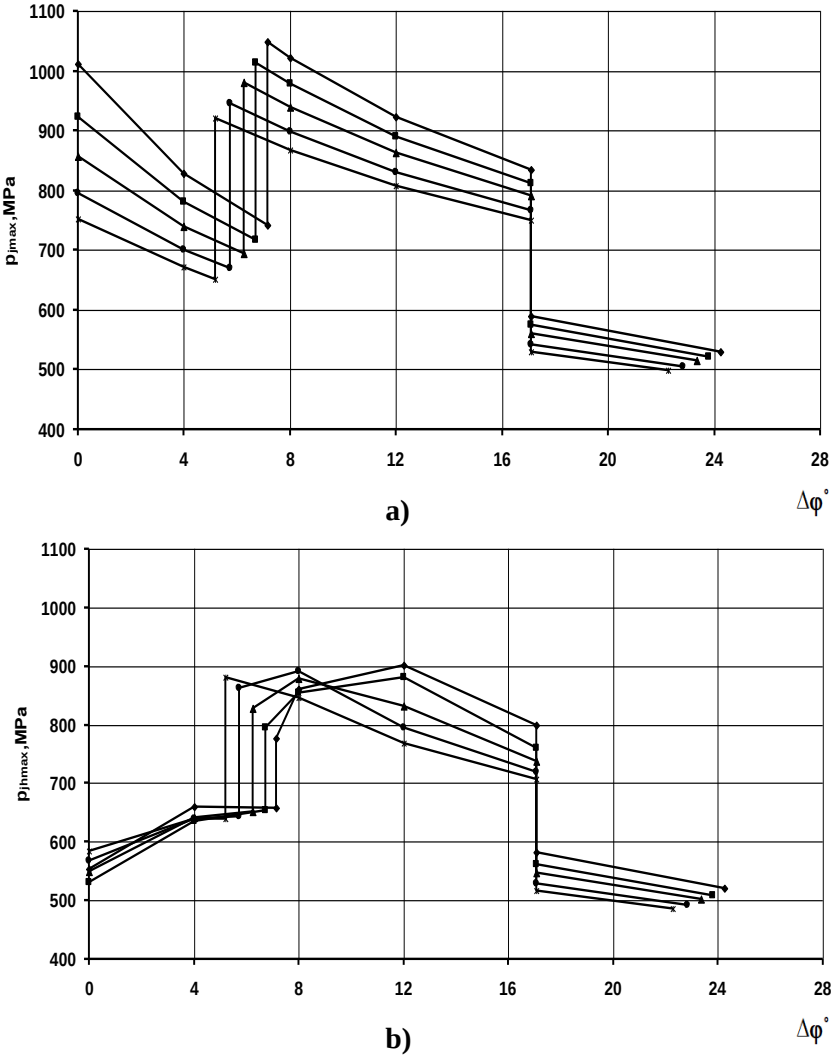

Fig. 2. Contact and tribocontact pressures in the internal section (own study)

As for this section, $p_{j\max}$ is approx. 1.48 times higher than that in the frontal section. The change in $p_{j\max}$ is similar to one given above (Fig. 1b).

Fig. 3 shows the diagrams of linear wear of gear profiles in the engagement zone in the internal section.

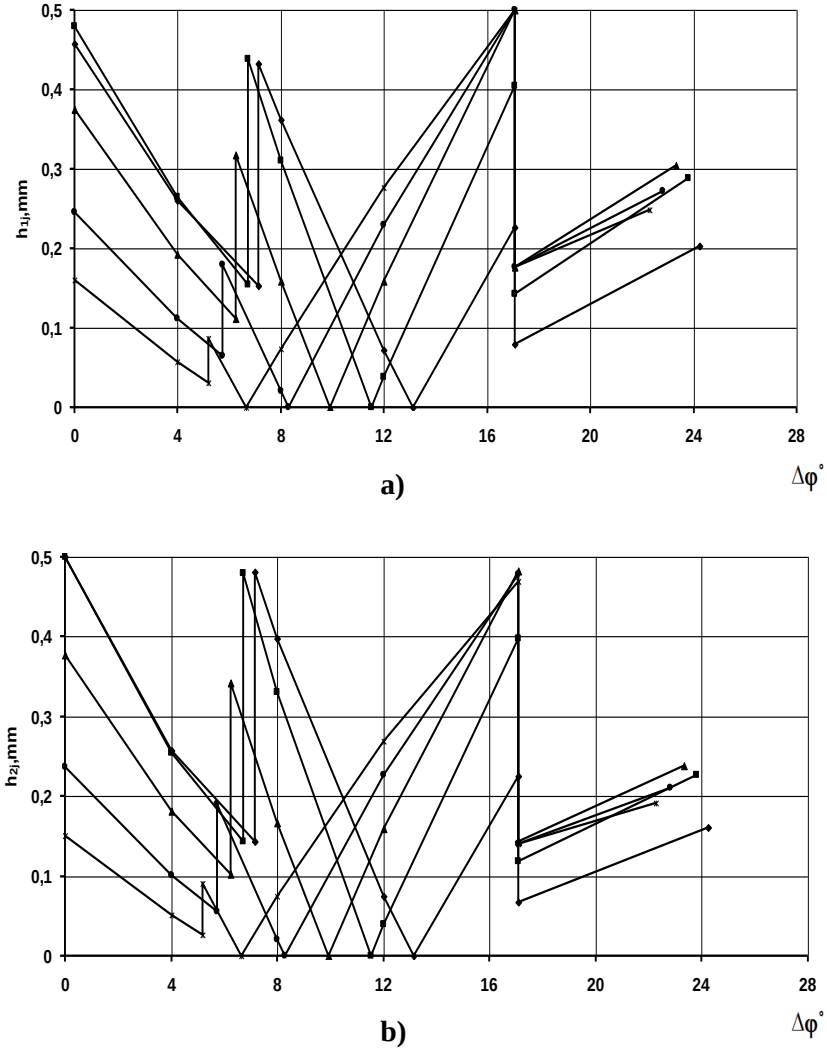

Fig. 3. Linear wear of corrected teeth: a) pinion, b) gear (own study)

Depending on a value of $x_1 = -x_2$, the maximum acceptable wear of cylindrical gear teeth occurs at the entry of the left-hand zone of double tooth engagement ($x_1 = -x_2 = 0$; 0.1) and at the exit of single tooth engagement ($x_1 = -x_2 > 0.1$).

Fig. 4 illustrates the effect of the minimal life of gears (gear tooth profile points where h_{2*} is attained) on the displacement coefficients $x_1 = -x_2$.

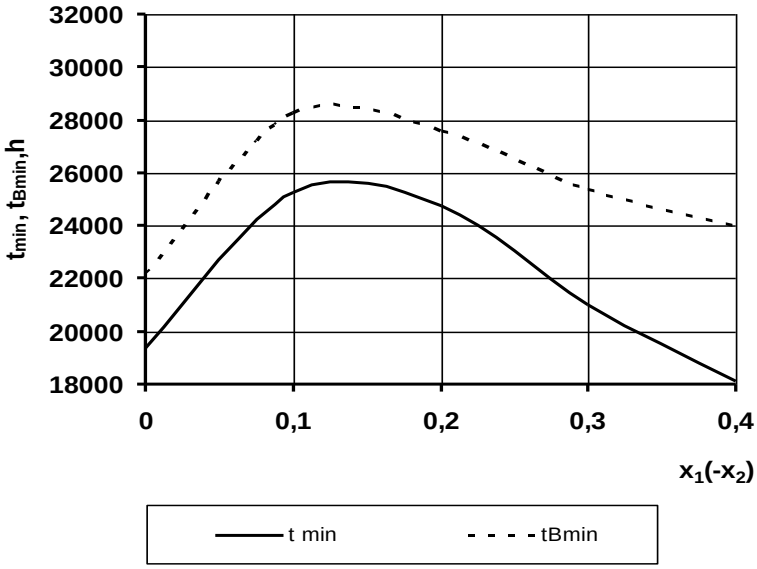

Fig. 4. Gear life: t_{min} when p_{jmax} = const, $t_{B\,min}$ when $p_{jh\,max}$ = var (own study)

Accordingly, the gear life t_{Bmin} takes into account changes in p_{jmax} due to tooth wear, while t_{min} is described by the assumption that p_{jmax} remains constant. For a selected range of change in the displacement coefficients, the optimal gear life is at $x_1 = -x_2 \approx 0.13$.

4. CONCLUSION

The results have demonstrated that:

1. In spur gears with double-single-double tooth engagement, the initial contact pressures p_{jmax} will be higher in the internal section of the gear by 1.475 times than in the frontal section due to a decrease in the module. That means that increasing of p_{jmax} is proportional to decreasing of the module's value.
2. The highest values of p_{jmax} can be observed at the entry of single tooth engagement in both sections.
3. The regularities concerning a decrease in p_{jmax} and p_{jhmax} in the left-hand zone of engagement can similarly be observed with increasing the displacement coefficients $x_1 = -x_2$.
4. We determined optimal displacement coefficients for spur gears $x_1 = -x_2 = 0.13$ which will produce the highest possible gear life.
5. The linear wear h_{1j}, h_{2j} of gear teeth in the internal section are alike.
6. Spur gears have the lowest acceptable life in their internal section.

REFERENCES

Brauer, J., & Andersson, S. (2003). Simulation of wear in gears with flank interference – a mixed FE and analytical approach. *Wear, 254*(11), 1216-1232. doi:10.1016/s0043-1648(03)00338-7

Chernets, M. V. (2013). Influence of spur gear tooth engagement on its contact strength. *Problems of Tribology, 69*(3), 109-113.

Chernets, M. V., & Chernets, Y. M. (2014). Investigation of tooth engagement conditions in cylindrical involute gear on contact strength, wear and durability. Part 3. Changeable conditions of interaction in uncorrected engagement. *Problems of Tribology, 74*(4), 49-53.

Chernets, M. V., & Chernets, Y. M. (2015). Investigations of tooth engagement conditions in cylindrical involute gear on contact strength, wear and durability. Part 4. Changeable conditions of interaction in corrected engagement. *Problems of Tribology, 75*(1), 69-76.

Chernets, M. V., Kelbinski, E., & Yarema, R. Y. (2011). Generalized method for the evaluation of wear in cylindrical involute gears. *Materials Science, 47*(1), 45-51.

Chernets, M. V., Yarema, R. Y., & Chernets, Y. M. (2012). A method for the evaluation of the influence of correction and wear of the teeth of a cylindrical gear on its durability and strength. Part 1. Service life and wear. *Materials Science, 48*(3), 289-300. doi:10.1007/s11003-012-9505-y

Drozdov, Yu. (1975) *To the development of calculation methods on friction wear and modeling. Wear resistance* (pp. 120-135). Moscow: Science.

Flodin, A., & Andersson, S. (1997). Simulation of mild wear in spur gears. *Wear, 207*(1-2), 16-23. doi:10.1016/s0043-1648(96)07467-4

Flodin, A., & Andersson. S. (1999). Wear simulation of spur gears. *Tribotest, 5*(3), 225-250. doi:10.1002/tt.3020050303

Grib, V. (1982). *Solution of tribotechnical tasks with numerous methods*. Moscow: Science.

Kahraman, A., Bajpai, P., & Anderson, N. E. (2005). Influence of tooth profile deviations on helical gear wear. *Journal of Mechanical Design, 127*(4), 656-663. doi:10.1115/1.1899688

Pasta, A., & Mariotti, G. V. (2007). Finite element method analysis of a spur gear with a corrected profile. *Journal of Strain Analysis for Engineering Design, 42*(5), 281-292. doi:10.1243/03093247jsa284

Applied Computer Science, vol. 12, no. 3, pp. 85–99

Submitted: 2016-08-08
Revised: 2016-08-29
Accepted: 2016-09-13

computer algorithm, economy and management,
information applications systems

Łukasz WOJCIECHOWSKI[*], *Tadeusz CISOWSKI*[**],
Józef MARCINIAK[***], *Bogdan PALCHEVSKYI*[****]

COMPUTER APPLICATION SYSTEM FOR OPERATIONAL EFFICIENCY OF DIESEL RAILBUSES

Abstract

The article presents a computer algorithm to calculate the estimated operating cost analysis rail bus. This computer application system compares the cost of employment locomotive and wagon, the cost of using locomotives and cost of using rail bus. An intensive growth of passenger railway traffic increased a demand for modern computer systems to management means of transportation. Described computer application operates on the basis of selected operating parameters of rail buses.

1. SUBURBANAND REGIONAL RAIL SERVICES

Until recently, regional rail services were operated by electric three-car multiple units, EN57 and EN71, as well as SP42 or SM32 diesel locomotives to haul up to four cars on non-electrified routes. The aforementioned electric or diesel trains were heavy vehicles with high axle loads ranging from 160÷170 kN. These vehicles had numerous shortcomings, including high energy consumption, lack of operational reliability, low acceleration (1.2 m/s^2), lack of smooth

[*]Lublin University of Technology, Nadbystrzycka Street 36, 20-618 Lublin, +48 81 538 45 85, l.wojciechowski@pollub.pl
[**]Department of Logistics, Polish Air Force Academy, Dywizjonu 303 Street 35, 08-521 Dęblin, tadeuszc@poczta.onet.pl
[***]University of Technologyand Humanities in Radom, Malczewskiego Street 29, 26-600 Radom, +48 361 77 43, j.marciniak@uthrad.pl
[****] National University of Technology in Lutsk, Lwowska Street 75, 43-018 Ukraine, bogdan_pal@ukr.net

running due to noise and vibration on a vertical and horizontal plane, low braking rate, low travel comfort (lighting, heating), inefficient and usually non-operational sanitary facilities which are difficult to maintain clean. In addition, these units did not have train destination side plates, which made orientation difficult for passengers getting on and out of the train from side travel directions. Passengers also reported difficulties with getting on and out of trains at high-platform stations. The use of standard train sets led to destruction of railway tracks, the technical condition of which was and still is far from being satisfactory, high consumption of electric energy and diesel oil, as well as degradation of the environment due to vibration, noise and pollution. The above factors contributed to the development of modern multiple units based on modern computer systems with new, passenger-friendly constructional and operational parameters which meet EU requirements (Sobaszek, Gola & Świć, 2014).

Suburban and regional rail services at distances of approx. 150 km on electrified lines with a higher traffic density are operated by electric multiple units EN 57.On secondary non-electrified lines (it is estimated that there are about 6500km of such lines), the traffic is operated by SM42, SP42 and SP32 diesel locomotives with two or three second-class passenger cars.

The PKP Polish Railways plans to close these lines down due to their unprofitability. Apart from low commercial speed of trains on secondary lines, the operation of rail traffic using diesel locomotives is very expensive.

This cost can significantly be reduced if a locomotive, e.g. SP42 with two cars, is replaced with a railbus, e.g. Regio Tramp 215M (two-unit) or 213M (single-unit).

Compared to diesel locomotives, the use of the above railbuses brings the following benefits (Stokłosa & Cisowski, 2008; Cisowski & Wojciechowski, 2011):

- the cost of materials, operation and maintenance of a high-speed engine manufactured by MAN (such engines are applied in Regio Tramp 215M and 213M buses) are lower than the cost of materials, operation and maintenance of a diesel engine type a8C22 (used in SP42 locomotives),
- fuel and engine oil consumption by 2 engines of a 210M railbus is by 13% lower than that by the a8C22 engine.

The operational costs of a railbus are significantly lower than those of the analyzed trainset due to a lower railbus weight and thus its lower impact on the track.

The data listed in the above table demonstrate that the number of passengers in both cases is almost the same, but fuel consumption is much lower in the case of railbuses (Dębiński, Kiercz, Kowalski & Kądziołka, 2011).

In addition, travel comfort in railbuses is higher. Finally, the lower weight of railbuses means that the rail tracks are destroyed to a smaller extent.

Table 1 provides a comparison of the operational parameters of two Regio Tramp railbuses and an SP42 locomotive.

Tab. 1. Comparison of a railbus and SP42 locomotive with two cars used in computer algorithm (own study)

Type of trainset or railbus	Unit	SP42 locomotive +2 cars 120A	Regio Tramp 215	%215 M/ SP42
Weight	[t]	159.5	58	36
Number of passengers	[pc]	128	120	94
Weight of passengers	[t]	8.96	8.4	94
Engine type	-	A8C22	2x2866LUH-21	-
Number and arrangement of cylinders	-	8V50°	R6	-
Rated power	[kW]	588	2x250	85
Rated rotational speed	[1/min]	1000	2000	-
Rated fuel consum./unit	[g/kWh]	224	195	87
Engine oil consumption	[g/kWh]	1.12	1.135	101
Fuel consumption in normal conditions	[kg/h]	131.7	114.5	37
Engine oil refill consumption	[kg/h]	0.659	0.244	37
Idle-run fuel consumption	[kg/h]	9.0	2x2.2	49

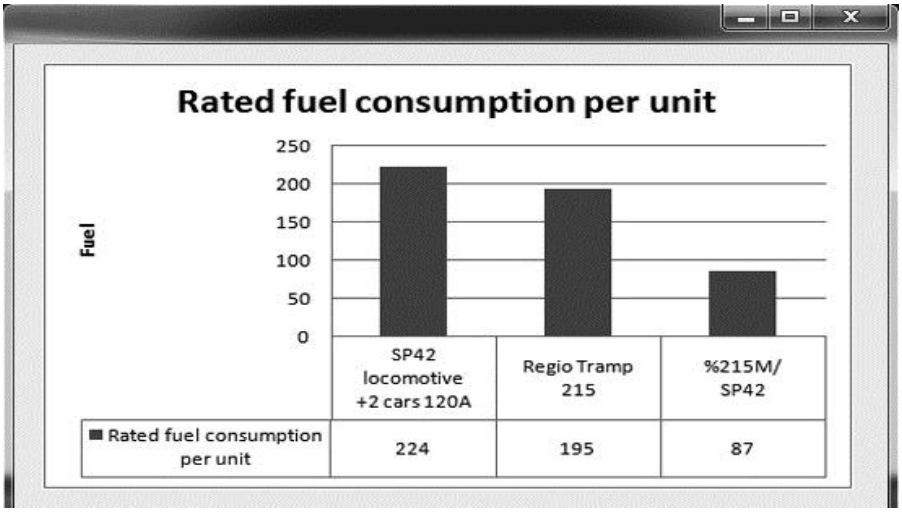

Fig. 1. Result of algorithm calculating fuel consumption (per unit) (own study)

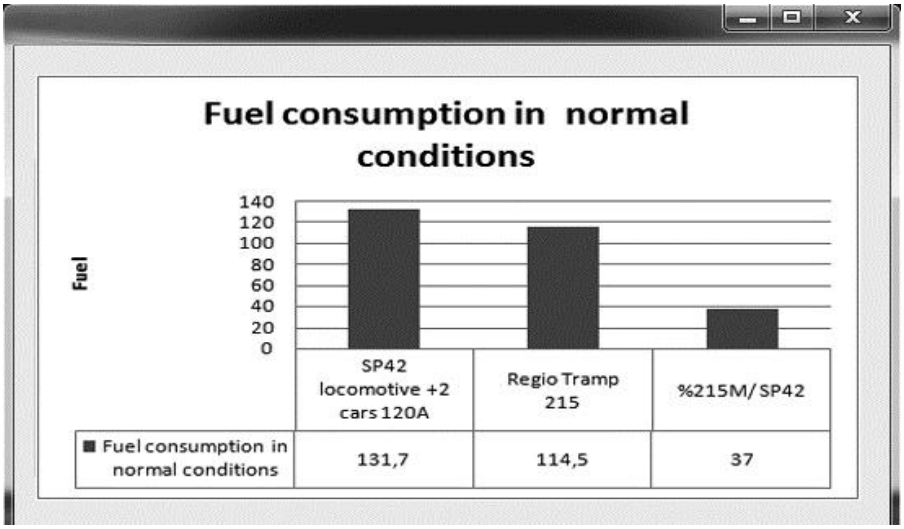

Fig. 2. Result of algorithm calculating fuel consumption (normal) (own study)

The first step comparison vehicles of computer algorithm are presented in fig. 1.:

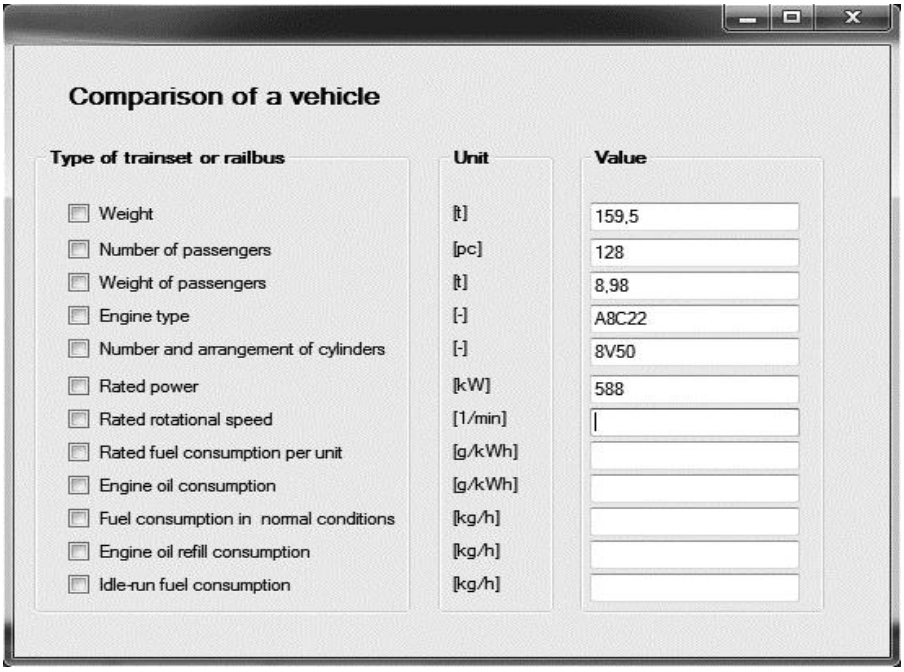

Fig. 3. Comparison vehicles (own study)

2. PROPERTIES OF RAILBUSES MANUFACTURED IN POLAND AND ABROAD

Railbuses are light traction vehicles manufactured by a number of companies worldwide (Gola, Montusiewicz & Świć, 2011; Świć, & Gola, 2013), including Siemens (the Netherlands), Adtranz (Germany), Bombardier/DWA (Germany), Wagonka Studenka (Czech Republic), Fujii Hi (Japan), Alstom (Germany), Goninan (Australia), DE Dietrich (France).

The parameters of railbuses manufactured by foreign companies are listed in Table 2.

Railbuses can develop a speed ranging from 90÷150 km/h, yet their operational speed is usually approx. 120 km/h.

Their engine power ranges from 200÷2x380 kW. The number of seats ranges from 36÷74. The maximum unit power of such bus is 12.9 kW/t.

These buses are powered by under-floor diesel engines manufactured by such companies as MAN Eurol, Volwo Euro I, MTn Euro I, MTN Eurol, Dentz, Man Euro II and Niigata DMF.

In Poland, railbuses are predominantly manufactured by three companies:

- ZNTK Poznań, the manufacturer of Regio-Tramp 213M and Regio Tramp 215M,
- KOLZAM Racibórz, the manufacturer of 208M and SPA-66/AS-66,
- ZNTK Bydgoszcz, the manufacturer of 214M.
- Table 3 gives the comparison of parameters of railbuses manufactured in Poland.

Regio Tramp 213M and 215M (Figs. 1 and 2) are light modern low-floor diesel railbuses for passenger service on normal-track lines.

These vehicles offer a broad spectrum of possibilities owing to their modular equipment which can be tailored to user requirements.

These vehicles can either consist of up to three units interconnected with a coupler and a bridge (e.g. 214M) or a single unit (e.g. 213M).

One of the most important features of these vehicles is that they can automatically change their wheel track from 1435 mm to 1520 mm.

These vehicles are relatively inexpensive and have low maintenance costs, which in fact increases the profitability of passenger service on the lines excluded from railway traffic by the PKP Polish Railways.

Tab. 2. Technical data of railbuses manufactured by foreign companies (own study)

Manufacturer	Country of user	Year of construction	Track [mm]	Operational speed [km/h]	Power [kW]	Length [mm]	Number of seats /standing room	Power per weight [kW/t]	Notes
SIEMENS	Netherlands	1980	1435	120	2x320	26170	-	-	-
Adtranz	Germany	1990	1435	129	2x257	25500	53/13	12.9	Engine MAN Euro I
Bombardier/ DWA	Germany	1990	1435	100	265	16540	53/13	11.5	Engine Volvo Euro I
Wagonka Studencka	Czech Republic	1990	1435	90	206	13250	36	11.1	Engine Volvo Euro I
Fujii HI	Japan	1990	1067	110	296	20000	3x35	8.5	Engine Niigata DMF
Alstom	Germany	1992	1435	120	315	27260	60/13	7.7	Engine MTU Euro I
Goninan	Australia	1994	1600	135	2x231	25900	50	9.2	Engine Bentz
ABB	Australia	1994	1435	150	3x380	3x25250	3x54	7.0	Engine Commins
SIEMENS	Germany	1995	1435	100	2x228	24800	74/ 100	11.12	Engine Euro II
Alstom	Germany	1999	1435	120	2x257	28900	63/17	10.5	Engine MAN Euro II
De Dietrich	France	2000	1435	140	2x257	28900	63/17	10.5	Engine MAN Euro II

Tab. 3. Comparison of buses manufactured in Poland (own study)

Type	207M + 207 Mr	208	SDA-66/AS-66	207Ma+207 Mra+207Mb	213	214 M
Manufacturer	ZNTK Poznań	KOLZAM Racibórz	KOLZAM Racibórz	ZNTK Poznań	ZNTK Poznań	PESA Bydgoszcz
Number of units	1÷2	2	1	3	1	1
Length with bumpers	30920 mm	19200 mm	16500 mm	45940 mm	17000 mm with automatic clutch	18000 mm
Unladen weight	54000 kg	38800 kg	23200 kg	82000 kg	27500 kg	23520 kg
Power	200 kW	157 kW	92/110 kW	2x200 kW	250 kW	250 kW
Type of gear	hydraulic	hydro-mechanical	mechanical	hydraulic	hydro-kinetic	hydro-kinetic
Maximum speed	90 km/h	90 km/h	90 km/h	90 km/h	120km/h	110 km/h
Seats	96	60	66	136 + 4	38	60
Standing room	140	68	74	196	52	70

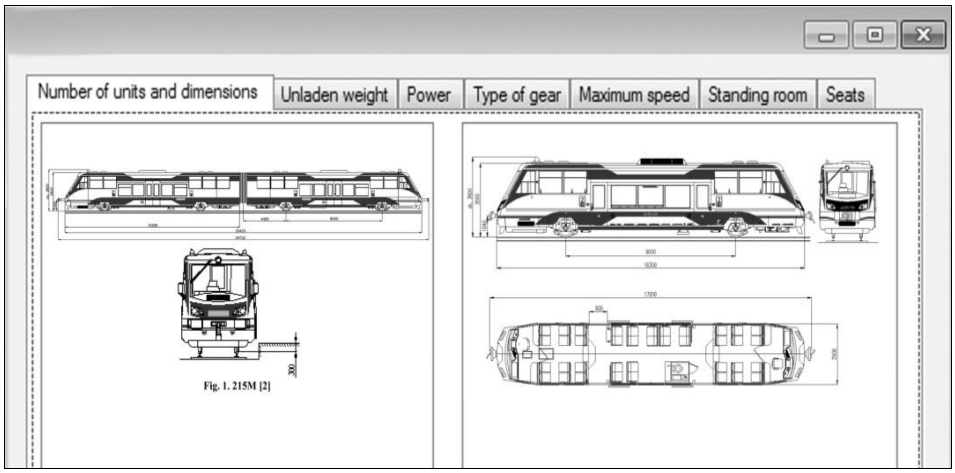

Fig. 4. Computer algorithm to comparison of buses (own study)

The main operational advantages of these vehicles include:

- reduced environment-polluting emissions due to the application of diesel engines which comply with the EURO2 standard (Lalik, 2008),
- reduced noise due to the application of shields and increased floor thickness, with particular emphasis on thermal and sound insulation,
- low axle-load of 140÷150 kN and thus a less destructive impact on rail tracks,
- relatively low energy consumption due to the application of light materials in vehicle design,
- reduced vehicle weight due to light steel design, the application of diesel engines with low fuel consumption and the use of heat from the engine and gear cooling system for vehicle heating,
- lower financial outlays on vehicle inspection and maintenance due to the application of maintenance-free subassemblies which wear to a little extent and do not require constant supervision,
- the use of environment-friendly materials, e.g. water-soluble painting materials,
- the use of recyclable materials, e.g. steel and parts made of plastics.

3. SELECTED PARAMETERS OF RAILBUSESUSED IN THE CALCULATION ALGORITHM

A selection of operational parameters of railbuses used in the calculation algorithm is illustrated using 208M as an example. According to the manufacturer's nomenclature (Basak & Biliński, 2007), 208M is a third-generation bus characterized by high comfort of travel (they are easy to get in and out of), modular design, low floor, on-board diagnostics, air-conditioned cars, and a closed WC system. Third-generation buses have a lower floor in the entire passenger space, while the floor height in the central part of the bus is 575÷600 mm (Basak & Biliński, 2007). The power units are mounted on an independent carrying frame, which considerably facilitates operation and maintenance processes. The buses are equipped with under-floor Power Pack integrated power units (Marciniak, 2009; Cisowski & Wojciechowski, (2011).

These buses are characterized by (Basak & Biliński, 2007):

- low purchase and operational costs, which leads to a higher profitability of passenger service on both local and regional lines,
- are adapted for getting in from both high and low platforms, i.e. from the level of a rail head (sliding doors),
- suitable for different levels of traffic due to their modular design and multiple travel,
- can be used for both cross-border and regional traffic on secondary lines as well as on lines which run in mountainous and sub-mountainous areas,

- high body inclination and small railway track arcs,
- are adapted to transport disabled passengers (getting in/getting out),
- separate space for the transport of large luggage and bicycles,
- ergonomic chairs with “vandal-resistant” design,
- ecological (closed) WC cabins adapted for disabled passengers,
- a modern hydro-mechanical under-floor drive system,
- a modern ecological combustion engine which complies with the EURO II standard,
- are equipped with an on-board computer which enables both drive system control and on-board diagnostics.

4. ANALYSIS OF ESTIMATED RUNNING COSTS OF A RAILBUS – RESULTS OF THE WORK CALCULATION ALGORITHM

The analysis of running costs involved calculating an estimated cost of transporting about 40 passengers at a distance l = 100 km by an SP42 locomotive with one 134-type car and by a 207-type railbus.

All calculations were based on the generated results of the works calculation algorithm. The algorithm in the course of calculation takes into account:

- route recalculation,
- energy consumption,
- final conversion,
- fuel consumption,
- specific fuel consumption
- the cost of fuel,
- converting liters of fuel per 1 kg of fuel.

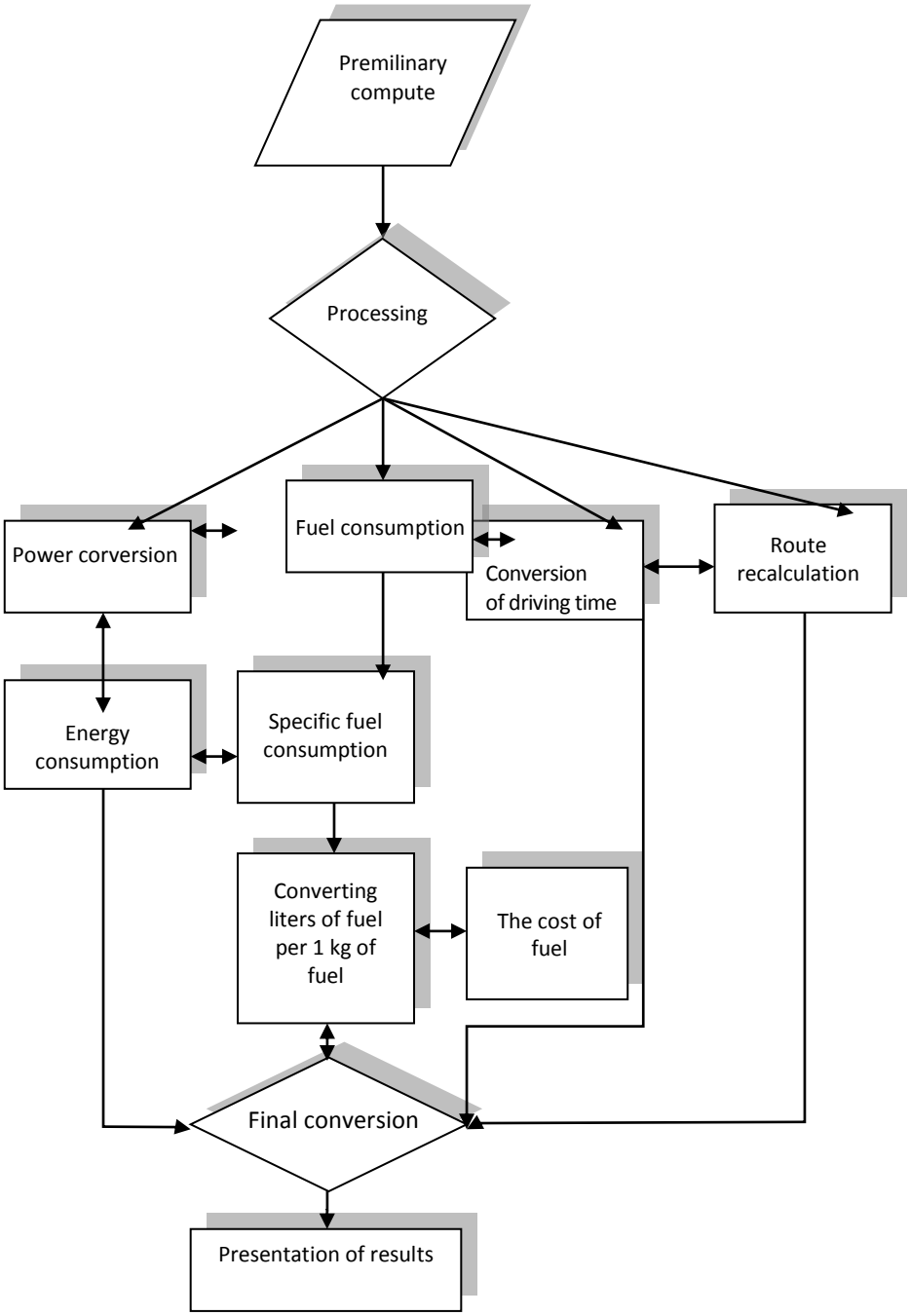

Fig. 5. Graph computer algorithm steps (own study)

Below are the steps in the process of computing the computer application:

Stage 1. Calculate the cost of the operational cost of SP42 locomotive with one car:

Step 1. Power of SP42 – P=588.2 kW (Stokłosa & Cisowski, 2008),
Step 2. Route – l = 100 km,
Step 3. Time of travel – t = 2 h,
Step 4. Unit fuel consumption – p = 224.4 [g/kWh],
Step 5. Energy consumption – E = 2·588.2 = 1176.4 kWh,
Step 6. Fuel consumption – P = 224.4·1176.4 = 263984.16 g ≈ 264 kg,
Step 7. Converting fuel into litres – 1 kg of fuel ≈ 1.3 litre,
P = 264·1.3 = 343.2 l,
Step 8. Cost of 1 liter diesel oil – 2.7 zloty,
Step 9. Fuel cost – Kp = 343.2 x 2.7 = 926.64 zloty.

Stage 2. Calculate the cost of the operational cost of K1 locomotive:

Step 1. It was assumed that the cost of one-day operation of this locomotive was 4000 zloty, which means that for 2 hours of operation:

$$K_1 = \frac{4000 \cdot 2}{24} = 333{,}5 \text{ zloty} \tag{1}$$

Step 2. A conductor was employed in the car for passenger service. An average monthly salary of the conductor was estimated at 2000 zloty per 200 hours a month.
The cost of conductor work for 2 hours (train travel):

$$K_2 = \frac{2000 \cdot 2}{200} = 20 \text{ zloty} \tag{2}$$

Step 3. It was assumed that the cost of one-day operation of a 134-type passenger car was 2000 zloty.
The operational cost of this car was:

$$K_3 = \frac{2000 \cdot 2}{24} = 166{,}66 \text{ zloty} \tag{3}$$

Step 4. K4 denotes the consumption of other operational materials K4 = 50 zloty (lubricating oil for wheel flanges, engine lubricant, sand, cooling water).

The total cost of 100 km travel (locomotive with one car):

$$K = \sum K_i = 926{,}64 + 333 + 20 + 166{,}66 + 50 + 1496{,}30 \text{ zloty} \tag{4}$$

Stage 3. Calculate the cost of the operational cost of 207 railbus:
Step 1. Engine power – P=200 kW,
Step 2. Route – l = 100 km,
Step 3. Time of travel – t = 2 h,
Step 4. Unit fuel consumption – p = 209 g/kWh,
Step 5. Energy consumption – E = 2·200 = 400 kWh,
Step 6. Fuel consumption – P = 209·400 = 83600 g = 83.6 kg,
Step 7. Converting fuel into litres:
P = 83.6 x 1.3 = 108.68 ≈ 109 l,
Step 8. Cost of fuel:
1 l engine oil costs 2.7 zl/l,
Kp = 109 x 2.7 = 294.3 zloty.

Stage 4. Calculate the cost of the operational cost of a railbus:
Step 1. It was assumed that the cost of one day of operation of a railbus was 1500 zloty, which means that for 2 hours of operation:

$$K_1 = \frac{1500 \cdot 2}{24} = 125 \text{zloty} \tag{5}$$

No conductor on the bus. Operational materials K4 = 25 zloty

Step 2. The total cost of 100 km travel (railbus):

$$K = \sum K_i = 294{,}3 + 125 + 25 = 444{,}30 \text{ zloty} \tag{6}$$

Step 3. A ratio between the locomotive and railbus costs:

$$k = 1496{,}30 / 444{,}30 = 3{,}96 \text{ zloty} \tag{7}$$

Tab. 4. Comparison of costs of 100 km travel of a locomotive with one car and a railbus–results of the work calculation algorithm (own study)

Cost specifications	Diesel locomotive with one car	Railbus
Fuel consumption [zl]	926.64	294.3
Operational cost K1 [zl] locomotive/railbus	333	125
Conductor work cost K2 [zl]	20	-
Car use cost K3 [zl]	166.66	-
Cost of operational materials K4 [zl]	50	25
Total cost	1496.30	444.3

Beloware presented results of cost specifications Diesel locomotive with one car and Railbus.

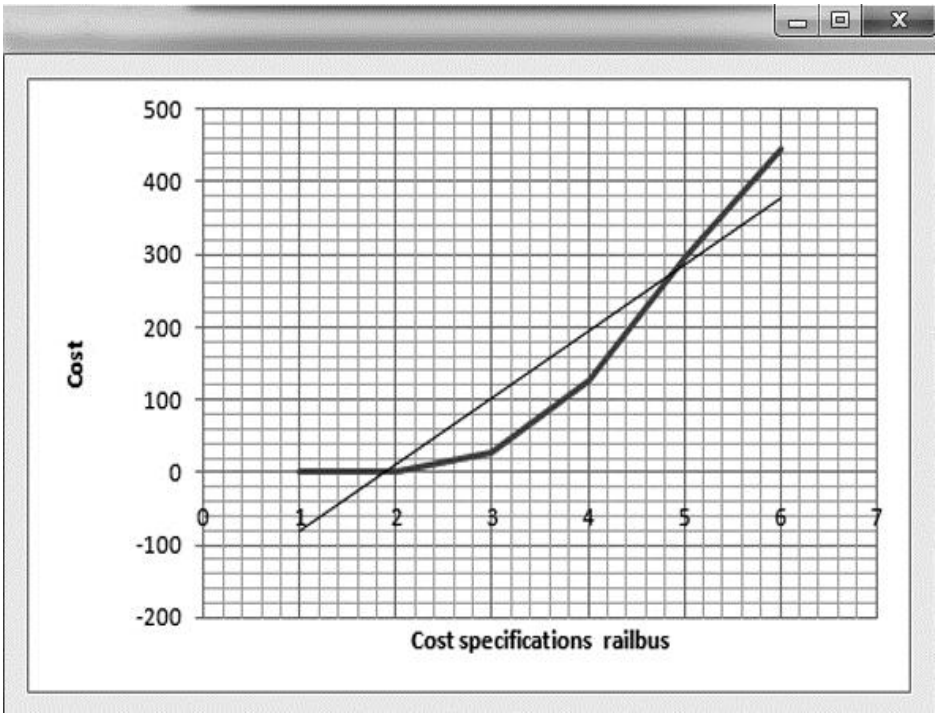

Fig. 6. Calculation results of computer algorithm for Railbus (own study)

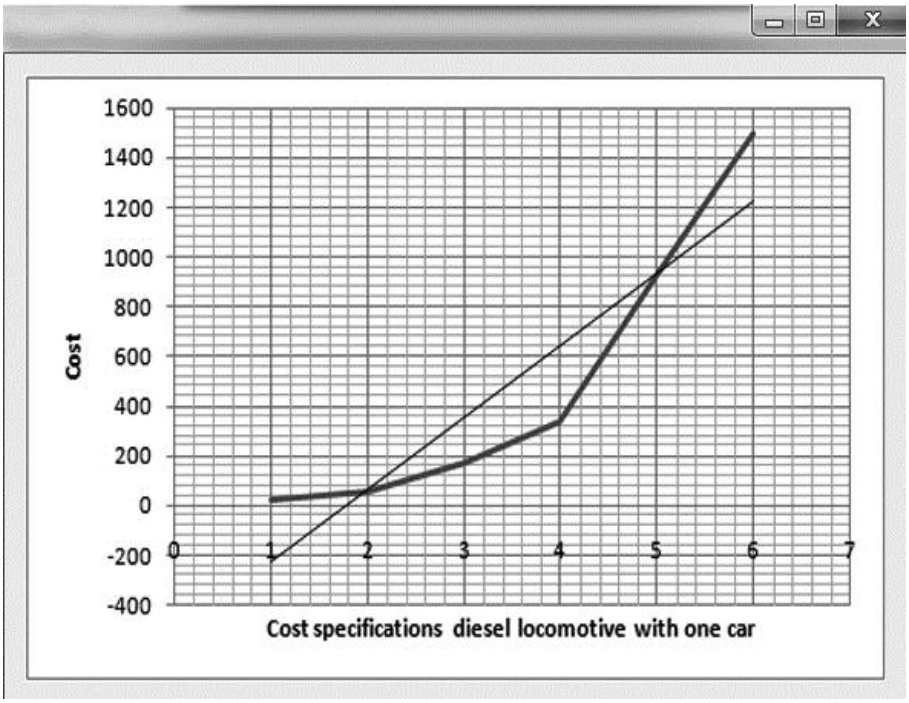

Fig. 7. Calculation results of computer algorithm for Diesel locomotive with one car (own study)

An algorithm analysis reveals that buses of this type can be used on lines which are in relatively low technical condition and have an axle load of 13÷14 t/axle. Their maximum speed is 90 km/h. The buses have seats for 60÷66 passengers, with standing room for 68 and 74. Railbus operating costs are lower more than 70% than diesel locomotive with one car.

3. CONCLUSIONS

Based on the analysis results, the following observations and conclusions have been drawn:

1. Computer algorithms for estimating operating costs are an effective tool to assist transportation process,
2. As a consequence, the maintenance of regional trains required and still requires considerable financial outlays,
3. Economic effectiveness of passenger railway services on secondary railway lines can be significantly increased if light rail vehicles are used instead of a diesel locomotive with two passenger cars.

4. P. 1 demand can be met if light railbuses, Regio Tramp 215M or 213M, are used.
5. 215M and 213M buses manufactured in Poland can compete with foreign products of a similar type.
6. 215M and 213M railbuses ensure high travel comfort, and they are easy and economic to operate.

REFERENCES

Basak, S., & Biliński, J. (2007). The modernization of the electric traction series EW60 (6 Web). *Technique of Railway Transport, 5-6*, 44-53.

Cisowski, T., & Wojciechowski, Ł. (2011). Synthesis models and algorithms to identify situations in the management of transport streams. *Advances in science and technology*, *9*, 98-119.

Cisowski, T., & Wojciechowski, Ł. (2011). The new approach in regulating the management of transport streams. *Advances in science and technology*, *10*, 112-121.

Dębiński, M., Kiercz, K., Kowalski, S., & Kądziołka, T. (2011). Overview of design solutions selected electric multiple units, *Rail Vehicles*, *1*, 48-54.

Gola, A., Montusiewicz, J., & Świć, A. (2011). Computer Aided FMS machine tools subsystem selection using the Evolutionary System of Multicriteria Analysis. *Applied Computer Science*, *7*(1), 18-29.

Lalik, M. (2008). *The test report number M/57.01/07 – Electrical performance tests trainset 16Ek*. Warszawa: CNTK Warsaw.

Marciniak, J. (2009). *Operation of railway vehicles of new generation*, Radom: Radom University of Technology.

Sobaszek, Ł., Gola, A., & Świć, A. (2014). Creating Robust Schedules Based on Previous Production Processes. *Actual Problems of Economics*, *158*(8), 488-495.

Stokłosa, J., & Cisowski, T. (2008). Intermodal transport over short and long distances. *Maintenance and reliability*, 3, 77-82.

Świć, A., & Gola, A. (2013). Economic Analysis of Casing Parts Production in a Flexible Manufacturing System. *Actual Problems of Economics*, *141*(3), 526-533.

INSTRUCTIONS FOR AUTHORS

1. The journal „Applied Computer Science" Publisher original papers written in English.
2. The published papers paper must concern problems of computer applications in production engineering, economy and management or technology.
3. The paper should be prepared using *Paper template* and be not shorter than 8 and not longer than 14 pages.
4. Units of measurement should be presented simply and concisely using System International (SI) units.
5. Manuscripts should be sent together with the filled in *Submission form* by one of the authors of the manuscript to the Editorial Board's e-mail address: acs@pollub.pl.
6. Papers must be submitted on the understanding that they have not been published elsewhere and are not currently under consideration by another journal published by any other publisher.
7. The submitting author is responsible for ensuring that the article's publication has been approved by all the others coauthors.
8. The Editorial Board sends the acknowledgment of the submissions. Only an acknowledgment from the Editorial Board officially establishes the date of receipt.
9. The Editor Board inform authors about the progress of assessment and publication processes. The publisher will do everything possible to ensure prompt publication.
10. After receiving positive reviews and after acceptance of the paper for publication, the text must be submitted in a Microsoft Word document format. Drawings and photos should be additionally submitted in the form of graphical files in the *.tif, *.jpg, *.gif or *.cdr formats. Bitmap images should be of 300 dpi resolution at least unless the resolution is intentionally set to a lower level for scientific reasons.
11. The Editorial Office reserves the right to abridge and adjust the manuscripts.
12. Authorship of the paper should be limited to those who have contributed substantially to the work.

13. Guest authorship and ghostwriting is unacceptable and will be retraced if any detected cases will expose, with the academics being reported to their institutions.
14. The contents of the articles are ultimately the responsibility of the contributor. Accordingly, the Publisher and the Editorial Board accept no liability whatsoever for the consequences of any inaccurate of misleading data, opinion or statement.

ASSESSMENT PROCESS

1. All submitted papers are subject to peer review and are expected to meet standards of academic excellence.
2. Manuscript are accepted for publication by:
   - The Subject Redactor,
   - Two independent reviewers from outside the institution of the author/authors, appointed by the Scientific Board,
   - The Language Redactor.
3. All submitted papers firstly are sent to the proper Subject Redactor (according to the author's indication of the paper's scientific area) who decides if the manuscript is relevant to the subject of Applied Computer Science. Negative decision of the Subject Redactor is tantamount to rejection of the manuscript and ends the assessment procedure.
4. Reviewers are selected in accordance with the principle of avoiding conflict of interests (examples of conflicts of interest include a personal relationship between reviewer and author, occupational subordination, direct scientific cooperation).
5. Reviewers prepare the reviews using the *Review form.* The review is provided in written form and concludes with an explicit recommendation to accept or reject the paper for publication.
6. Reviewers do not know the name of paper's author/authors (reviewer receives the text of the manuscript signified by *ID-text-number* given by the Editors)
7. The names of the reviewers for the individual publications are not revealed and are anonymous to the authors.
8. If a negative review is given, the submission is rejected.
9. The reviewer can discuss the manuscript with the Statistical Redactor or/and Language Redactor.
10. On receiving the required number of reviews, the Editors pass them immediately to authors. The Editors require that authors prepare answers to reviewers' comments, which are then sent to referees.
11. When the answers to reveiwers' comments are accepted by reviewers, the Editorial Board makes a decision of publishing the manuscript. Decision with the expected date of publication is sent to the submitting author.

“GHOSTWRITING” PROCEDURE

(based on guidelines of the Ministry of Science and Higher Education, Poland)

Introduction

Reliability is one of the foundations in the education. Readers should be assured that the author’s results of work are transparent, fair and honest. Authors should present works in such a way whether they are the direct authors, or used in support of a natural or legal person. Therefore, the provide information about entities that contribute to the formation of publication (their substantive or financial contribution, etc.) is necessary. It is a sign of good morals and corporate social responsibility. Opposite behaviors are the phenomenon of “ghostwriting” and “guest authorship”.

“Ghostwriting” and “guest authorship”

“Ghostwriting” is the concealment participation of a person having a significant contribution to the formation of publication. If the author's contribution in the formation of the publication is negligible or even not taken place, and it is still included as an author or co-author – then we have to deal with the phenomenon of “guest authorship”.

Procedure

In order to prevent the “ghostwriting” and “guest authorship” cases authors of the publication should reveal the contribution of individual authors in the creation of the publication. They should provide information about the authorship of ideas, assumptions, methods, etc. used for the development of publication. The main responsibility for the article bears author.

Moreover the authors should present information about sources of funding of publications, contribution of research institutions, associations and other entities (“financial disclosure”).

“Ghostwiring” and “guest authorship” are forms of scientific misconduct and therefore each detected case will be exposed. The editors will notify the institutions employing authors and scientific societies. All cases of scientific misconduct (especially violations and breaches of ethics applicable in science) will be documented.